Influence of salt and regional tectonics on the structural and sedimentary basin development, Tiddlybanken Basin, southeastern Norwegian Barents Sea

Amalie Skibeli Herrem

Master Thesis in Geosciences
Sedimentology, paleontology and stratigraphy
60 Credits

Department of Geosciences
Faculty of Mathematics and Natural Sciences

UNIVERSITY OF OSLO

May 2022

Supervisors: Reidar Müller, Muhammad Hassaan, Jan Inge Faleide, Ivar Midtkandal

Influence of salt and regional tectonics on the structural and sedimentary basin development, Tiddlybanken Basin, southeastern Norwegian Barents Sea.

This work is published digitally through DUO – "Digitale Utgivelser ved UiO".

http://www.duo.uio.no

Preface

This master's thesis (ECTS 60) is submitted to the Department of Geosciences, University of Oslo (UiO), in the candidacy of the Master of Science in Geosciences (ECTS 120) following the Sedimentology, paleontology and stratigraphy program. The main supervisor of this thesis is Associate Professor Reidar Müller (UiO), together with the co-supervisors Senior Engineer Muhammad Hassaan (UiO), Professor Jan Inge Faleide (UiO, UiT), and Associate Professor Ivar Midtkandal (UiO).

This thesis serves as a contribution to the Research Center for Arctic Petroleum Exploration (ARCEx), funded by the Research Council of Norway (grant number 228107) together with ten academic and six industry partners (Equinor, Vår Energi, Aker BP, Lundin Energy Norway, OMV and Wintershall Dea).

Data availability statement

The seismic and well data that support the findings of this study are available from the Norwegian Petroleum Directorate (NPD), Schlumberger Multiclient, and Lundin Energy Norway, respectively. Restrictions apply to the availability of these data, which were used under license for this study.

Acknowledgments

First, I want to express my gratitude and sincere appreciation to my main supervisor Reidar Müller for his encouragement and guidance at every stage of this process. I am also appreciative to my co-supervisors, Muhammad Hassaan, Jan Inge Faleide, and Ivar Midtkandal, for your productive discussions and critical assessments of various drafts. A special thank you goes out to my co-supervisor, Muhammad Hassaan, who has been a great help throughout this project. Hassaan provided many great ideas for this thesis, and whenever I had a question or needed help, he was there. Additionally, thank you for teaching me Petrel during my Bachelor's degree. I would also like to extend a thank you to the IT department and student administration at the Department of Geoscience. Your guidance has been crucial when working on my master thesis. I am sincerely grateful to ARCEx (Research Centre for Arctic Petroleum Exploration), based in Tromsø, for providing financial support to my M.Sc. project, which is funded by the Research Council of Norway (grant number 228107), together with ten academic and six industry partners (Equinor, Vår Energi, Aker BP, Lundin Energy Norway, OMV and Wintershall Dea).

Secondly, I want to thank my fellow students and friends in the Geoscience M.Sc. program at UiO. They have made the time working on this thesis enjoyable and the past five years absolutely great, in addition to providing guidance and support.

Finally, a personal thank you goes to my partner, Marius Hauge Arnesen, and my family for taking such an interest in my studies. Your endless support and encouragement throughout this process mean the world to me.

Amalie Skibeli Herrem

Oslo, Norway. May 16th, 2022

Abstract

The Tiddlybanken Basin in the southeastern Norwegian Barents Sea is an excellent example of a salt-influenced rift basin, salt structure evolution, and rim-syncline stratigraphic accumulation. Due to increased subsidence during salt withdrawal, the rim-syncline comprises thick successions of the Triassic-Middle Jurassic fluvio-deltaic basin infill. Advanced seismic attribute mapping revealed a wide range of interactions between the salt wall growth and sediment routing within the Upper Triassic-Middle Jurassic strata. The data utilized in the Tiddlybanken Basin was a conventional three-dimensional (3D) and extensive, reprocessed two-dimensional (2D) seismic data sets integrated with two new (2019) exploration wells.

Late Devonian-early Carboniferous NE-SW regional extensional stress resulted in three half-grabens in the study area, affecting the distribution of evaporite layers. The northwestern part of the salt wall was developed by passive diapirism during the late Triassic due to the availability of halite. In comparison, the central and southeastern parts did not reach further than a pedestal stage due to a lack of mobile halite. During the Triassic-Jurassic, the salt wall is recorded to have been active in three different pulses. The channel systems crossing the salt wall during late Carnian and early ?Norian indicates inactivity of the salt wall. During the Triassic-Jurassic transition, the pre-salt Carboniferous rift structures were reactivated by far-field stresses from the Novaya Zemlya fold-and-thrust belt. The reactivation led to the rejuvenation of the northwestern part of the salt wall and the development of the Signalhorn Dome. Sediment routing within the rim-syncline resulted in diversion through lateral migration and ponding due to changes in slope relief in late Norian-?Rhaetian. Erosion of the Signalhorn Dome resulted in distinct truncation patterns and an angular unconformity between Upper Triassic and the overlying Lower Jurassic strata.

A local basin started to form above the southeastern and central parts of the salt wall during the lower Jurassic. Concurrently, the salt wall growth in the northwestern part was active. The entire salt wall became inactive during the middle Jurassic, resulting in a tidal-influenced depositional environment. Cenozoic compressional stresses reactivated again the Carboniferous pre-salt structures, the Signalhorn Dome, and the salt wall. The northwestern and southeastern parts of the salt wall were rejuvenated. However, the central part was insignificantly affected by the reactivation. The widespread inversion throughout the

Norwegian Barents Sea resulted in regional uplift and erosion, stripping off most of the folded roof of the Tiddlybanken Basin and Signalhorn Dome.

Table of Contents

1 Introduction

This study provides an assessment of the stratigraphic infill architecture and evolution of halokinesis within the Tiddlybanken Basin. It discusses the possible causes of salt movement and their effects on basin configuration. This chapter introduces the motivation, previous research on the study region, particularly the evolution of the Tiddlybanken Basin, marginal Signalhorn Dome, and primary research objectives.

1.1 Study area

The Barents Sea is enclosed by the Russian and north Norwegian shoreline, the Novaya Zemlya, Franz Josef Land, Svalbard, and the Atlantic Ocean eastern margin (Figure 1.1a). The southeastern Norwegian Barents Sea comprises a complex series of basins, platforms, and highs, including the Nordkapp and Tiddlybanken basins, the Haapet, Veslekari, and Signalhorn domes, the west Fedynsky, Norsel highs, and the Bjarmeland and Finnmark platforms (Mattingsdal et al., 2015). This thesis will focus on the infill pattern within the Upper Triassic to Middle Jurassic sedimentary sequences (Realgrunnen Subgroup) in the Tiddlybanken Basin (Figure 1.1b). The Tiddlybanken Basin is located at the southwestern margin of the Fedynsky High towards the Finnmark Platform. The Tiddlybanken Basin includes a ca. 39 km long salt wall and is isolated by pronounced rim-synclines with an NW-SE trend (Hassaan et al., 2020b). A salt-cored anticlinal is located on the western and southwestern margin of the basin, named Signalhorn Dome (Gernigon et al., 2018; Hassaan et al., 2020a, 2020b; Mattingsdal et al., 2015; Rowan et al., 2017). The dome has an elongated ellipse shape with a length of ca. 58 km long. Few previous studies have focused on this specific area (Hassaan et al., 2020a, 2020b; Rojo et al., 2019; Rojo et al., 2018; Rowan & Lindsø, 2017) because it was a disputed region between Norway and Russia until 2011.

A conventional 3D seismic dataset of very good quality, ST14004, is being presented in this study. The dataset will further increase the understanding of halokinetic movement and basin infill patterns of the Tiddlybanken Basin. The Realgrunnen Subgroup was earlier believed to

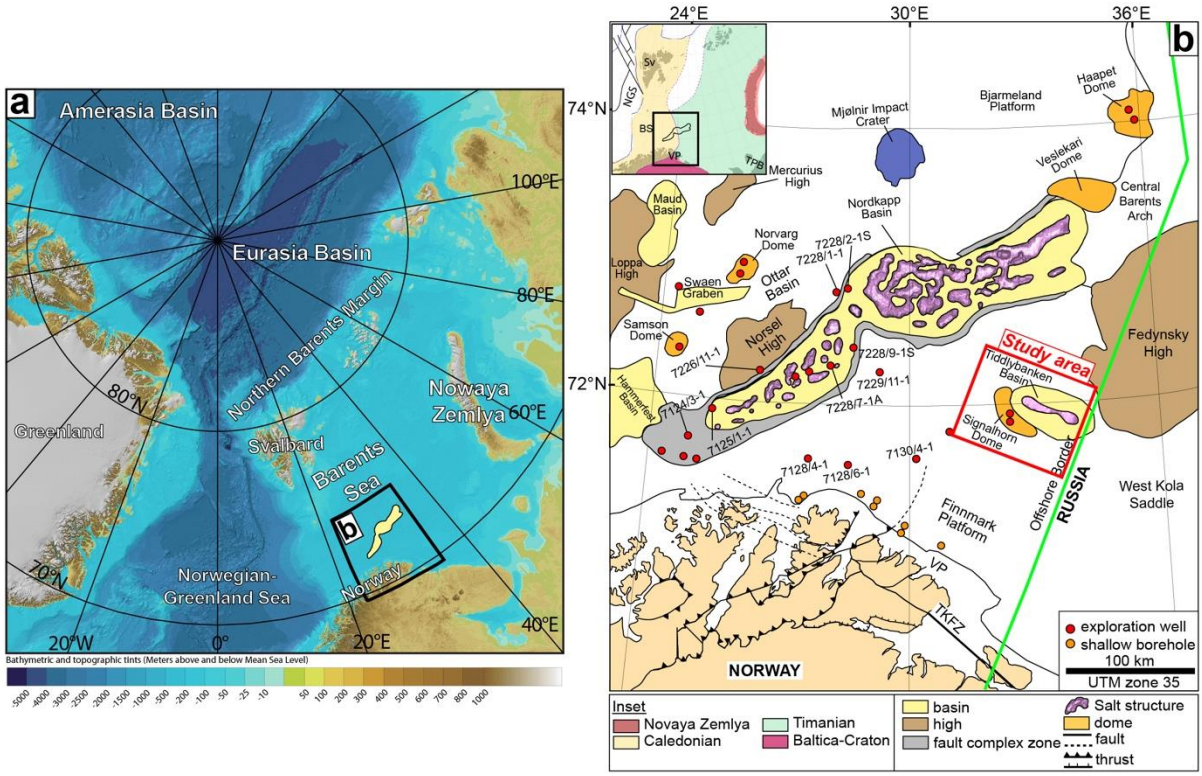

Figure 1.1: (a) *The Barents Sea in the Arctic modified after (Jakobsson et al., 2012).* ***(b)*** *Structural element near the study area (Hassaan, 2021) modified from (Gabrielsen et al., 1990; Mattingsdal et al., 2015). Sv: Svalbard; BS: Barents Sea; VP: Varanger Peninsula; TPB: Timanian-Pechora Basin; NGS: Norwegian-Greenland Sea; TKFZ: Trollfjorden-Komagelva Fault Zone.*

have been modestly influenced by tectonism (Figure 2.1). However, mounting evidence suggests that the tectonic imprint of the basin infill dynamics was considerable, for example, in the late Triassic to early Jurassic (Hassaan et al., 2020a, 2020b; Müller et al., 2019).

During the late Devonian-early Carboniferous, a NE-SW regional extensional stress regime formed three half grabens within the study area, which later influenced the salt deposited in Pennsylvanian to early Permian. Distinct truncation patterns and unconformities mapped show that far-field stresses from Novaya Zemlya fold-and-thrust belt had a much more significant impact on the basin infill history than previously thought (Line et al., 2020; Müller et al., 2019). The far-field stress regime caused reactivation of the pre-salt Carboniferous rift structures (Hassaan et al., 2020b).

1.2 Motivation

Salt-influenced rift basins might contain significant volumes of hydrocarbons and additionally offer trapping possibilities (Jackson et al., 2017; Warren, 2016). Due to the impermeable nature of evaporites, these traps can also be considered CO_2 storage sites. When salt is present in a basin, it will affect all aspects of a hydrocarbon system due to salt mobilization. The characteristics of salt in a hydrocarbon system are many: Salt flows create traps and influence the petroleum distribution in reservoirs. It works as a seal to the migration of fluid and as an effective conductor of heat, which elevates thermal maturity. Advanced 3D migration and computing power have revolutionized presalt and suprasalt hydrocarbon exploration (Warren, 2016). The visualization of the 3D cube provides an increased resolution, making it easier to interpret the exact shape of salt bodies and the salt-sediment interface. Sediment progradation and regional tectonic stresses are essential to understanding the activity of salt mobilization.

1.3 Research objectives

The seismic 3D dataset ST14004 in the Tiddlybanken area has been analyzed. The two wells 7132/2-1 and 7132/2-2 penetrated the succession in question. The seismic analysis combined with core and well data enhances the understanding of how the complex infill history of the Tiddlybanken Basin developed.

The investigations presented in this thesis will cover a detailed analysis of the temporal and spatial correlation between regional tectonic events and halokinesis. The interaction between the basin infill and 3D seismic image could answer several gaps in the geologic development of the Tiddlybanken Basin, southeastern Norwegian Barents Sea:

1. When did salt initially mobilize in the Tiddlybanken Basin, and what is the development timing for the Signalhorn Dome?
2. What were the mechanisms for salt mobilization?
3. Was the salt mobilization homogeneous or heterogeneous along the strike of the salt wall?

4. What are the impacts of salt mobilization and regional tectonics on the sedimentological development and distribution of the Realgrunnen Subgroup within an isolated salt-influenced rift basin?

These objectives are achieved by creating detailed time-structure and -thickness maps of the sedimentary successions within the study region, assessing RGB blending maps, available well (core and well logs), and seismic data (2D and 3D).

1.4 Research background

This section highlights a selection of recent research on salt tectonics of the Norwegian Barents Sea and structural analysis of the Tiddlybanken Basin to develop relevant research background. A broader review of the regional geology in the study region, theoretical concepts, data and methods are presented in chapters 2, 3, and 4. Until 2011, the area east of Nordkapp Basin was in disputed waters between Norway and Russia and therefore closed to exploration. The region included the salt-related Tiddlybanken Basin, which has not been studied much as the Nordkapp Basin.

Numerous salt-related minibasins have been studied in the Norwegian Barents Sea to better understand halokinesis and its influence on basin infill architecture. Therefore, several salt-tectonic and evolution studies have been conducted in this area. Examples of recent studies related to the evolution of the Tiddlybanken Basin are a master thesis by Reppen (2016), assessments of the Norwegian Barents Sea by Rowan et al. (2017), the Nordkapp Basin and Tiddlybanken Basin by Rojo et al. (2017, 2019) and Hassaan et al. (2020a, 2020b). These studies focused on the relationship between crustal rifting and evaporite deposition, base-salt relief influence, nature of the layered evaporite sequences (LES), triggering mechanisms and evolution of salt-related deformations, the effect of halokinesis on sedimentation accumulation, and creation of accommodation and routing of fluvial systems within salt-related basins.

Reppen (2016) focused on the structural evolution and fluvio-deltaic sedimentary architecture of the Snadd formation in the Tiddlybanken Basin and Nordkapp Basin. The study concluded that the interaction between salt diapirism and fluvio-deltaic systems caused fill-spill infill

patterns within the rim-syncline. The Signalhorn Dome has a salt pillow underneath it, which controls the rim-syncline sedimentation. Fluvial systems interacting with salt structures will migrate alongside the topographic highs during the deposition of the Snadd Formation (Reppen, 2016).

Rowan et al. (2017) suggested four suprasalt intervals within the Tiddlybanken Basin. The first and earliest is a pre-kinematic sequence of Middle Permian to Lower Triassic strata. Secondly, a Lower-Middle Triassic sequence pinches out towards the salt wall and is truncated by the middle-Triassic unconformity. A middle Triassic-Jurassic interval above the Middle Triassic unconformity (MTu) thickens towards the salt wall. The last interval is a Cretaceous unit that folds along the flanks of the salt wall and is interpreted to truncate the seafloor.

The triggering mechanism of salt movement during the early Triassic has been discussed by Rowan et al. (2017) and Hassaan et al. (2020a, 2020b). No evidence of differential loading was observed within the Tiddlybanken area by Rowan & Lindsø (2017), which is why they concluded that the first triggering was contraction related to the Permo-Triassic Uralian Orogeny. Under regional subsidence, Triassic delta systems sourced from the southeast Urals (Glørstad-Clark et al., 2010; Klausen et al., 2015; Klausen et al., 2018a; Line et al., 2020) prograded westward and caused minor salt triggering due to differential loading during the earliest Triassic (Hassaan et al., 2020a, 2020b). Salt mobilization accelerated in the early-mid Triassic due to additional sediment load. However, rejuvenation of the salt wall occurred probably due to far-field stresses from the Novaya Zemlya fold-and-thrust belt in the east (Triassic-Jurassic transition) and transpressional Eurekan/Spitsbergen orogeny to the northwest (early-mid Eocene).

2 Geological setting

This chapter focuses on describing the stratigraphic and structural framework and geological evolution of the southeastern Norwegian Barents Sea and the Tiddlybanken Basin in particular.

2.1 Structural framework

The Barents Sea is located north of Norway and Russia, covering an area of 1.4 million km^2 (Smelror et al., 2009). The Norwegian-Greenland Sea encloses the Barents Sea in the west, the Svalbard archipelago in the northwest, and the Russian islands of Franz Josef Land and Novaya Zemlya in the northeast and east. Novaya Zemlya divides the Barents Sea from the Kara Sea to the east (Figure 1.1).

North Novaya Zemlya, the North Barents, and the South Barents basins were formed in the foredeep zone of the Uralian tectonic belt (Doré, 1995). The most significant sedimentary basins were developed om the Russian sector, west of Novaya Zemlya Basin. Further west in the Norwegian Barents Sea, the Hammerfest Basin is bounded to the north by the Loppa High. The Ringvassøy-Loppa Fault Complex (N-S orientation) separates the western from the eastern Norwegian Barents Sea basins (Doré, 1995; Smelror et al., 2009).

The Southeastern Norwegian Barents Sea includes the Tiddlybanken and Nordkapp basins, the Signalhorn, Haapet, Veslekari domes, the West Fedynsky and Norsel highs, and the Finnmark and Bjarmeland platforms (Doré, 1995; Faleide et al., 1993; Mattingsdal et al., 2015). These structural elements were influenced by the Pennsylvanian-early Permian evaporites, where the prominent Nordkapp Basin includes numerous salt diapirs and salt walls, while the Tiddlybanken Basin comprises a central NW-SE oriented and uni-dimensional salt wall (Hassaan et al., 2020b; Rojo et al., 2019).

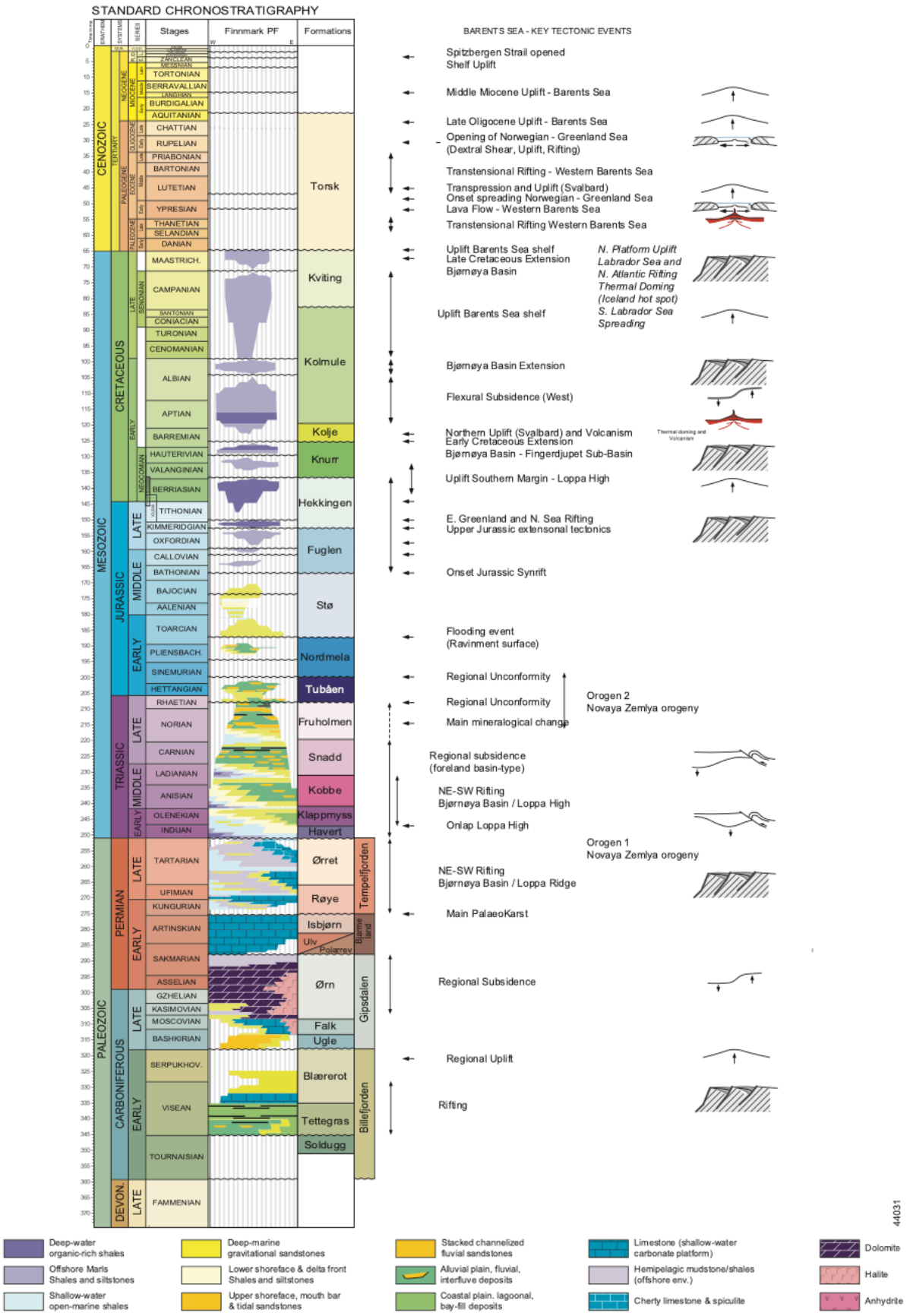

Figure 2.1: *Stratigraphic framework and key tectonic events in the Barents Sea (Jacquin, 2015).*

2.2 Stratigraphic framework

2.2.1 Stratigraphy of Late Carboniferous to Late Permian

The **Gipsdalen Group** (Figure 2.1) includes the Falk and Ørn formations which deposited evaporites and warm water carbonates during Pennsylvanian to early Permian (Gudlaugsson et al., 1998; Larssen et al., 2002). A shift in the depositional environment caused the deposition of cool-water carbonate platforms during the early-mid Permian. This refers to the **Bjarmeland Group** (Figure 2.1) which include Isbjørn and Polarrev formations (Beauchamp, 1994; Stemmerik, 2000). During the middle to late Permian, Tempelfjorden Group were deposited that include Røye and Ørret formations and comprised cool-water carbonates.

2.2.2 Stratigraphy of Early to Late Triassic

The Early-Late Triassic successions record a period of relatively stable tectonics and widespread subsidence in the Barents Sea region. The Induan to Carnian succession includes the Havert, Klappmys, Kobbe, and Snadd formations, older to younger (Figure 2.1).

The **Havert Formation** (Induan-Early Olenekian, earliest Triassic) has a distinct southern derived source in Fennoscandia but is mainly sourced from the Uralides in the southeast/east (Glørstad-Clark et al., 2010).

The **Klappmys Formation** (Early Olenekian-Late Olenekian, Early Triassic) has a similar depositional trend as the Havert Formation. A general coarsening and shallowing upward trend is characterized in this formation. The formation base comprises open-marine shales, while the uppermost part includes non-marine deposits such as tidal to fluvial channels and coastal plain deposits (Glørstad-Clark et al., 2010).

The **Kobbe Formation** (Anisian, Middle Triassic) consists mainly of shaly upper and lower shelf deposits with a coarsening and shallowing upward trend (Glørstad-Clark et al., 2010; Klausen et al., 2018a). The succession is a forestepping clastic deltaic system.

The **Snadd Formation** (Ladinian to early Norian, Middle-Late Triassic) is recorded as a siliciclastic wedge prograding from the southeast, sourced from the erosion of the Uralide Orogen (Klausen et al., 2015). It is represented as a late stage of the Early Mesozoic infilling of the Barents Sea Basin. The Snadd Formation comprises a range of depositional environments, from offshore shales through shallow marine to fluvial.

2.2.3 Stratigraphy of Late Triassic to Middle Jurassic

The Realgrunnen Subgroup successions (Norian to Bajocian) cover a period with reduced local subsidence and minor local faulting. The Realgrunnen Subgroup (Figure 2.1) contains the normal regressive offshore to deltaic Fruholmen Formation (Norian-Rhaetian), the forced regressive Tubåen Formation (Rhaetian-Sinemurian), the overall transgressive Nordmela (Sinemurian-Pliensbachian) and Stø (Pliensbachian-Bajocian) formations (Klausen et al., 2018b). The Realgrunnen Subgroup consists mainly of sandstones deposited in coastal plain and deltaic to shallow marine environments (Lord et al., 2019; Müller et al., 2019; Mørk, 1999), whose thickness locally varies considerably.

The **Fruholmen Formation** (Norian to Rhaetian, Late Triassic) is bounded by a maximum flooding surface at the base and the Rhaetian unconformity at the top (Klausen et al., 2016; Line et al., 2020). The Fruholmen Formation is subdivided into three members: the Akkar Member (prodeltaic to offshore marine mudstones), Reke Member (fluvio-deltaic sandstones and floodplain/tidal flat mudstones), and the Krabbe Member (deltaic) (Klausen et al., 2019). Large areas of the Barents Sea were uplifted during the late Triassic-early Jurassic, which resulted in erosion of Triassic sediments (Müller et al., 2019; Smelror et al., 2009).

The **Tubåen Formation** (late Rhaetian to early Hettangian, Late Triassic-Early Jurassic) is marked by the Rhaetian unconformity at the base and a subaerial unconformity at the top. The succession varies in thickness, where a thickness of 261 m has been recorded along the western margin (Klausen et al., 2016) but might be completely absent in other parts near the study area (e.g., the Bjarmeland Platform). The Tubåen Formation comprises sedimentary facies of

alluvial fan, braided plain, delta front, and mouth bar with a local transition to high energy marginal marine deposits (Ryseth, 2014).

The **Nordmela Formation** (Sinemurian to late Pliensbachian, Early Jurassic) is bounded by a flooding surface at the base and an unconformity at the top. The succession is a transition to fine-grained sandstones and siltstones. It is characterized by large areas with deposition of shoreface, coastal and alluvial plain deposits which locally became more tidal-influenced towards the top (Ryseth, 2014).

The **Stø Formation** (Late Pliensbachian to Bajocian, Middle Jurassic) is defined at the base by a regional unconformity and a major flooding surface at the top (regional drowning of Barents shelf). The succession generally consists of nearshore and inner shelf facies, including multiple hiatuses, resulting from an interplay between tectonics and relative sea-level changes (Müller et al., 2019; Ryseth, 2014). An overall transgression and deepening upward characterizes the succession (Olaussen et al., 1984).

2.3 Structural evolution

This section describes the main tectonic and stratigraphic events that developed the features and structures in the Norwegian Barents Sea, particularly the region in the vicinity of the Tiddlybanken Basin (Figures 1.1B and 2.2). For the purpose of this study, events that might have caused the formation of Tiddlybanken Basin and Signalhorn Dome are also described in more detail. The Barents Sea has experienced predominantly four tectonic phases from Late Paleozoic to Paleogene (Faleide et al., 2018; Henriksen et al., 2011a). It consists of a complex mosaic of basins and platforms originating from these tectonic events (Doré, 1995). The Caledonian mountain-building episode culminated around 400 m.y. (million years ago). It represented the closure of the Iapetus Ocean and the separation between Eurasia and

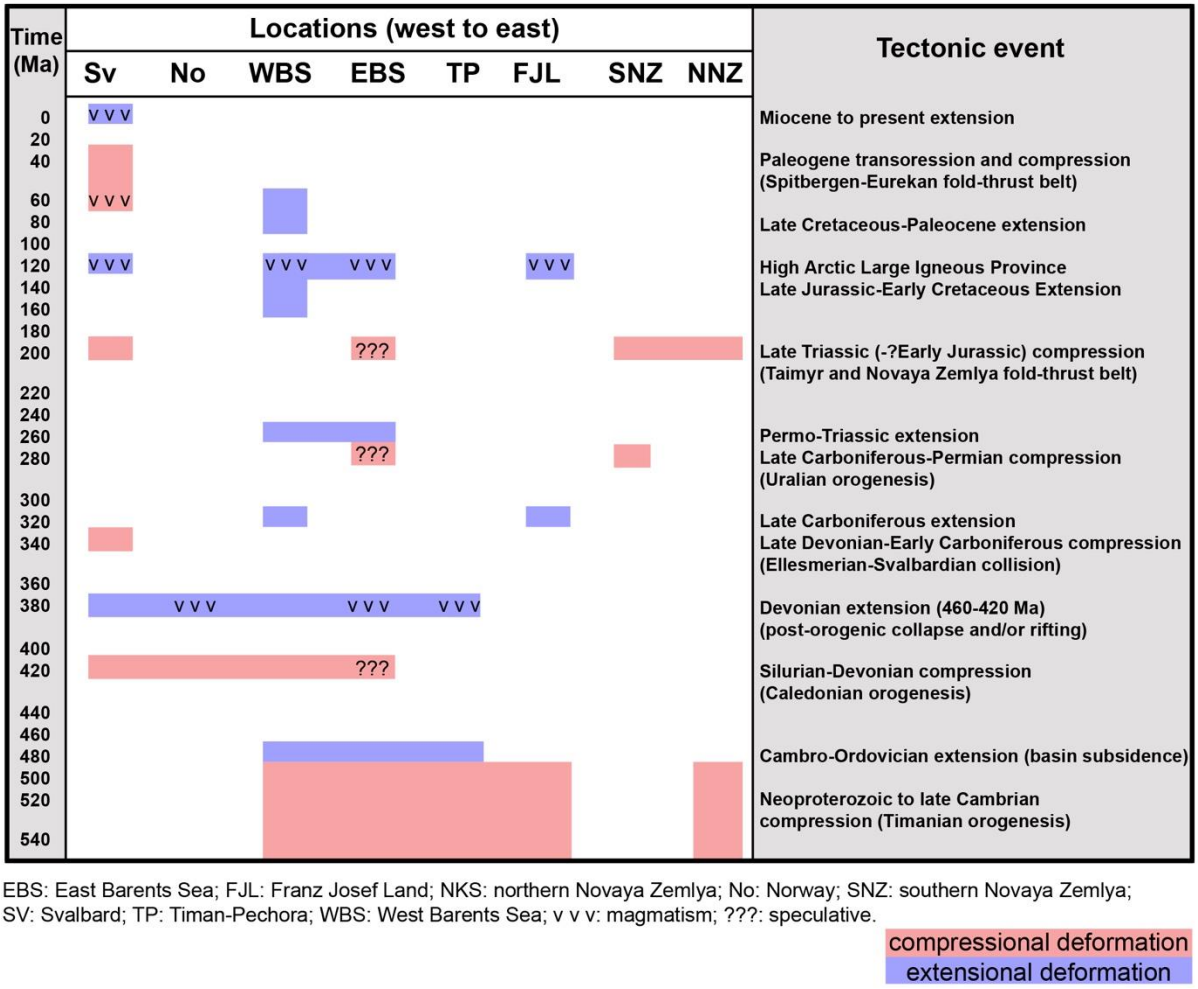

Figure 2.2: *Tectonic synthesis of the Barents Sea and nearby structural elements. Regional compression and extension are displayed in different regions (Hassaan, 2021).*

Laurentia plates. The post-Caledonian geological history is dominated by four major rift phases (Figure 2.2; Faleide et al., 2018):

1. Late Paleozoic rifting (Devonian-Carboniferous)
2. Permo-Triassic extension
3. Middle Jurassic-Early Cretaceous rifting - opening of Euramerican Basin in the north.
4. Late Cretaceous to Early Cenozoic Break up and opening of the Northern North Atlantic Margin.

2.3.1 Paleozoic

In the southeastern Norwegian Barents Sea, the late Devonian was characterized by a central structural high (Fedynsky High) surrounded by depressions to the south and north of it. During late Devonian-early Carboniferous, an extensional stress regime with a NE-SW orientation created, most likely, the NW-SE striking graben structures located in the southeastern Norwegian Barents Sea (Figures 2.3 and 2.4) (Hassaan et al., 2020a).

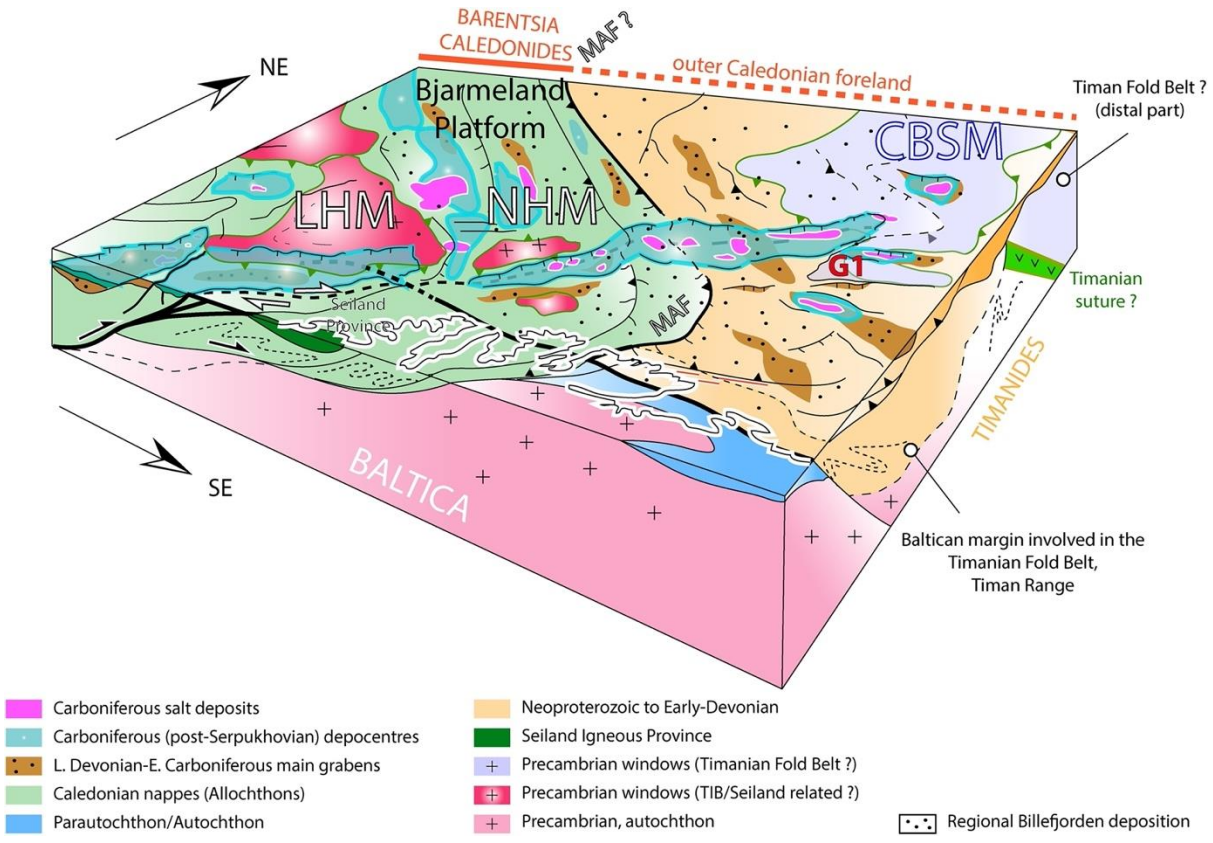

Figure 2.3: *Basement inheritance and late Paleozoic configuration in the Southeast Barents Sea (Hassaan, 2021) modified from (Gernigon et al., 2018). LHM: Loppa High magnetic domain; NHM: Norsel High magnetic domain; CBSM: Central Barents Sea magnetic domain; MAF: Middle allochthon Front.*

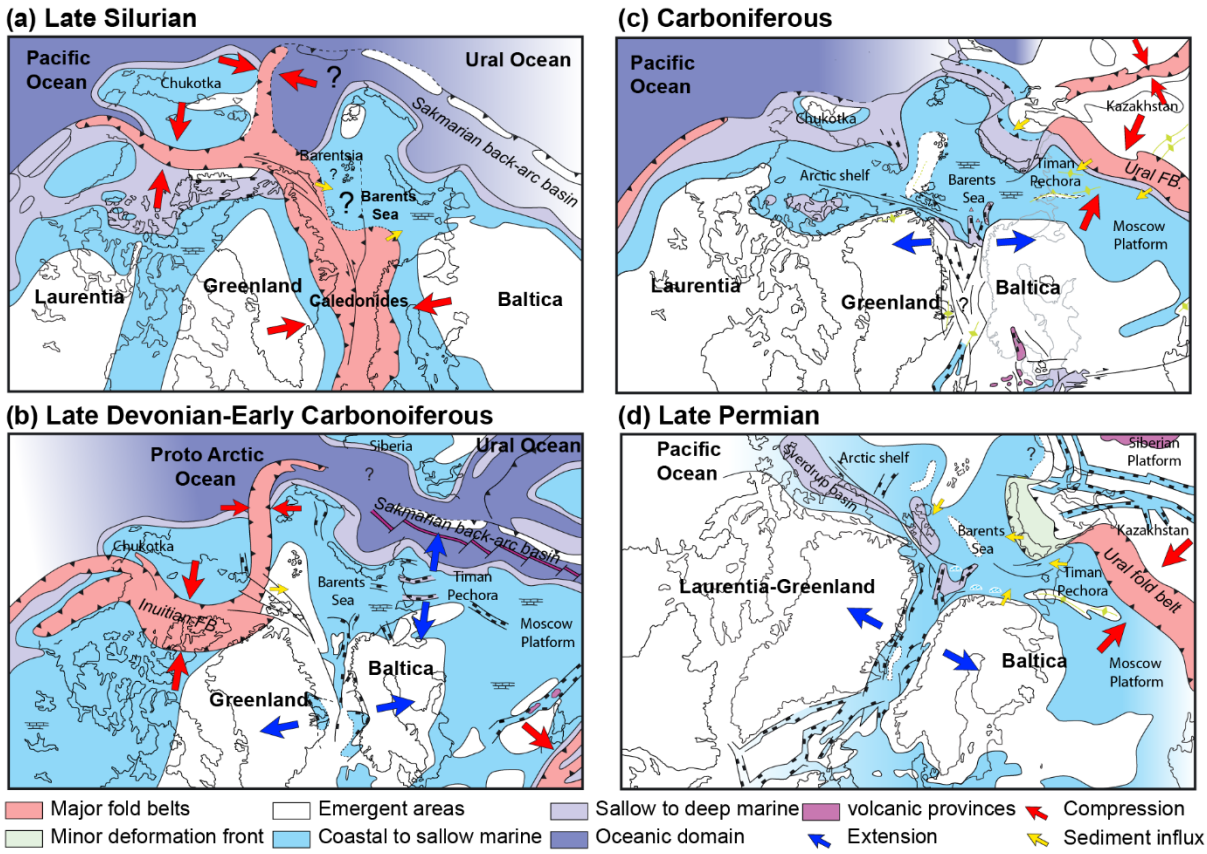

Figure 2.4: *Paleozoic geodynamic evolution of the North Atlantic and Arctic regions (Hassaan, 2021) modified from (Smelror et al., 2009).*

In the late Devonian to early Carboniferous NE-SW oriented extensional stress regime and the pre-existing Timanian structures developed a complex graben system below the Tiddlybanken Basin and Signalhorn Dome (Figure 2.5). It can be divided into three half-graben units GU1, GU2, and GU3 (Hassaan et al., 2020b). An NW-SE to NNW-SSE trending horst is situated along the southwestern and western margin of the Tiddlybanken Basin. The horst separates GU1 and GU2 half-grabens and is believed to have resulted from the Timanian structural grain (Figure 2.3).

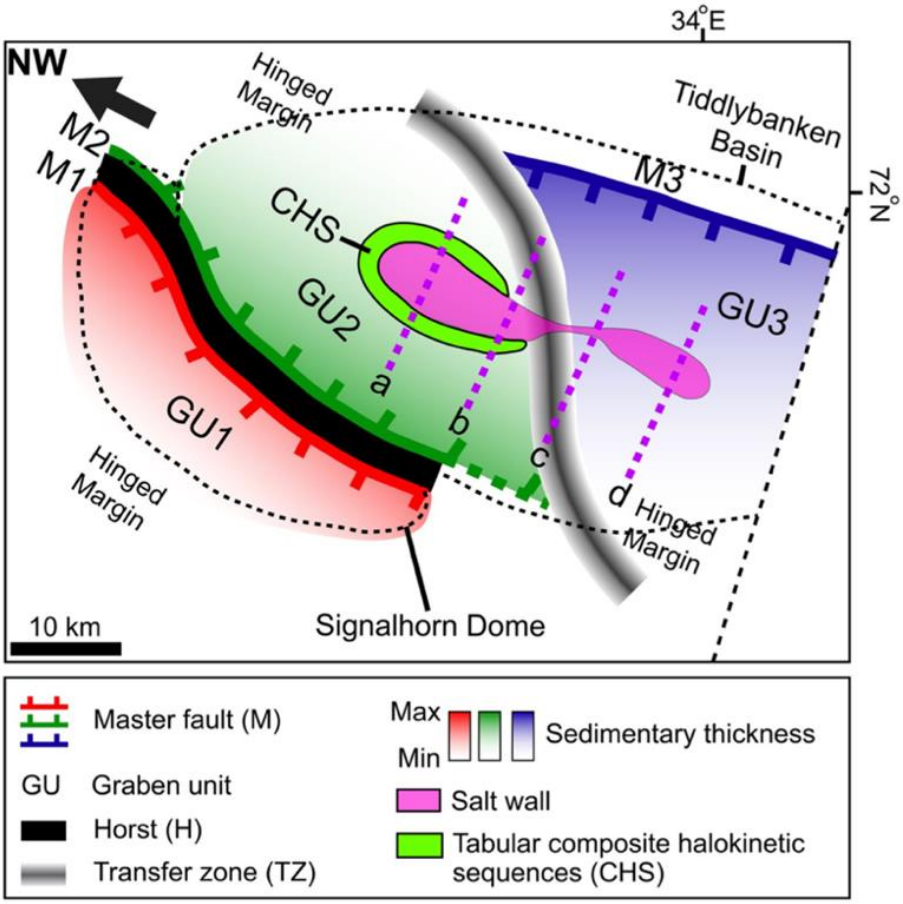

Figure 2.5: *Map illustrating the structural elements in the area. Half-grabens, horst, and transfer zone control the pre-evaporite geometries on the passive diapirism and reactivation (Hassaan et al., 2020b).*

Regionally, this crustal extensional event corresponds to the collapse of the Caledonides, which led to the development of a series of NE-SW half-grabens separated by structural highs, followed by regional sag basins covering significant parts of the current Barents Shelf (Figure 2.2) (Henriksen et al., 2011a). However, in the southeastern Norwegian Barents Sea, the NW-SE trending rift structures formed in a NE-SW oriented extensional regime are linked to widespread extensional tectonics in the Russian Barents Sea and the corresponding structures reflect an underlying Timanian basement grain (Hassaan et al., 2020a).

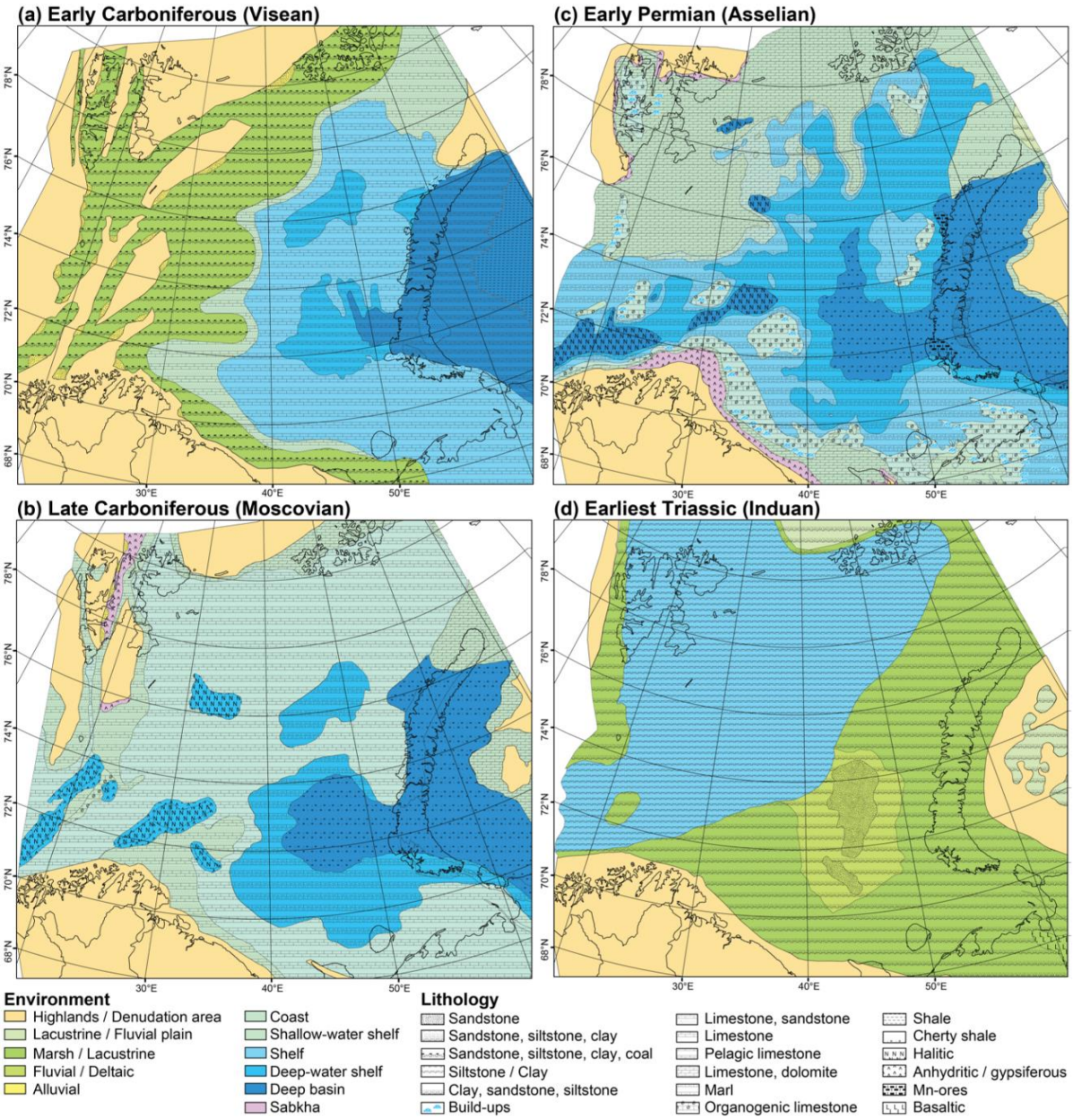

Figure 2.6: *Paleozoic paleogeography of the North Atlantic and Arctic regions (Hassaan, 2021) modified from (Smelror et al., 2009).*

The graben structures became the preferential sites for rifting and deposition of the syn-rift early Carboniferous Billefjorden Group (Figures 2.1 and 2.6a) (Bugge et al., 1995; Worsley, 2008). Subsequently, the Carboniferous-Permian plate collision caused the Uralian Orogeny that induced uplift of the eastern Barents Sea (Faleide et al., 2008). This led to the distinct change in basin physiography in late Paleozoic-early Triassic times. The Nordkapp Basin and the basins flanking the Novaya Zemlya were affected locally by post-Permian subsidence (Henriksen et al., 2011a).

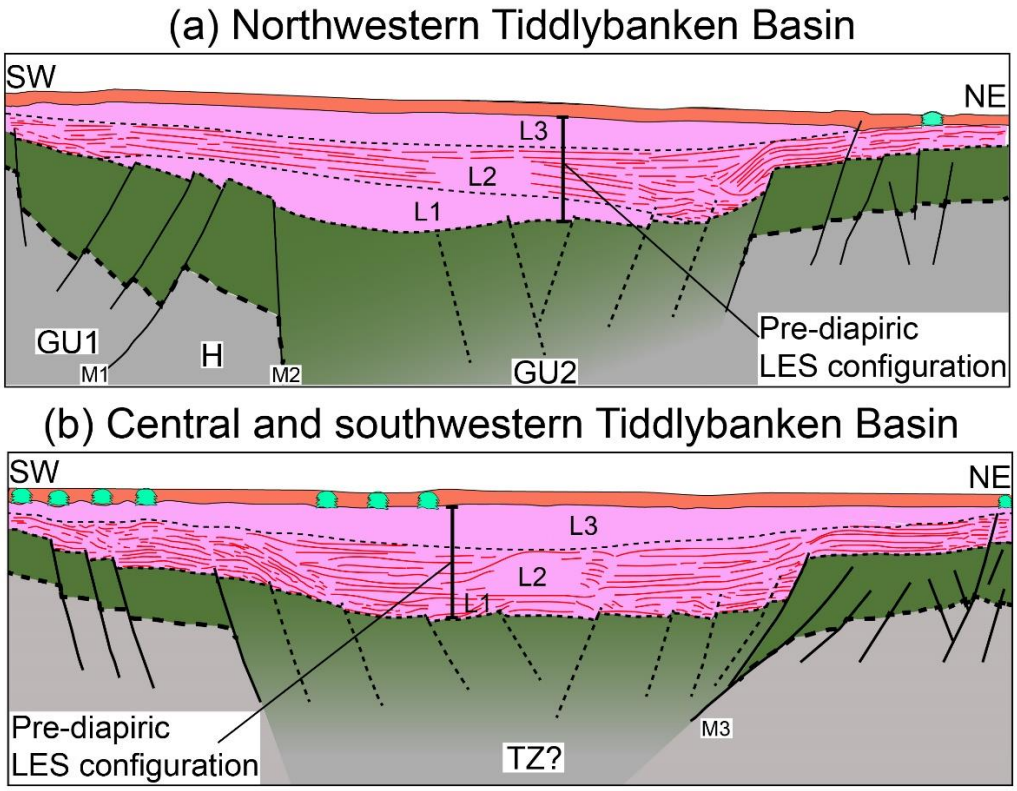

Figure 2.7: *Pre-diapiric layered evaporitic sequences configuration at the end of Permian in the different segments of the Tiddlybanken Basin (Hassaan, 2021).*

In the Tiddlybanken Basin, the elevation of the transfer zone affected the deposition of the deepest evaporitic layer (Hassaan et al., 2020b). The transfer zone acted as a barrier to flow in the area, resulting in two depocentres, the northwestern and southeastern (Figure 2.5). Halite-rich evaporite layers were deposited in the northwestern part of the salt wall and below the Signalhorn Dome (Figure 2.7a). In contrast, in the southeastern part of the salt wall, mixed-layer non-mobile evaporites were accumulated (Figure 2.7b).

Further west, the Hammerfest Basin created an additional post-Permian depocenter, divided by major faults from the Loppa High and Finnmark Platform (Henriksen et al., 2011a). The Nordkapp and Tiddlybanken basins are separated by the Finnmark Platform, where the basinal orientation axes are almost 90 degrees from each other (Figure 1b). The characteristic feature of both basins is the deposition of large quantities of evaporites during the Pennsylvanian to early Permian and the development of complex salt structures (Hassaan et al., 2020b; Henriksen et al., 2011a; Rojo et al., 2019; Rowan & Lindsø, 2017). Carbonates were deposited on a broad shelf during Bashkirian to Artinskian/Early Kungurian times (Figures 2.3 and 2.6b). This was followed by the Gzelian-Asselian/Sakmarian deposition of basinal evaporites and the

growth of marginal carbonate build-ups (Gudlaugsson et al., 1998; Smelror et al., 2009). By the time Sakmarian-Artinskian was over, a shallow-water carbonate platform was established on a regional scale. The clastic deposition dominated the region during the late-early Permian. During Late Carboniferous, the climate changed from humid tropical to sub-tropical and arid (Henriksen et al., 2011a). Later, the western part of the Barents Shelf was transgressed, causing warm water conditions throughout the Barents-Pechora shelf (Smelror et al., 2009).

2.3.2 Mesozoic

The early-late Triassic successions record a period of relatively stable tectonics and widespread subsidence in the Barents Sea area except for local activities (Glørstad-Clark et al., 2010; Henriksen et al., 2011a; Klausen et al., 2015). Accommodation was created due to subsidence, and large amounts of Triassic clastic sediments were deposited during a short period sourced from the Uralides and Fennoscandia (Figures 2.6d and 2.8a) (Bjorlykke, 2010; Faleide et al., 2010; Glørstad-Clark et al., 2010; Klausen et al., 2015; Riis et al., 2008).

Palynological evidence is used to evaluate the paleoclimate during the Early Triassic (late Smithian) to Late Triassic (Rhaetian) of the Barents Sea (Hochuli et al., 2010). The Triassic period was an extreme "hot-house," with ice-free polar areas and flora associated with warm temperatures. A humid climate with increased rainfall and more prolonged precipitation episodes was assumed in the Ladinian to Early Carnian time. Generally, warm and humid conditions continued throughout the Late Carnian to Norian times, in contrast to the drier conditions to the south (Ryseth et al., 2003). Furthermore, a more humid climate was established during the transition from Triassic to Jurassic.

The thick deltaic wedges developing during the early Triassic from the southeast (Figure 2.6d) resulted in the salt moving laterally and upwards through the sedimentary successions. These salt movements occurred in several phases during the Triassic and Paleogene (Dengo et al., 1992; Rojo et al., 2019; Rowan & Lindsø, 2017). As a result, today's salt forms large, almost vertical salt diapirs into the Nordkapp and Tiddlybanken basins and smaller domes on the corresponding margins. The Tiddlybanken Basin formed due to the well-developed salt wall with a rim-syncline surrounding the salt structure (Hassaan et al., 2020b; Rowan & Lindsø,

2017). On the southwestern margin of the basin, a salt anticlinal was formed, the Signalhorn Dome. The depositional environment of an area dominated by salt structures gets heavily affected during the growth of the salt diapirs (Banham et al., 2013).

The middle Jurassic-early Cretaceous rifting corresponds to a significant structural-depositional re-arrangement of the Barents Sea marked by a major regional Base Cretaceous Unconformity (BCU) (Figure 2.8d, f) (Henriksen et al., 2011a). Regional extension and strike-slip movements in the Late Jurassic-earliest Cretaceous formed the Bjørnøya, Tromsø, and Harstad basins as prominent rift basins in the southwestern Barents Sea (Bjorlykke, 2010; Faleide et al., 2010; Faleide et al., 2008; Faleide et al., 1993). All structural elements formed due to the subsidence became buried by the lower Cretaceous shelf-platform sedimentary complex (Midtkandal et al., 2020). However, thinning of the lower Cretaceous above the salt diapirs has been attributed to continued salt supply from the source layers in the Nordkapp Basin (Koyi et al., 1993b; Rojo & Escalona, 2018).

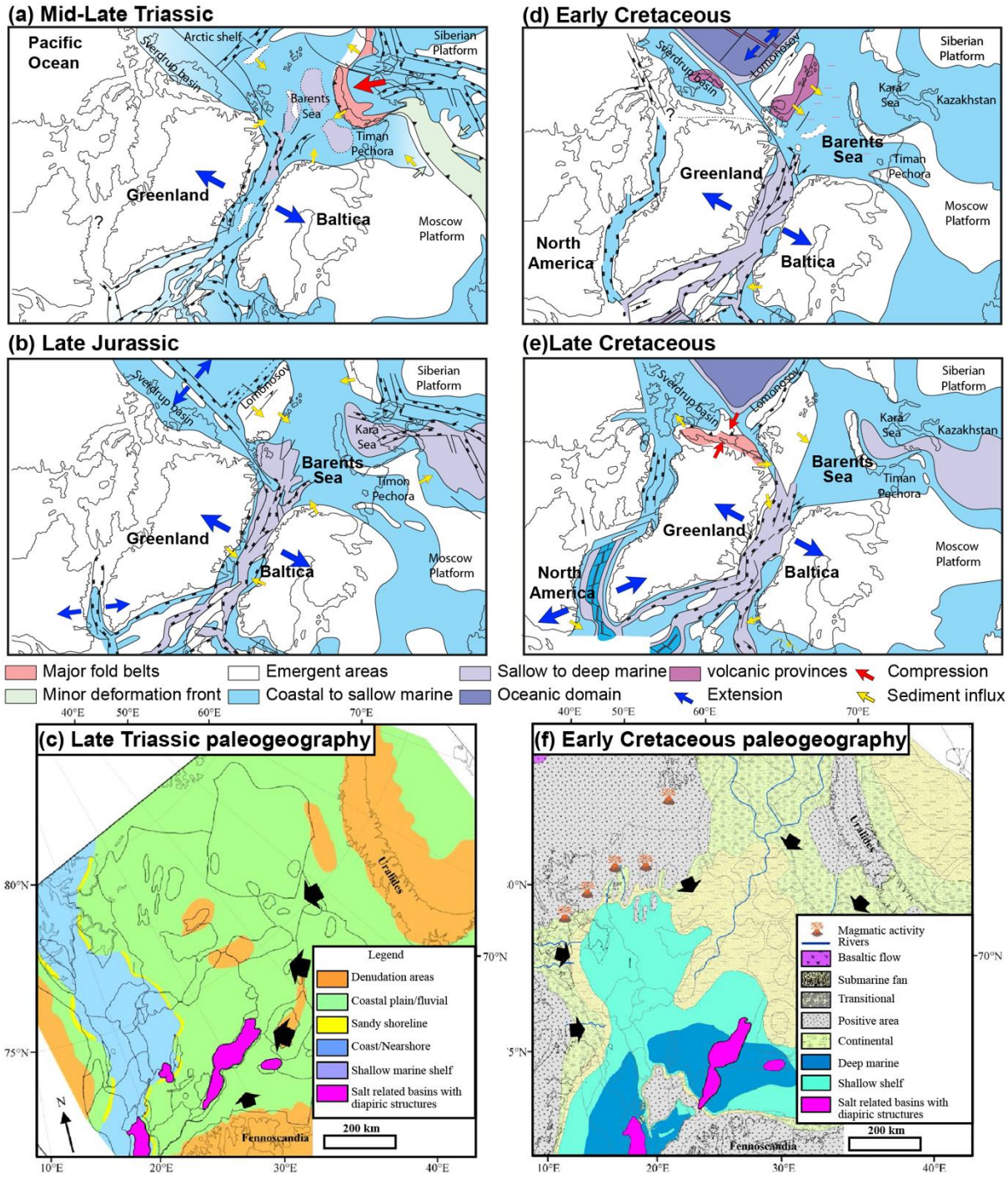

Figure 2.8: (a-b and d-e) *Mesozoic geodynamic evolution of the North Atlantic and Arctic regions (Hassaan, 2021) modified from (Smelror et al., 2009).* ***(c and f)*** *Late Triassic and Early Cretaceous paleography in the Barents Sea shelf edge clinoforms prograded towards northwest and south, respectively, passing across evaporite-influenced rift basins with ongoing halokinesis (Black arrows illustrate the progradation direction) (Hassaan, 2021) modified from (Henriksen et al., 2011a; Rojo et al., 2019).*

2.3.3 Cenozoic

A mega-shear system (De Geer Zone) formed narrow pull-apart basins at the western Barents Sea-Svalbard margin during the Late Cretaceous-Paleocene (Figure 2.9) (Faleide et al., 1993; Knutsen et al., 1997; Kristensen et al., 2018; Ryseth et al., 2003). During the Paleocene-Eocene transition, the opening of the Norwegian-Greenland Sea resulted from the tectonic stresses from the East (Eldholm et al., 2002; Faleide et al., 2018). In the Paleogene, the northwestern Barents Sea-Svalbard margin was affected by the Eurekan orogeny, while the south mainly experienced transtensional deformation. Major glaciations in the Pliocene-Pleistocene resulted in uplift and erosion in the entire Barents shelf (Figure 2.9c) (Baig et al., 2016; Henriksen et al., 2011b).

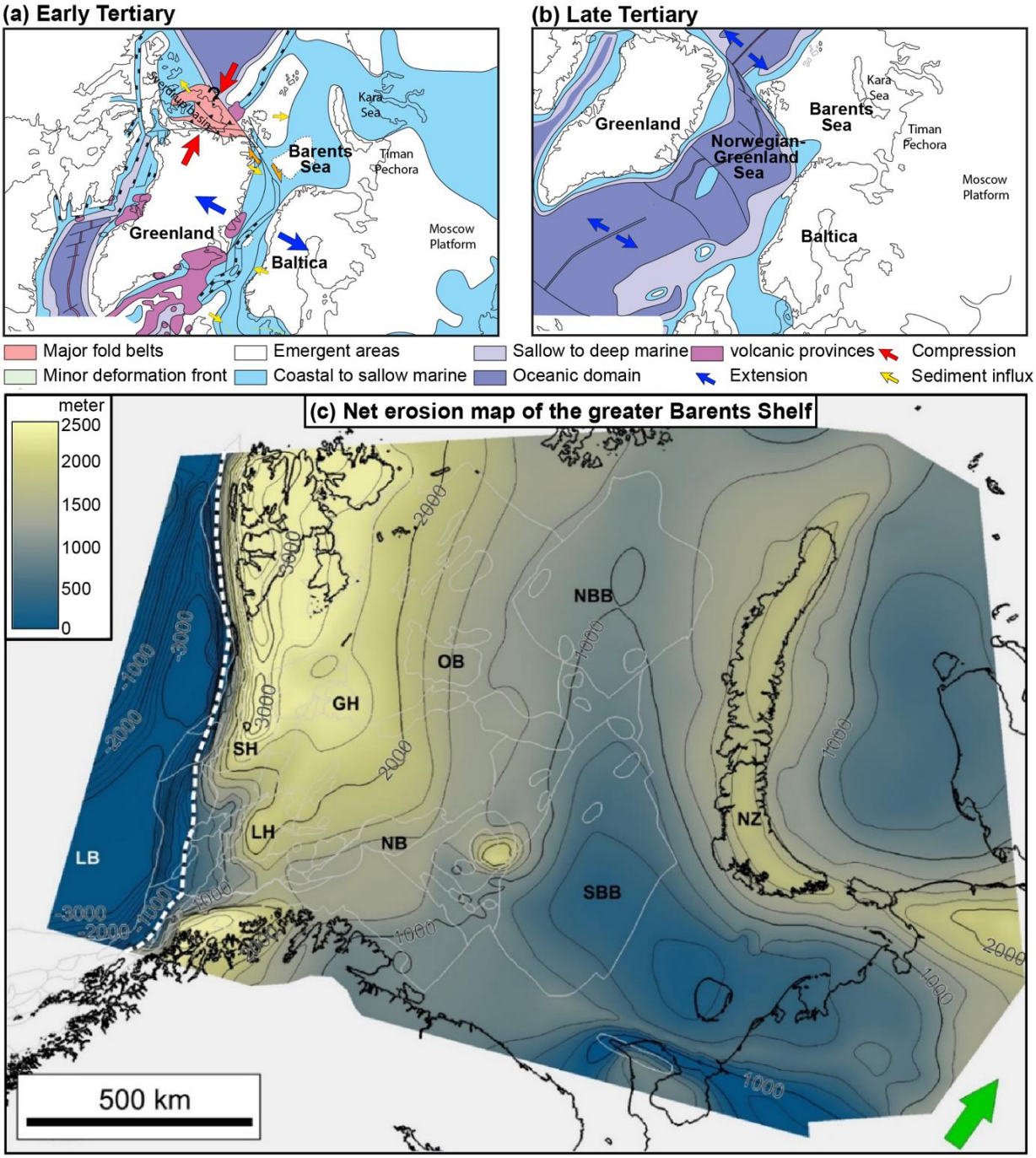

Figure 2.9: (a-b) *Tertiary geodynamic evolution of the North Atlantic and Arctic Regions (Hassaan, 2021) modified from (Smelror et al., 2009).* ***(c)*** *Compiled net erosion map for the greater Barents Shelf (Hassaan, 2021) modified from (Lasabuda et al., 2021). To the west, the contours within the map also show sedimentary thicknesses in the depositional areas. Note that the contours may also show higher net erosion than 2500 m (more than the optimum value shown in the color scale). Abbreviations used: BP: Bjarmeland Platform; GH: Gardarbanken High; LB: Lofoten Basin; LH: Loppa High; NB: Nordkapp Basin; NBB: North Barents Basin; NZ: Novaya Zemlya; OB: Olga Basin; SBB: South Barents Basin; SH: Stappen High.*

3 Theory

It is essential to understand the theoretical key concepts of salt and its properties before addressing the influence of salt on the structural and sedimentary basin development. In the Barents Sea, the Triassic-Jurassic interval predominantly consists of prograding and retrograding depositional sequences (Glørstad-Clark et al., 2010; Klausen et al., 2015). These successions consist of deep marine to fluvial deposits. The basin infill of the Triassic-Jurassic stratigraphic succession is controlled by fluvio-deltaic mechanisms and salt tectonics, contributing to the sedimentation patterns and accommodation.

3.1 Salt tectonics – Key concepts

Evaporites are deposited in constrained basins (Warren, 2016), where the inflowed water evaporites (Hudec et al., 2007). There are four main settings where evaporites are deposited: (1) cratonic basins, (2) syn-rift basins, (3) post-rift passive margins, and (4) continental collision zones and foreland basins. These basins tend to lie at roughly 30° latitude, where dry, cold, high-pressure air descends in Hadley circulation cells to create arid and semiarid areas. Salt tectonics is defined as deformation caused by the flow of salt and may involve contraction and extension (Warren, 2016). Salt is a common feature in many sedimentary basins and is a part of the stratigraphic column. Rock salt consists mainly of halite, which can flow (Figure 3.1)(Hudec & Jackson, 2007). It depends on what stages of evaporation the area has undergone. Properties of salt differ from siliciclastic rocks, and it has a much lower density (Figure 3.1) (Fossen, 2016).

Salt flow triggering mechanisms include differential loading, tectonic forces, gravitation, thermal gradient, or buoyancy. Differential loading involves lateral variations of the overlying stratigraphic strata density, weight, and thickness (Hudec & Jackson, 2007; Jackson et al., 1995). Buoyancy was believed to be a first-order triggering mechanism for a long time. Now it is considered a second-order mechanism. As the salt is deposited, the surrounding sediments have a lower density than the salt, but after ca. 2 km, the surrounding sediments become denser and more compact than the salt (Fossen, 2016).

Property	Halite	Anhydrite/Gypsum
Density	2100 – 2200 kg/m^3	2980 kg/m^3
Seismic velocity	4500 m/s	6500 m/s

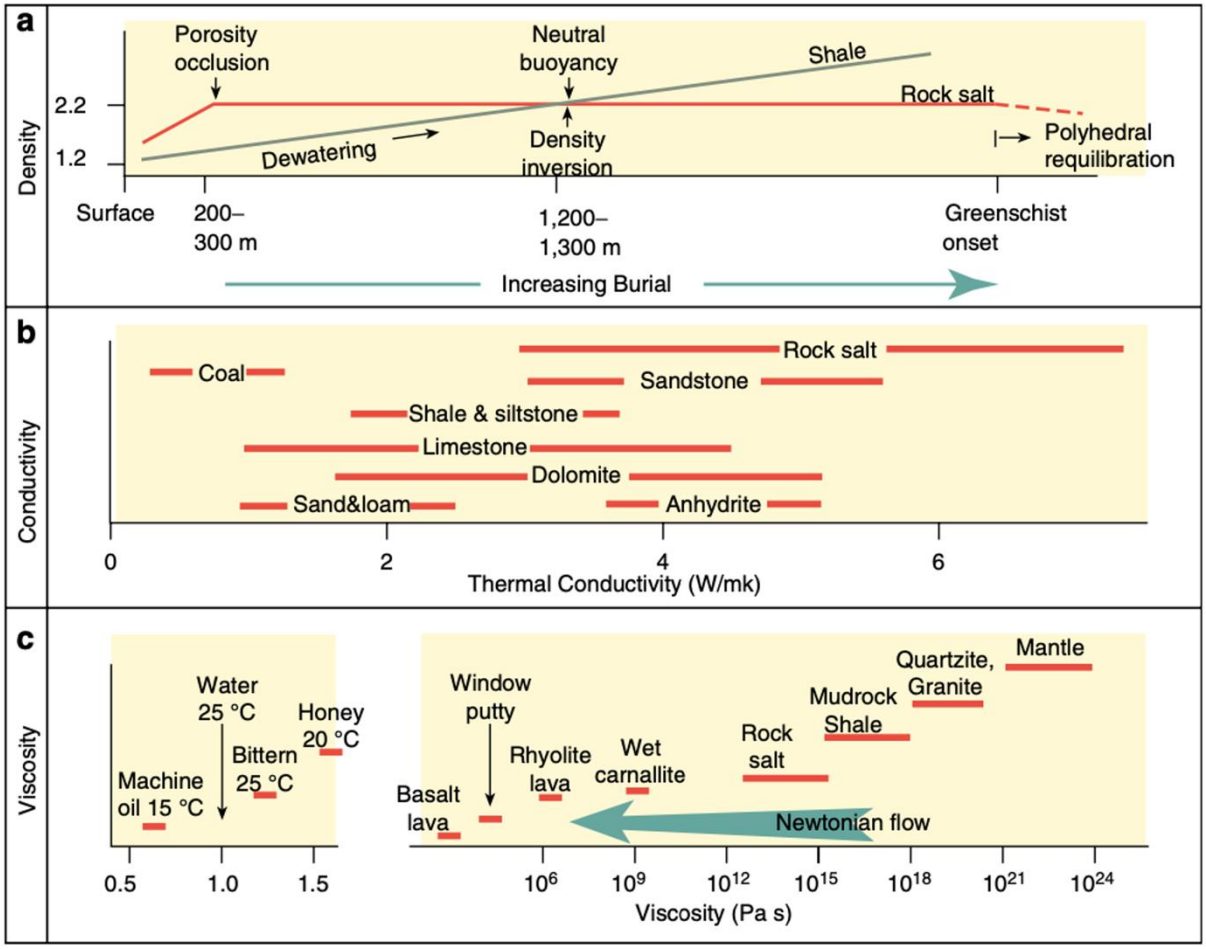

Figure 3.1: *Physical properties of rock salt compared to other lithologies (Warren, 2016).* ***(a)*** *Density changes with burial.* ***(b)*** *Thermal conductivity.* ***(c)*** *Viscosity.*

Salt flows like a fluid (geologic time scale), causing deformations in the overlying strata. Various geometries and structures form due to the movement of the salt (Figure 3.2). Diapirism is often related to tectonic events that either force or give deformation and faulting possibilities. Highs and lows are often formed, creating syn-halokinetic accommodation and thickening and thinning sequences in the basins (Figure 3.4) (Hudec & Jackson, 2007). Gravitational gliding and gravitational spreading are two models presented to cause salt movement. Gravity gliding is mainly driven by marginal tilt. Extension occurs in the upper-slope area; meanwhile, in the lower-slope, contractional structures form.

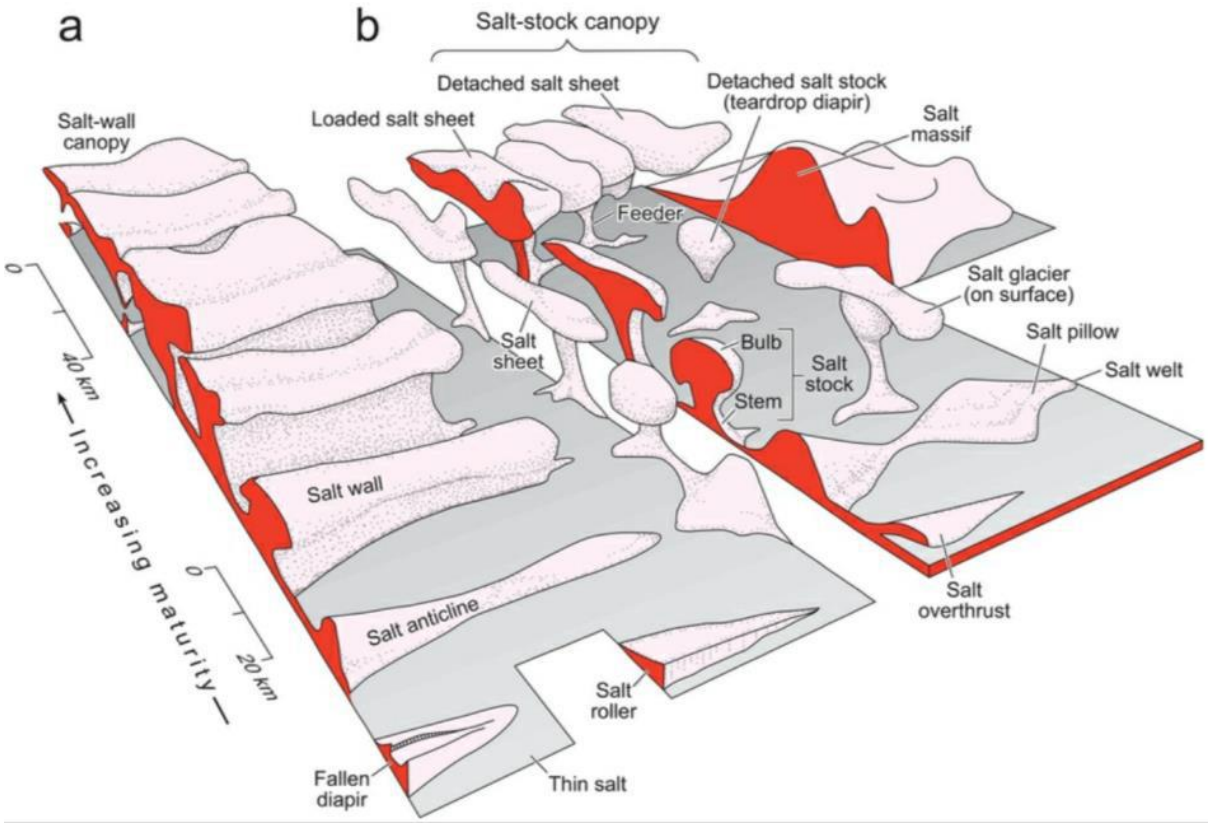

Figure 3.2: *Names of salt structures are derived from cross-sectional shape and map geometry where diverse salt geometries hint about the evolution mechanisms (Jackson & Hudec, 2017).*

The extension migrates downdip, and contraction migrates up-dip, causing inversion structures. For example, gravity spreading is caused by sedimentary deposition from a prograding delta.

3.1.1 Diapir growth

There are three types of diapirism: Reactive, active, and passive (Figures 3.3 and 3.4) (Hudec & Jackson, 2007; Rowan et al., 2021). Reactive diapirism is a response to regional extension that creates space and weakens the overburden, making it easier for the salt to rise towards the surface (Figure 3.3a). Either loading, contraction, or buoyancy cause active diapirism (Figure 3.3b). The salt rises after its deposition, resulting in penetration of its overburden. Passive diapirism occurs when the salt crest remains at or near the surface while sediments accumulate around the diapir (Figure 3.4) (Fossen, 2016; Hudec & Jackson, 2007).

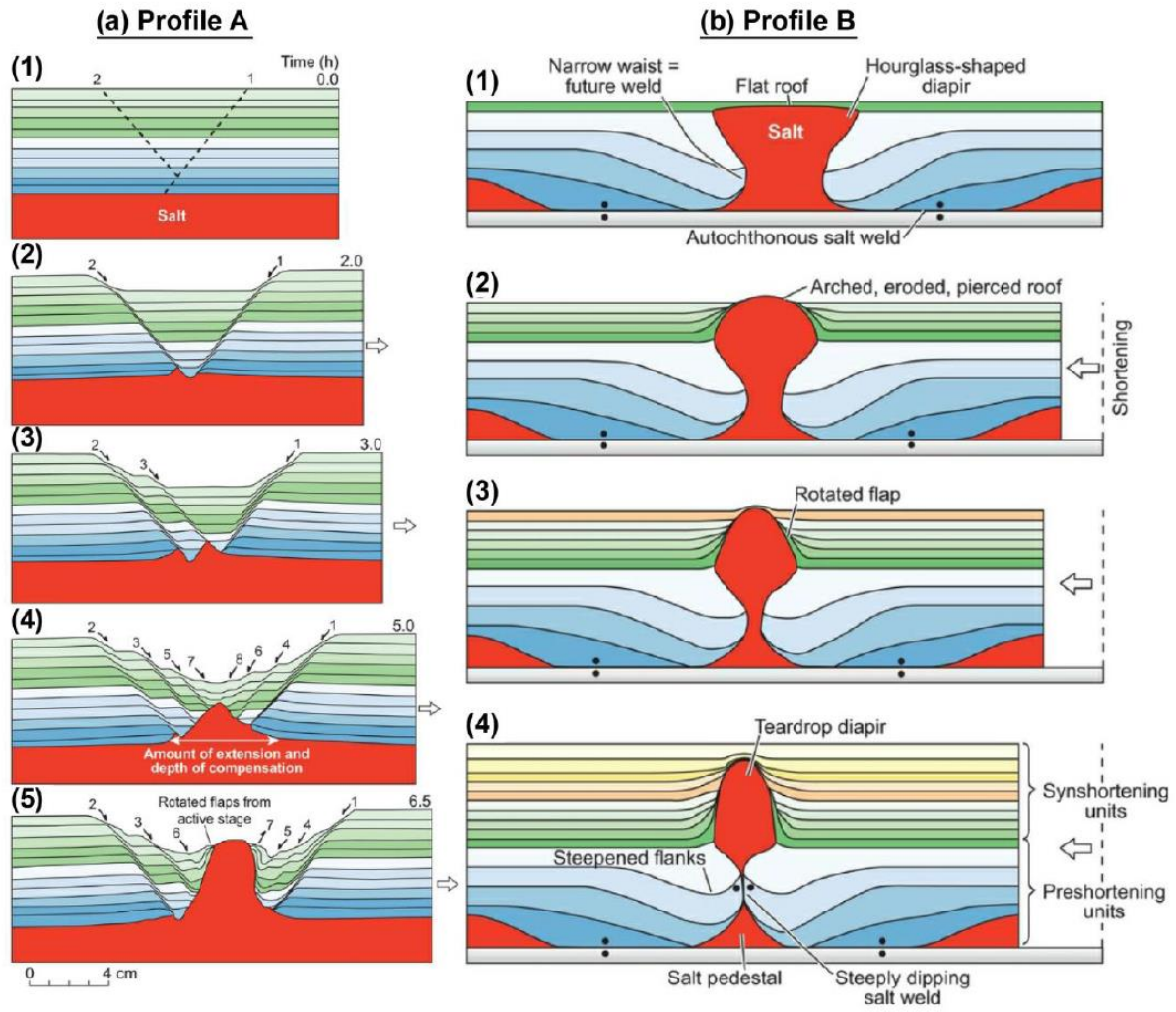

Figure 3.3: (a) *Profile A shows a reactive diapir rises because of thin-skinned regional extension. These cross-sections of an evolving reactive wall are from otherwise identical physical models extended by 0 cm, 2 cm, 3 cm, 5 cm, and 6.5 cm, respectively. All the overburden is prekinematic. In the final stage (5), active diapirism had begun. Faults are numbered in order of formation (modified from Jackson and Vendeville, 1994).* ***(b)*** *Profile B displays a rejuvenated diapir that is laterally squeezed, flanking strata steepen, the stem of the diapir narrows, and can eventually pinch-off as the bulb becomes taller and its roof arches. Passive diapirs stop growing halokinetically after exhausting their source layers. Still, they can be rejuvenated by lateral shortening as salt is displaced upward by the converging sides of the diapir (Hassaan, 2021) modified from (Jackson and Hudec, 2017).*

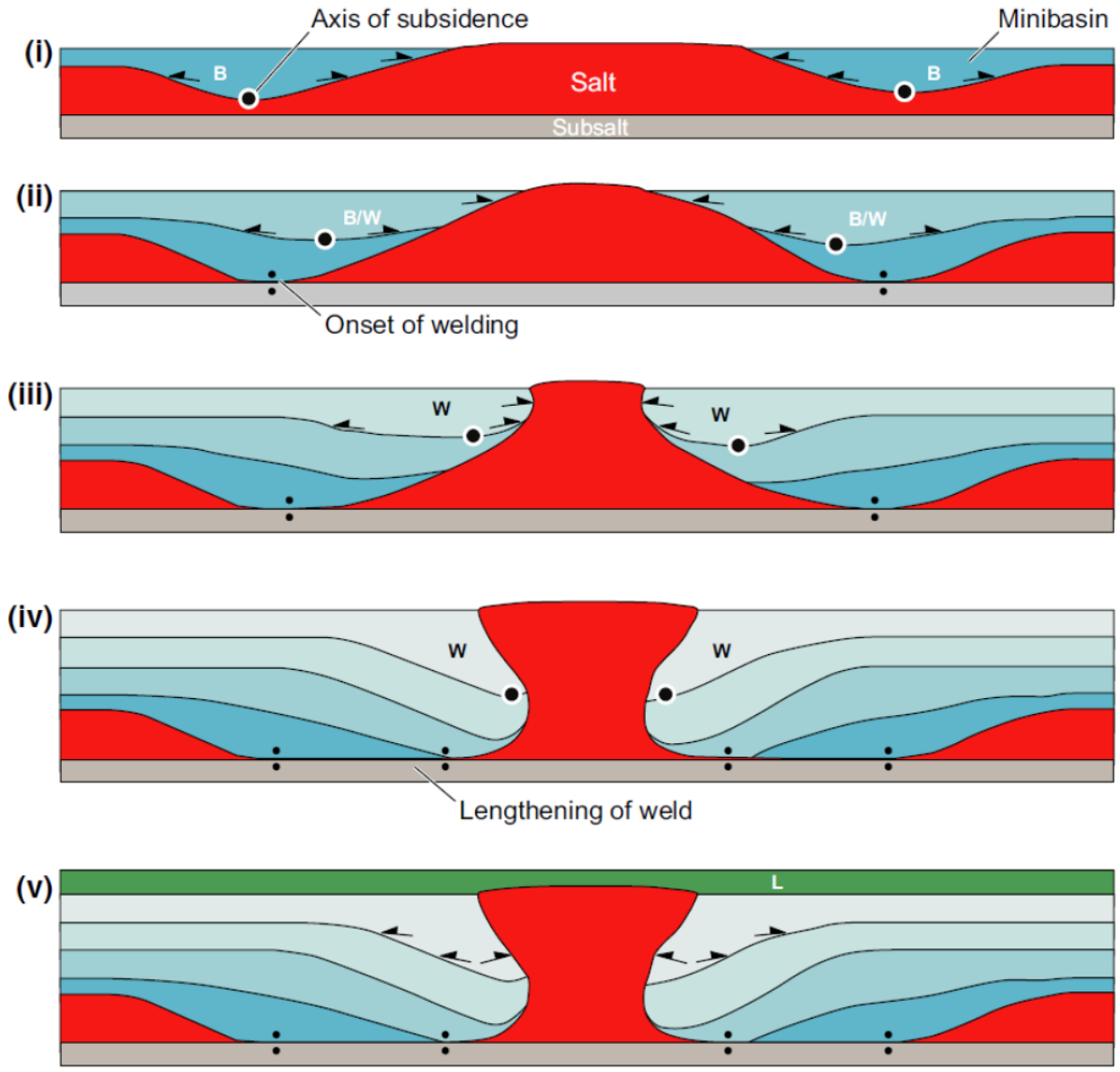

Figure 3.4: *Passive diapirism with the development of bowl (B), wedge (W), and layer (L) stratigraphic/seismic–stratigraphic units during minibasin subsidence and passive diapirism (terminology after Rowan and Weimer, 1998). Note progressive shifts in the axis of subsidence associated with welding and the transition from a primary* ***(stages I and II)*** *to secondary* ***(stages III-IV)*** *peripheral sink (sensu Trusheim, 1960).*

Geometry and shape of the diapir and surrounding strata are determined by the relationship between the sedimentation rate (A) and salt supply rate (R) (Figure 3.5) (Fossen, 2016; Hudec & Jackson, 2007). The sediment and salt supply (along with many other factors) will vary in time and space along a diapir, therefore different stacking geometry (Figure 3.6a). For instance, investigating these types of stacking patterns will contribute to locating channel routing in a minibasin.

Halokinetic sequences are bounded by unconformities and vary through time and space along a diapir (Giles et al., 2012). Once many HS are stacked on top of each other, it is called

Composite Halokinetic Sequence (CHS) (Figure 3.6b). If the diapir rise rate is greater than the sediment accumulation (R > A), hook HS will form, resulting in a tabular CHS as they stack each other (Figure 3.5a and Figure 3.6). Contrarywise this, wedge HS and tapered CHS sequences form when the diapir rise rate does not manage to keep up with the sediment accumulation (R < A) (Figure 3.5c, Figure 3.6). HS and angular unconformities are evidence of salt movement (halokinesis) and, as a result, the revealment of salt diapirism. Seismic reflection patterns like truncations, pinch-outs, offlaps, and onlaps near a salt structure may indicate salt movement (Giles et al., 2002; Hudec & Jackson, 2007).

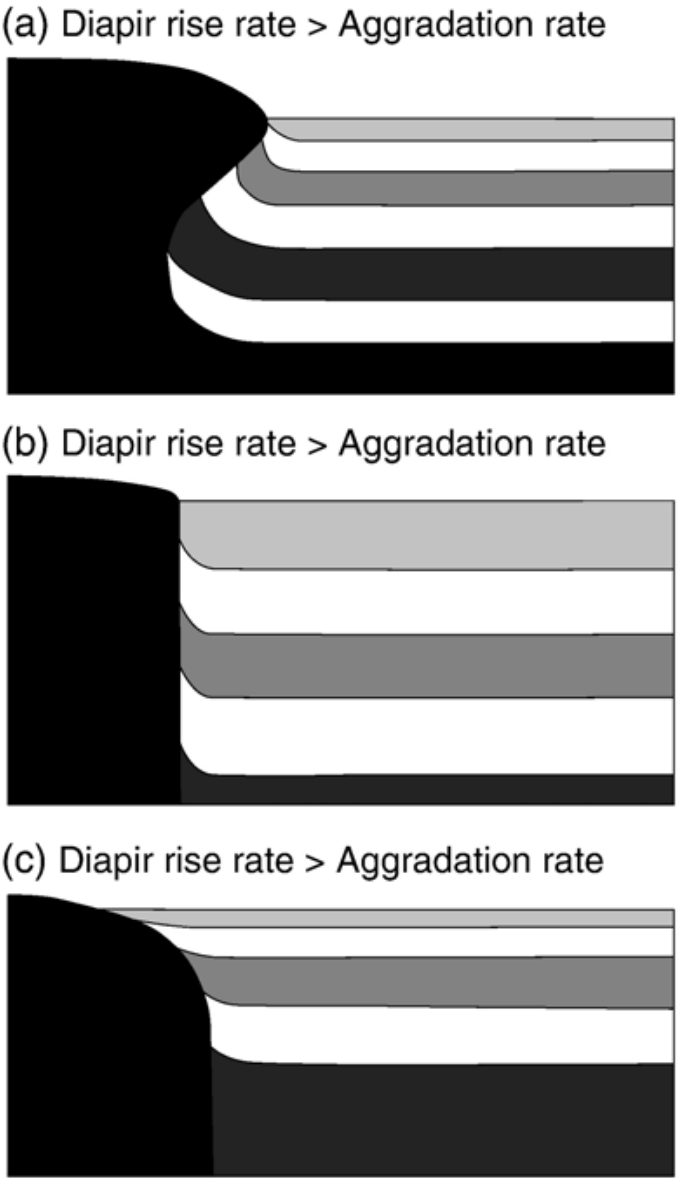

Figure 3.5: *Comparison of passive diapirs (cross-sectional view) with different aggradation/diapir rise rate relationship (Hudec & Jackson, 2007).* ***(a)*** *Diapir rise rate exceeds aggradation rate, causing a widening upward of the diapir shape.* ***(b)*** *Diapir rise rate is equal to aggradation rate, resulting in vertical diapir walls.* ***(c)*** *Aggradation rate outpaces the diapir rise rate, forming a narrowing upward diapir shape.*

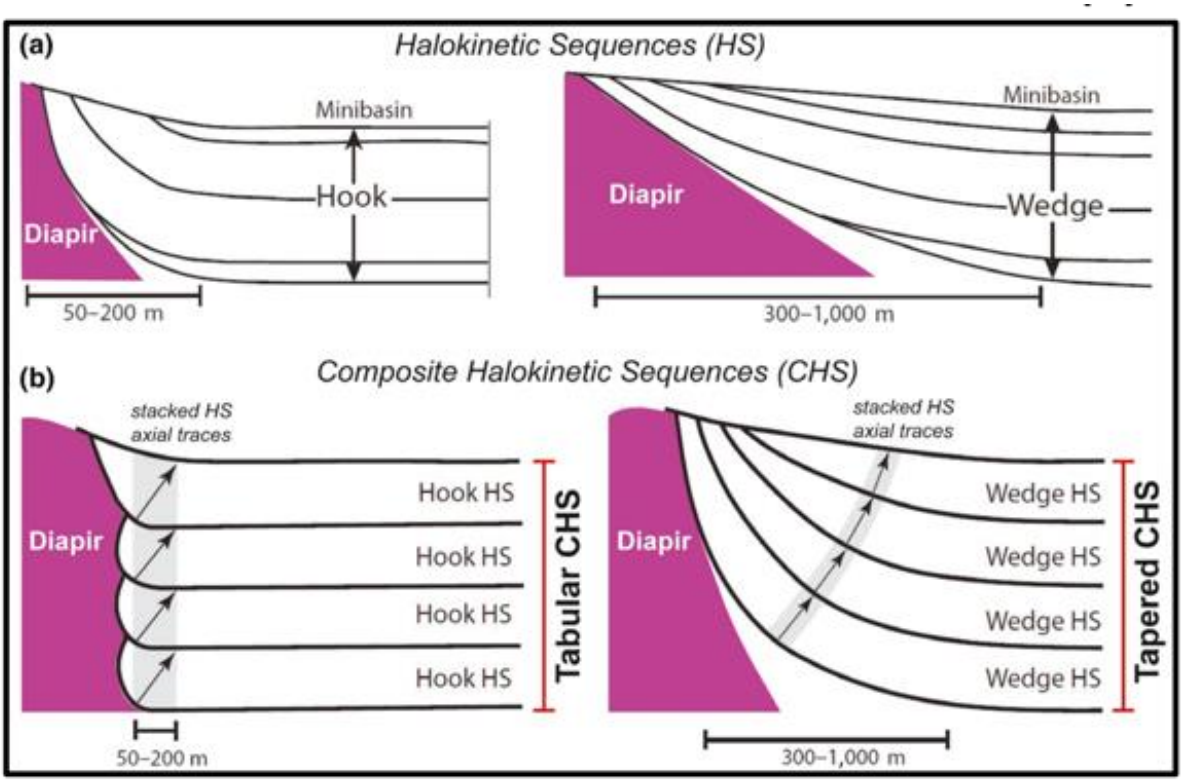

Figure 3.6: *End-members of halokinetic- and composite halokinetic sequences along the flanks of the salt structures (Giles & Rowan, 2012).*

3.1.2 Salt-walled minibasins and sedimentary infill processes

Primarily, minibasins form by differential loading or tectonic events and are often referred to as rim-syncline, withdrawal basin, or minibasin (Figures 3.7 and 3.8) (Peel, 2014). Minibasins are relatively small, typically 1-10 km across. Subsidence of the minibasin, and the movement of salt accommodating it, is driven by net lowering of the center of mass as denser sediments move downwards and less dense salt towards the surface (Figure 3.8). Minibasins formed by salt withdrawal are accommodated by the salt movement out from the subsiding area into, most probably, a rising area. Diapirs form adjacent to the minibasins, which may have different geometries and forms, bowls, or wedges (Figure 3.4). Minibasins are economically important due to their significant hydrocarbon recourses. Subsidence of the minibasin is controlled by the weight of the accumulating sediments, which holds most of the economic resource in the form of hydrocarbons.

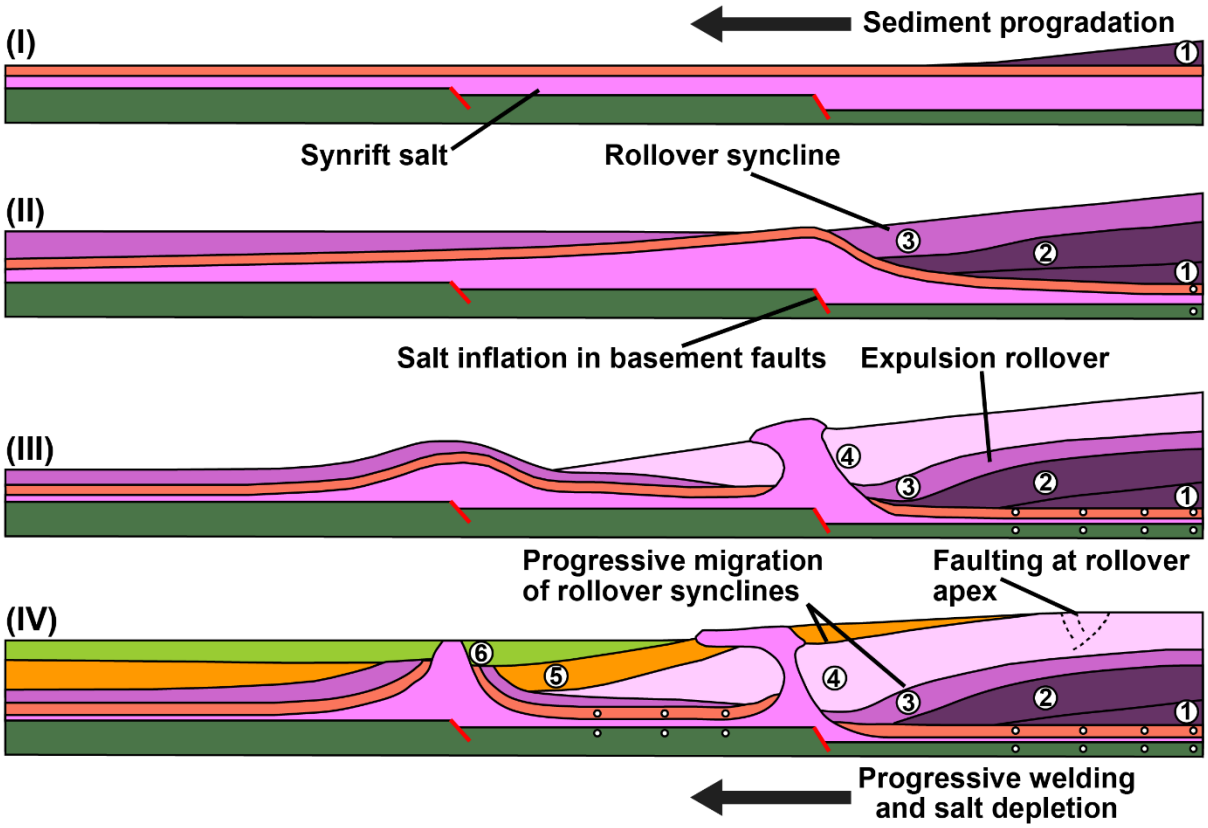

Figure 3.7: *Progradational sediment loading of a salt-influenced rift basin (Hassaan, 2021)*

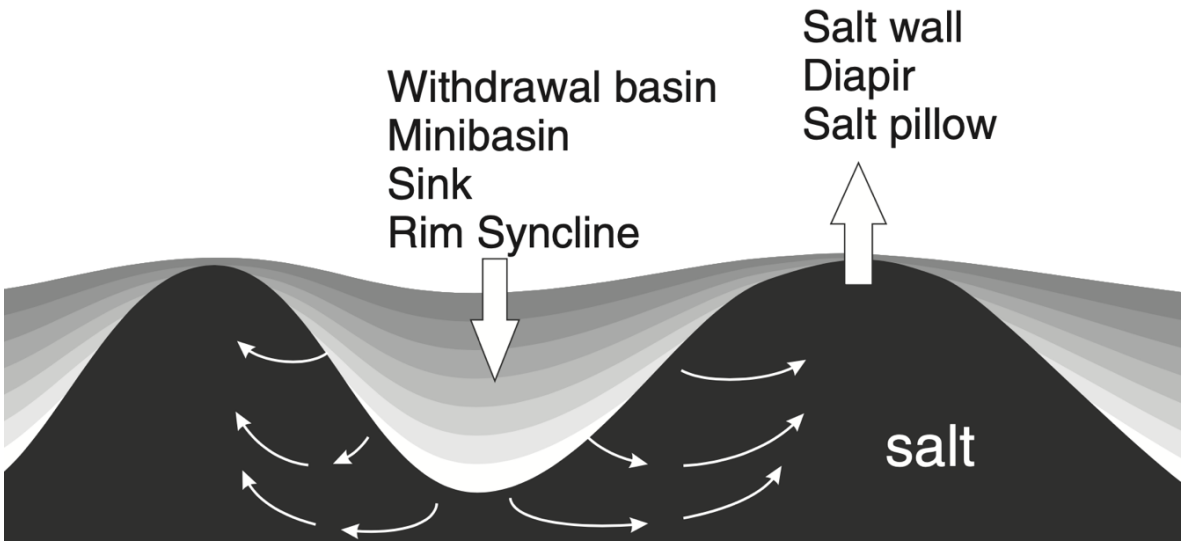

Figure 3.8: *Basic elements of a minibasin illustration area of salt depletion and sediment accumulation (Peel, 2014).*

3.1.3 Controlling parameters in minibasins

Infill patterns of fluvial sedimentations are primarily controlled by temporal and spatial variations in the rate of subsidence that influence the generation of accommodation, while the rate and style of sediment supply influence how the space is filled (Figures 3.5, 3.8, and 3.10) (Banham & Mountney, 2013). Secondary factors are basement geometry, salt thickness and composition, climate, and the inherited drainage direction. In a passive continental margin, several variables are essential for the resulting basin geometry (Figure 3.7). Surface and basal slope, extension, contraction, lateral translation over ramps, progradation of the shelf, and formation of the incised valley on the shelf are the different variables dealt with (Figure 3.9).

3.1.4 Fluvial and salt interaction

The interplay between sediment supply and rate of accommodation caused by halokinesis plays an essential role in controlling the basin infill (Figures 3.9 and 3.10). A salt-walled minibasin has a complex evolution. Fluvial strata within and between the minibasins are influenced by several factors that control the sediment distribution. Rim-synclines develop as the salt wall grows and subsidence occurs (Banham & Mountney, 2013). These factors will directly impact the fluvial drainage system (Figure 3.9). Accumulation of sediments within the minibasin increases the differential loading and enhances salt withdrawal. As more salt moves into the growing diapir, more accommodation is created. Sediment routing of the transportation system is controlled by the topographic highs and lows created by the movement of salt. As the deposition continues, the differential compaction will cause the salt to move. Sedimentation rate, salt supply rate, and subsidence (accommodation) are the controlling factors that decide fluvial routing within a minibasin (Figure 3.10) (Banham & Mountney, 2013). Infill architecture is determined by correlating the rate of subsidence and sedimentation, which either result in underfilled-, overfilled-or typically filled basins.

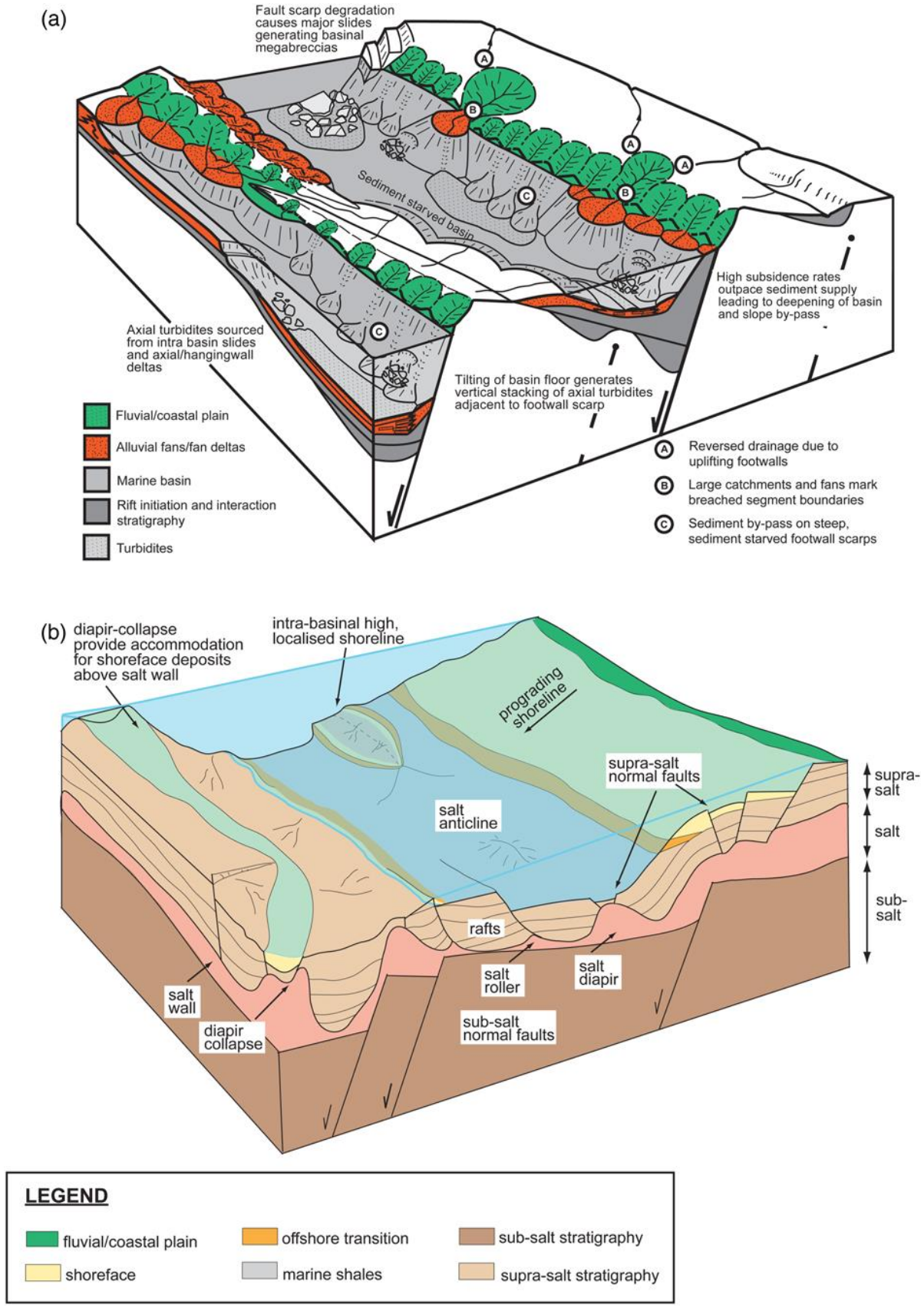

Figure 3.9: *Schematic block diagrams comparing the structural styles and coastal plain to marine depositional environments for* ***(a)*** *a generic, salt-free rift basin and* ***(b)*** *the salt-influenced Norwegian Central North Sea rift basin (Mannie et al., 2016).*

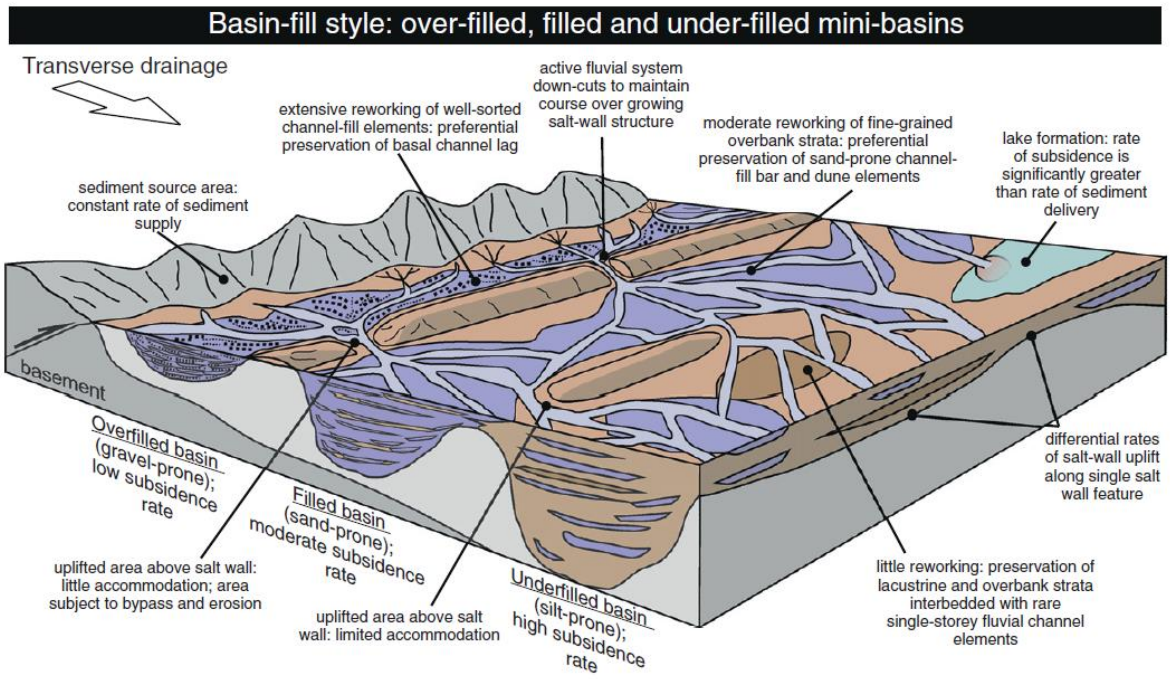

Figure 3.10: *Basin-fill style, demonstrating the development of over-filled, filled, and under-filled basin styles. The model depicts a system subject to a constant rate of sediment supply rate but for adjacent mini-basins that undertake variable rates of subsidence (Banham & Mountney 2013).*

4 Data and methods

4.1 Seismic data

Seismic reflection data give an image of the subsurface by measuring the time (ms) it takes for a seismic wave to propagate down to an interface and reflect up to the receiver (i.e., two-way-time; TWT). Acoustic impedance (AI) varies, affecting the strength of the seismic reflections. This is decided by the compressional wave velocity (v) and bulk rock density (ρ). Lithological variation within the subsurface reflects the acoustic impedance due to the density and velocity change as a function of depth and petrophysical properties (Brown, 2011). Seismic reflection data has extensively been applied in hydrocarbon exploration and can be acquired along a single line (2D seismic) or systematically over an area (3D seismic). 3D seismic data is, therefore, a good provider of seismic data volumes, which means that it is possible to create seismic lines with any orientation and horizontal sections.

The 3D seismic survey, ST14004, in the Tiddlybanken area is analyzed for this study (Table 4.1). WesternGeco AS acquired and processed the survey in 2014, and the quality is excellent due to the new broadband with a wide frequency range. The ST14004 survey covers ca. 5450 km^2 in the southeastern Norwegian Barens Sea, covering the blocks 7132/1-4 and 7132/10 over the structural elements Signalhorn Dome and Tiddlybanken Basin. Seismic 3D data, tied to well-logs, are used to map the studied interval across the Tiddlybanken Basin.

Understanding seismic survey polarity (2D and 3D) is essential to differentiate between several datasets. The Society of Exploration Geophysicists (SEG) has defined two polarity conventions, the normal and the reverse. A downward increase in acoustic impedance is displayed as a peak, while a downward decrease in acoustic impedance shows as a trough. These properties are defined as the normal polarity, while it is the opposite for the reverse. The general characteristics of the survey are SEG reverse polarity (European polarity/negative polarity) and zero-phase. In the seismic dataset of this study, a peak represents the seabed, meaning that the survey is consistent with normal polarity convention. Rotation of the zero-phase wavelet is observed in some cases.

Table 4.1: *Utilized seismic reflection database.*

Survey	3D/2D	Year	Acquisition Company/Authority	Recorded time (TWT, s)	Study area coverage (3D km²/2D km)	Location	Resolution
ST14004	3D	2014	Lundin Energy Norway (operator) and WesternGeco AS Norway (acquisition)	3.5	5450	Tiddlybanken Basin, Barents Sea	Excellent
NPD-BA-11	2D	2014	NPD/TGS	9	1935	Barents Sea	Good
OD1201	2D	2012	NPD	8.5	1536	Barents Sea	Good

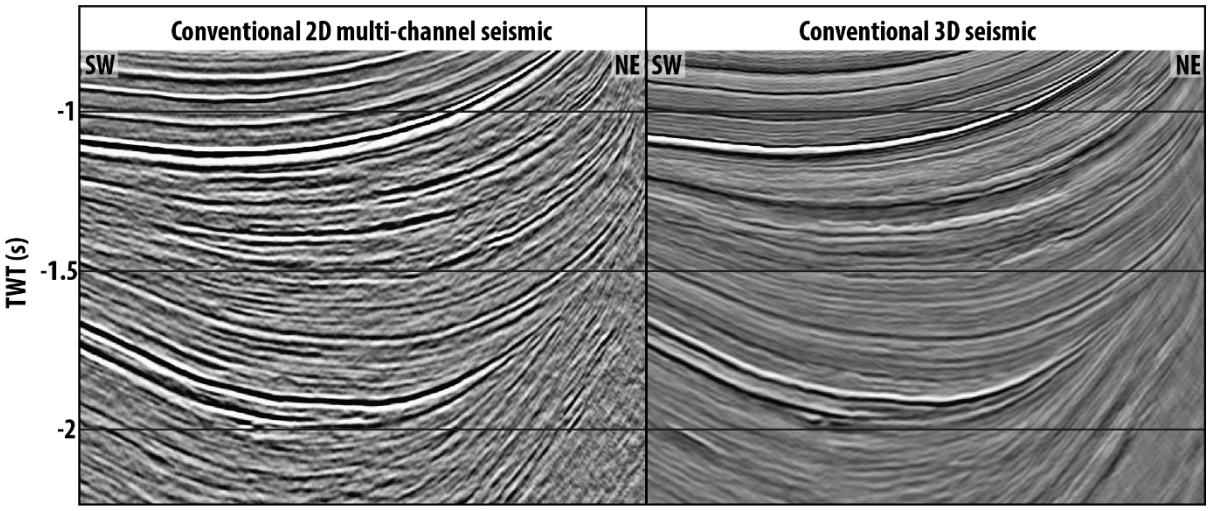

Figure 4.1: *Difference between conventional 2D multi-channel seismic and conventional 3D seismic data. 2D and 3D seismic data have more or less the exact vertical resolution, but 3D seismic data has a better horizontal resolution than 2D). Seismic data courtesy of Schlumberger Multiclient.*

The inline traces are trending NNE-SSW, and the crosslines are trending WNW-ESE. The inline and crossline interval is 12.5 m. The ST14004 survey is displayed in TWT (ms) that has a record down to -3500 ms TWT.

2D seismic data provides an image of the subsurface in one single line. This study analyzed two 2D seismic surveys, NPD-BA-11 and OD1201 (Table 4.1). The surveys extend beyond the 3D seismic survey and much deeper at depth. The seismic covers ca. 6600 km^2 with a total line length of ca. 2900 km along the Tiddlybanken Basin and Signalhorn Dome. NPD-BA-11 contains 25 good quality lines, and OD 1201 covers 18 good quality lines, with a line spacing of 4 km and 6 km, respectively. These 2D seismic lines allow for correlation between the 3D seismic survey. The 2D seismic lines are used to understand better the regional context of the area, both outside the 3D survey and within it for comparison (Figure 4.1). The 3D survey

includes only the northwestern part of Tiddlybanken Basin and terminates at the salt wall. The 2D seismic lines are crossing the salt wall and both related rim-synclines. The surveys include conventional 2D multichannel seismic (MCS) reflection profiles.

4.2 Well data

The available wells analyzed are located on the northwestern side of Tiddlybanken Basin, above the Signalhorn Dome, and were not publically available or included in previous studies. The two exploration wells 7132/2-1 and 7132/2-2 penetrate the succession in question (Table 4.2), and they are tied to the seismic data and logged. This provides essential input to the model for the basin infill of the area. Well 7132/2-2 penetrates the succession down to lower Permian time. It has been detected a shift in the GR-log toward higher values from 1480 ms upwards. Well 7132/2-1 is only penetrating succession down to Carnian time. Well tops and calibrated well-ties were provided by Lundin Energy Norway AS. The two wells were drilled by Equinor Energy AS in 2019, resulting in two dry wells. Figure 5.22 displays the two wells with the gamma-ray log to illustrate the variations within the interpreted horizons for this study.

Table 4.2 *Information about the two wells analyzed for this study.*

Well	**7132/2-1**	**7132/2-2**
Structural element	Signalhorn Dome	Signalhorn Dome
Drilling operator	Equinor Energy AS	Equinor Energy AS
Drilling permit	1740-L	1743-L
Drilling facility	West Hercules	West Hercules
Year	2019	2019
Content	Dry	Dry
Type	Exploration	Exploration
Oldest penetrated age	Late Triassic	Late Permian
Oldest penetrated formation	Snadd Fm.	Røye Fm.
Kelly bushing elevation (m)	31	31
Measuring depth (MD)	883	3528
NS UTM (m)/EW UTM (m)	7974242.39/480278.88	7971546.00/478721.28

4.3 Data limitations

Limitations and uncertainties are crucial matters when interpreting seismic data. Results from this study may be affected by either the data acquisitions stage (e.g., seismic resolution and spacing detector) or the data processing stage (e.g., signal-to-noise-ratio) (Sheriff, 1977). The resolution of seismic data is the minimum distance, either horizontally or vertically, between two features that can be distinguished individually. This is controlled by the wavelength (λ) of the seismic signal.

By measuring the distance between two peaks, the wavelength (λ) can be found. It is also possible to find the wavelength by dividing the seismic velocity (v) by the dominant frequency (f_d) of the seismic (Sheriff, 1977). Due to the increase of compaction with depth, the seismic velocity will increase; in addition, attenuation of higher frequencies causes a decrease in the dominant frequency. Therefore, the wavelength will increase with depth, causing a poorer resolution. Vertical resolution in conventional 3D seismic data usually ranges between 15-25 m and typically ranges between 1/4 and 1/8 of the dominant wavelength (λ_d). A simple process to estimate the dominant frequency (f_d) from seismic is to measure the time difference over, for example, ten peaks. For the ST14004 3D conventional seismic, the measurement of a cycle of ten peaks gave an average time of 20 ms and calculated to a dominant frequency of 50 Hz (Equation 4.1). Using an average velocity of 3000 m/s gave a dominant wavelength of 60 m (Equation 4.1). The vertical resolution of the ST14004 can then be estimated to range between 7.5-15 m (λ/8-λ/4), respectively.

$$f_d = \frac{1}{0.02} \approx 50\ Hz \rightarrow\ \lambda = \frac{v}{f_d} = \frac{3000\,\frac{m}{s}}{50\ Hz}\ \approx 60\ m$$

(4.1)

4.4 Method

This section of the chapter explains the methods and workflow applied in this study to achieve the key objectives; i) mobilization of salt in the Tiddlybanken Basin and development of the Signalhorn Dome, ii) triggering mechanism of salt mobilization, iii) impact of salt mobilization, and iv) impact of salt movements on sedimentological development and distribution of the Realgrunnen Subgroup within an isolated salt-influenced rift basin.

The workflow includes three main stages: preparation (literature study, software training, examination of data), seismic interpretation (detailed horizon interpretation, attribute maps), and minibasin analysis (structural evolution, halokinesis) (Figure 4.2). The seismic interpretation was carried out using mainly Petrel 2021© by Schlumberger and RGB Blends based on the frequency decomposition by Geoteric 2021©. Figures of thickness maps are all presented with the same color templates (e.g., "Hawaii" or "Batlow") created by Crameri et al. (2020) to reduce distortion effects and visual errors. Core material from well 7132/2-1 has been inspected, where the material comprised the Nordmela and Stø formations. The core was located at the Norwegian Petroleum Directorate in Stavanger and was acquired by Equinor Energy AS.

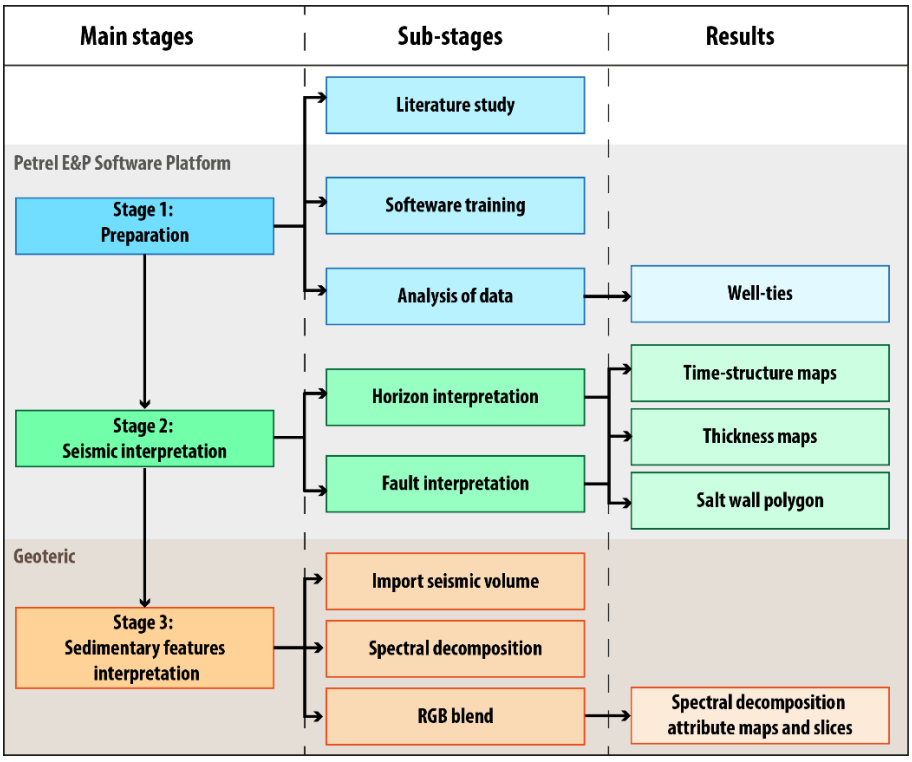

***Figure 4.2**: Flowchart illustrating the workflow applied in this study, consisting of three main stages divided into multiple-sub stages. Results are shown in the column to the right.*

4.4.1 Horizon mapping

Interpretation of seismic data allows studying the structural evolution, identifying depositional sequences, and describing the stratigraphic framework of the study area of interest. Detailed seismic data interpretation of the Tiddlybanken Basin and Signalhorn Dome is essential to create structure, thickness, and attribute maps to analyze basin infill patterns. The target for this study is the Middle Triassic-Lower Jurassic Realgrunnen Subgroup, which includes Fruholmen, Nordmela, Stø, and Tubåen formations (described in sections 5.2.4 and 5.2.5). To get a better understanding of the area, nine horizons have been interpreted (Table 4.3): Top Permian, Top Havert Formation, Top Kobbe Formation, Intra Snadd, Top Snadd Formation, Top Fruholmen Formation, Top Stø Formation, Top Fuglen Formation, and BCU.

A seven-stage operation has been done in this study (Figure 4.3). The first target was to interpret the key horizons within the surveys. The horizons were interpreted at least every 100 inline and crossline, creating a rough grid (Figure 4.3b). Areas of higher complexity, near the salt wall or faults, were interpreted with a decreased inline and crossline interval. Some packages of reflections thin and merge into one reflection. For example, the Top Stø Formation on top of the Signalhorn Dome is interpreted as the same reflector as the Top Fuglen Formation.

Flattening the interpreted horizon is a helpful tool when dealing with complex areas in the seismic data. The seismic will then vertically shift to a horizontal datum, which then characterizes the structural geometry at the time of deposition. The horizons were first interpreted on the 3D seismic data, using the well tops information. When the 3D seismic data gridding was complete, 2D seismic lines were interpreted based on the interpreted horizons.

A surface framework was established when the interpretation of inlines and crosslines created an excellent grid. 3D autotracking of this framework filled in the un-interpreted areas and created a continuous surface (Figure 4.3c). Signs of error from the auto-tracked interpretations were revised and interpreted with a decreased line spacing to create a more valid geological interpretation. Time-structure maps were created when the autotracked surface was of satisfactory quality and geological validity (Figure 4.3d). The time-structure maps were made with a grid increment of 200 x 200.

Table 4.3: *List of horizons interpreted within the ST14004 3D seismic volume in this study.*

Seismic horizon	Reflector pick (3D)	Reflector quality	Comments on upper boundary character
Top Hekkingen Fm.	Trough	Very strong, continuous	Base Cretaceous Unconformity.
Top Fuglen Fm.	Peak	Very strong, continuous	The reflector is representing a Kimmeridgian unconformity. Downward increase in acoustic impedance.
Top Stø Fm.	Trough	Medium strong, disrupted	Upward transition from a sandstone-rich to a mudstone-rich unit.
Top Fruholmen Fm.	Peak	Strong, disrupted	Sharp decrease in gamma-ray response, from the mudston-rich upper Fruholmen Fm. to the sandstone-rich Nordmela Fm. Also, an unconformity.
Top Snadd Fm.	Trough	Strong, continuous	Increasing gamma-ray values from the upper Snadd Fm. to a mudstone-rich lower Fruholmen Fm.
Intra Snadd Fm.	Peak	Strong (very strong in basin), continuous	An unconformity represent the reflector. Upward decrease in acoustic impedance from mudstone-rich to a more sandstone-rich unit.
Top Kobbe Fm.	Trough	Weak, disrupted	Upward increase in acoustic impedance from the upper sandy unit in Kobbe Fm. to a mudstone-rich lower Snadd Fm.
Top Permian	Trough	Very strong, continuous	Erosional unconformity divides the Havert Fm. with the underlying Ørret Fm.

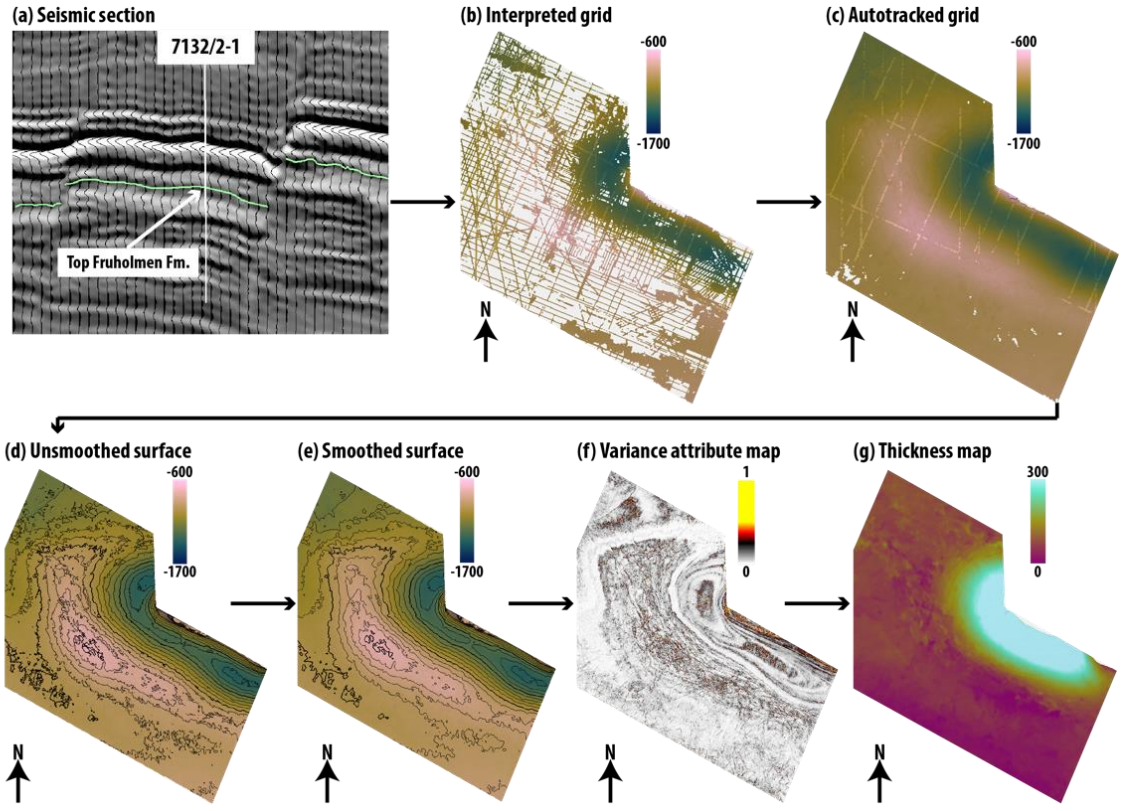

Figure 4.3: *Illustration of the seven stages of horizon interpretation. Top Fruholmen Fm. has been used as an example for this diagram.* ***(a)*** *Horizon interpretation correlated with well information,* ***(b)*** *interpreted grid,* ***(c)*** *autotracked grid,* ***(d)*** *time-structure map,* ***(e)*** *smoothed time-structure map,* ***(f)*** *variance attribute map, and* ***(g)*** *isochron map.*

The interpretation of horizons (Table 4.3) is tied to two exploration wells 7132/2-1 and 7132/2-2 located on top of the Signalhorn Dome (Figure 4.4). The top Permian is interpreted as a very strong trough, separating the salt with the unconformably overlying lower Triassic sandstones of the sequence S1. The layered evaporites with variable thickness and mobile character were deposited in the graben system that was later covered by early Permian carbonates. The Top Permian horizon has been interpreted throughout the whole study area. Middle Triassic Top Kobbe Formation is interpreted on a weaker trough, which is also present in most parts of the seismic data, except for near the salt wall due to erosion. A distinct unconformity within the rim-syncline is interpreted as a Base Carnian Unconformity. The seismic horizon is a strong internal peak within the sequence S4 (Snadd Formation), called Intra Snadd (described in section 5.2.3). The Intra Snadd reflector is more diffuse in the wells and the area outside of the basin. Top Snadd Formation is also represented by a diffuse trough in the well, turning into a strong reflector within the basin. Ladinian-early Norian deposits represent the sequence S4, which has various thicknesses towards the salt wall, described in section 5.2.3.

The Top Fruholmen Formation horizon coincides with the Upper Triassic unconformity. Top Fruholmen Formation is interpreted as a strong peak, with some disrupted areas on the dome and outside the basin where the sequence S5 (Fruholmen Formation) has most likely been eroded. The thickness within the basin is significant and will be described in section 5.2.4. The Jurassic formations Tubåen, Nordmela, and Stø, are interpreted as one medium-strong trough called Top Stø Formation. The reflector is strong within the basin but relatively diffuse and disrupted outside the basin. The thickness variation of sequence S6 is significant. All three formations are most likely present in the basin, but in the wells, only Nordmela and Stø formations can be interpreted as a considerably thin unit described in section 5.2.5.

Irregularities may result from complexities within the data or poor seismic quality. Therefore, a surface smoothing operation has been used with iterations no less than two (Figure 4.3e). If the smoothing operation is used too much, it may result in inaccuracies and should be used with caution. To ensure that the smoothing tool did not remove any critical geological structures or features, a revision of the seismic data was performed to ensure that the data was still valid geologically. The next stage of this procedure was to create a variance attribute cube (Figure 4.3f). The variance attribute cube is used to understand the different geological structures and was generated by the volume attribute function in the Petrel software.

The creation of time-thickness/isochron maps is the final step in this workflow (Figure 4.3g). They are made by measuring the vertical thickness between two time-structure maps. Analyzing thickness maps gives information on the variation in sedimentation accumulation, salt diapir growth, and depositional environment. These maps are essential for analyzing sedimentation rate versus salt supply rate, deposition of the different formations, and the related subsidence and salt evacuation.

4.4.2 Well-seismic-tie

Well data was used to establish detailed well-to-seismic ties to generate time-depth relationships analyzed with the available checkshot data to ensure correct horizon interpretation (Figure 4.4). It is essential to examine the data made for this analysis before performing horizon interpretation. Wellbores give a higher vertical resolution than seismic data but relatively little information laterally. Wellbores can be tied to seismic data, and it is in these areas, high certainty points are present. Well-ties were performed in Petrel using the two wells, 7132/2-1 and 7132/2-2, within the study area.

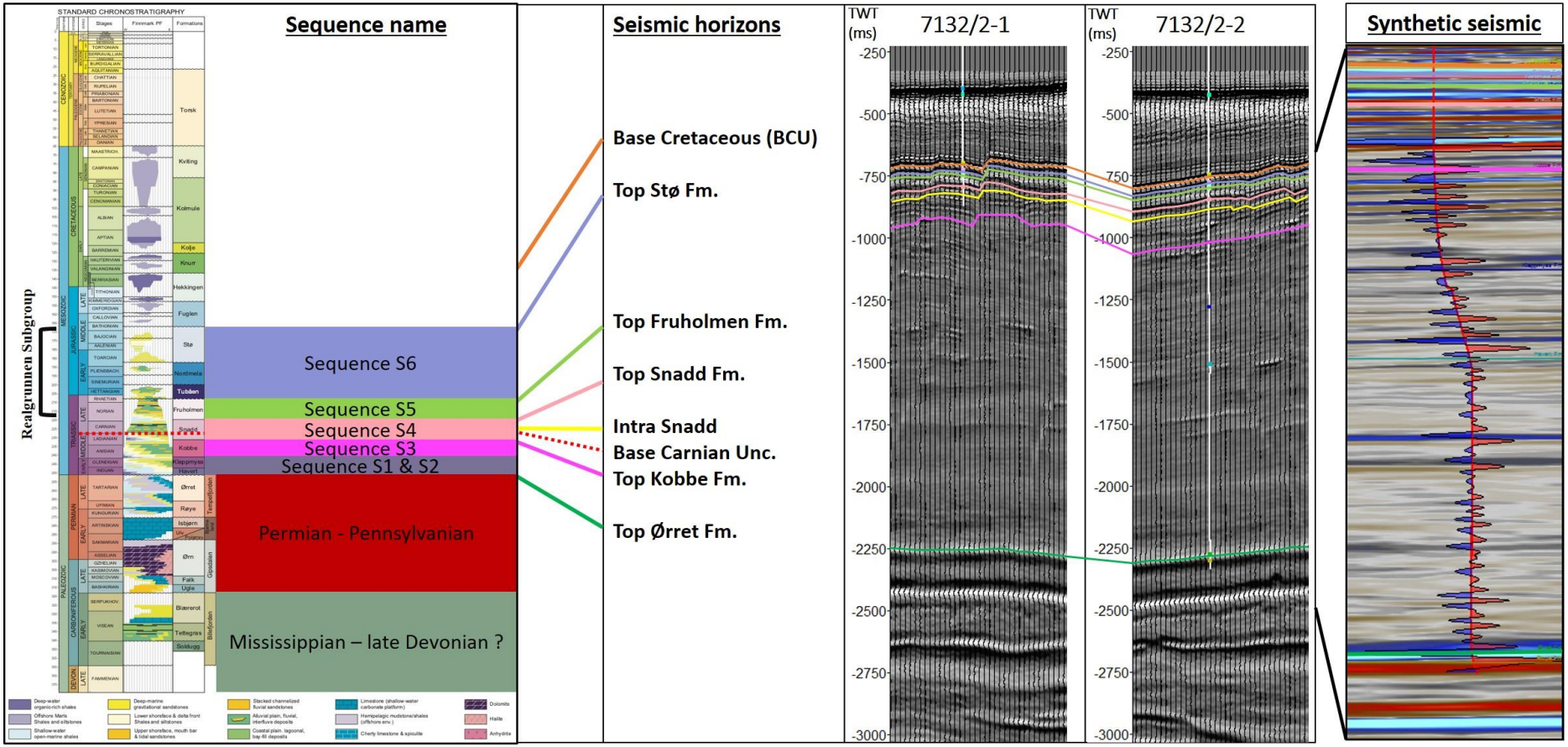

Figure 4.4: *Stratigraphic framework and key seismic horizons interpreted in the study area based on wells 7132/2-1 and 7132/2-2. Synthetic seismic from well 7132/2-2 is displayed to the furthest right, with the corresponding well tops.*

4.4.3 Spectral decomposition attribute map

Spectral decomposition Red-Green-Blue (RGB) color blended attribute maps are generated from the 3D seismic volume (Figure 4.5). Geoteric software is used to generate the RGB color blended maps. These maps give the possibility to analyze geomorphological features within the study area. Red-Green-Blue (RGB) corresponds to a specified frequency range (Othman et al., 2016), and spectral decomposition convert the seismic reflection data into the frequency domain. It displays the subsurface seismic interference at discrete frequencies. Spectral decomposition is used to image channel systems within the area of interest. The channels appear as white-colored features by mixing the three RGB frequencies. Spectral decomposition provides significantly detailed and more exact data than conventional attributes. Stratigraphic facies and facies boundaries, in addition to relative thickness, are revealed by the maps.

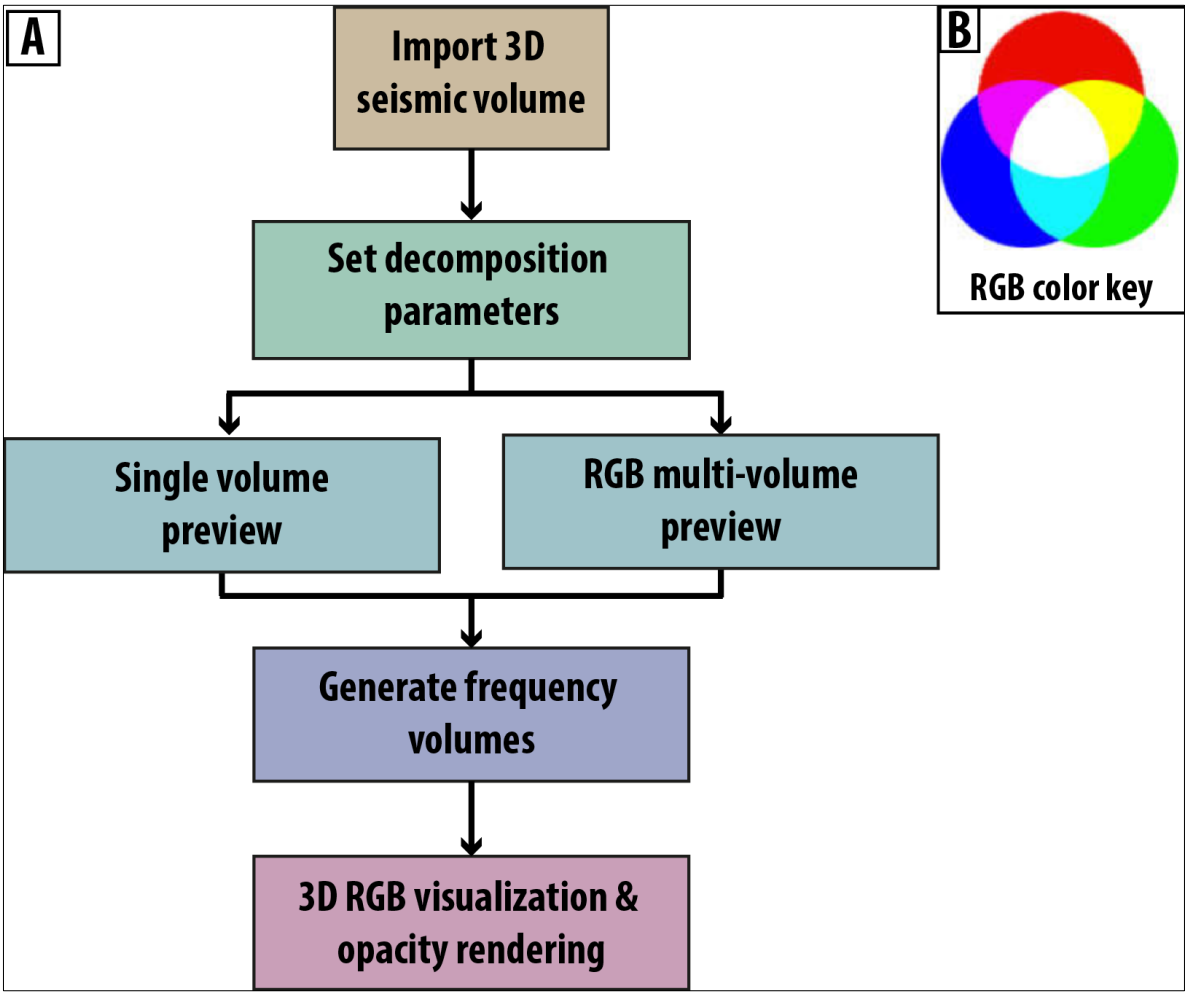

Figure 4.5: ***(A)*** *Flowchart illustrating the workflow applied in the spectral decomposition.* ***(B)*** *RGB color key used to describe the different color mixes used in the attribute maps.*

5 Results

5.1 Structural framework of the Tiddlybanken basin

The Tiddlybanken Basin is an example of a salt-influenced rift basin that consists of a uni-dimensional, NW-SE oriented, and ca. 39 km long salt wall that is surrounded by rim-synclines (Figures 2.10 and 5.1) (Gabrielsen et al., 1990; Hassaan et al., 2020b; Mattingsdal et al., 2015). The basin and salt wall can be divided into three parts: northwestern, central, and southeastern (Figure 5.1). The analysis of structural evolution is crucial to better understand the timing of accommodation creation and subsidence. The structural evolution of the Tiddlybanken Basin is therefore described in detail, focusing on the Realgrunnen Subgroup (Late Triassic-Early Jurassic). Important events like distinct unconformities within the basin, truncation of the sequence S5 (Fruholmen Formation), and thickness variations are described (Figure 5.2). Selected seismic sections, time-structure, and -thickness maps are being used to illustrate and explain the structural evolution. The pre-Permian NW-SE trending graben architecture developed during a transtensional deformation in the Late Devonian-Early Carboniferous is also described by Hassaan et al. (2020b) (see section 2.4.1 for details).

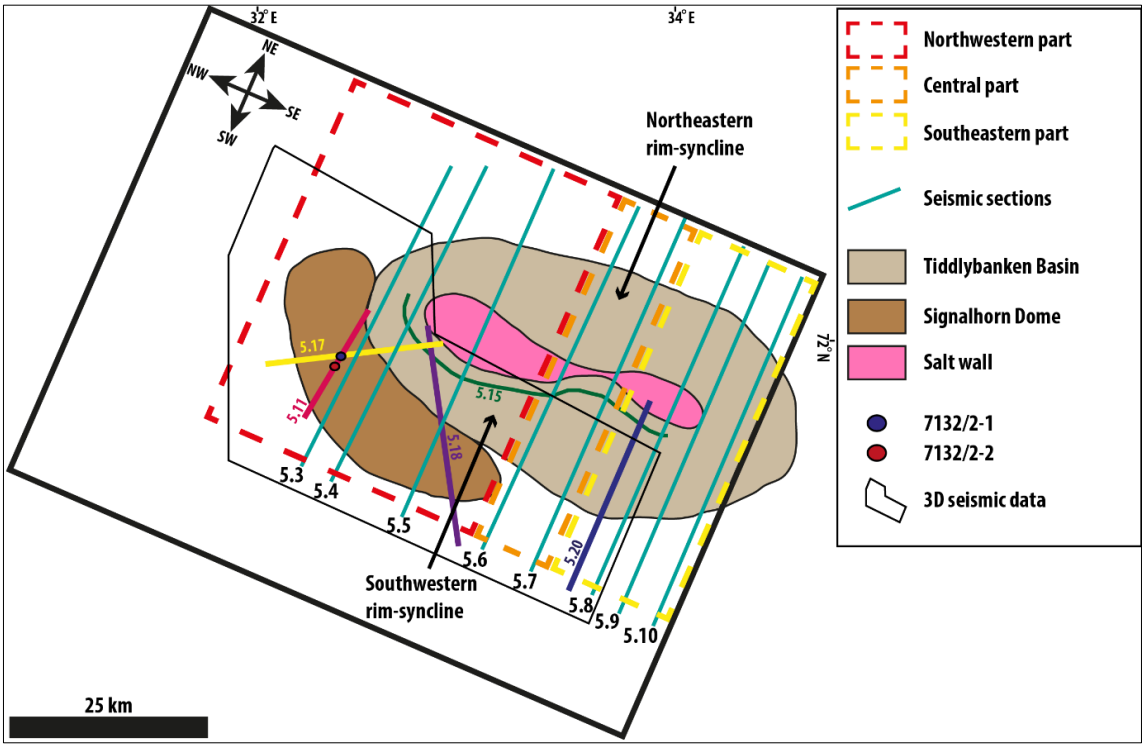

Figure 5.1: *Tiddlybanken Basin and Signalhorn Dome. Selected seismic sections are numbered by figure number (5.3-5.10). Selected arbitrary lines are marked with figure numbers.*

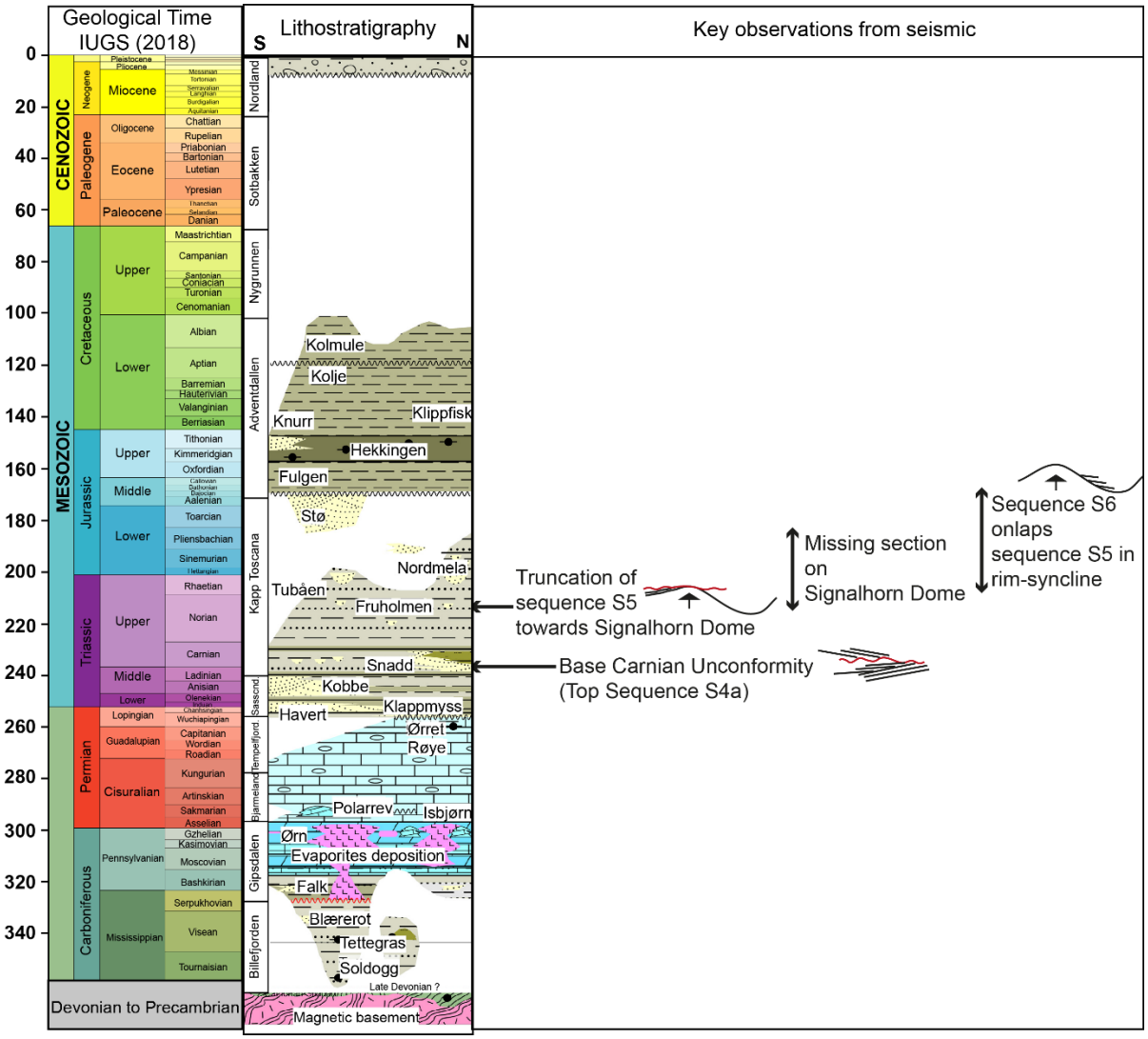

Figure 5.2: *Key observations from 3D seismic data from the Triassic-Jurassic time within the Tiddlybanken Basin. The lithostratigraphic column is based on regional information in the South Eastern Norwegian Barents Sea (Regional stratigraphy is based on Larssen et al. (2005) modified after Gernigon et al. (2018) and Rojo et al. (2019), and geologic timescale after IUGS (2018)).*

Mobile and non-mobile evaporites were deposited during Pennsylvanian to Early Permian within the graben system, which controlled the thickness and lithological alterations of the layered evaporitic sequences (see sections 2.3.1 for details). The base-salt relief affected the later development and distribution of the central salt wall and Signalhorn Dome.

5.1.1 Northwestern segment

A rim-syncline is present in the northern corner of the salt wall (Figure 5.3). The different sedimentary units have a general uniform thickness throughout the section, except the Realgrunnen Subgroup, which has a distinct thickness variation. Moving towards SE, a pillow-like salt structure connects with the salt wall and a rim-syncline on both sides of the pillow (Figure 5.4). Here, a clear difference in thickness can be observed. The sequences S1 and S2 (Havert and Klappmys formations) are upturned and thin towards the salt wall. The sequence S3 (Kobbe Formation) and the lower part of sequence S4 (Snadd Formation) have a distinctive pinch-out towards the salt pillow. The strata above the salt pillow are domed, in addition to a difference in thickness throughout the sequences. The sequence S4 shows a thinning above the pillow, while the sequences S5 and S6 are thicker above the salt pillow. Sequence S1 and the upper Triassic-Jurassic units are onlapping the salt wall, while sequences S2, S3, and lower S4 are apparently truncated or pinched out (Figure 5.5). The salt wall has a triangular base geometry (*sensu* Hudec and Jackson, 2007), which widens downward to ca. 15 km. A narrow stem of ca. 3.2 km is developed and is connected to a bulb-shaped overhang of ca. 6.6 km in width (Figure 5.5).

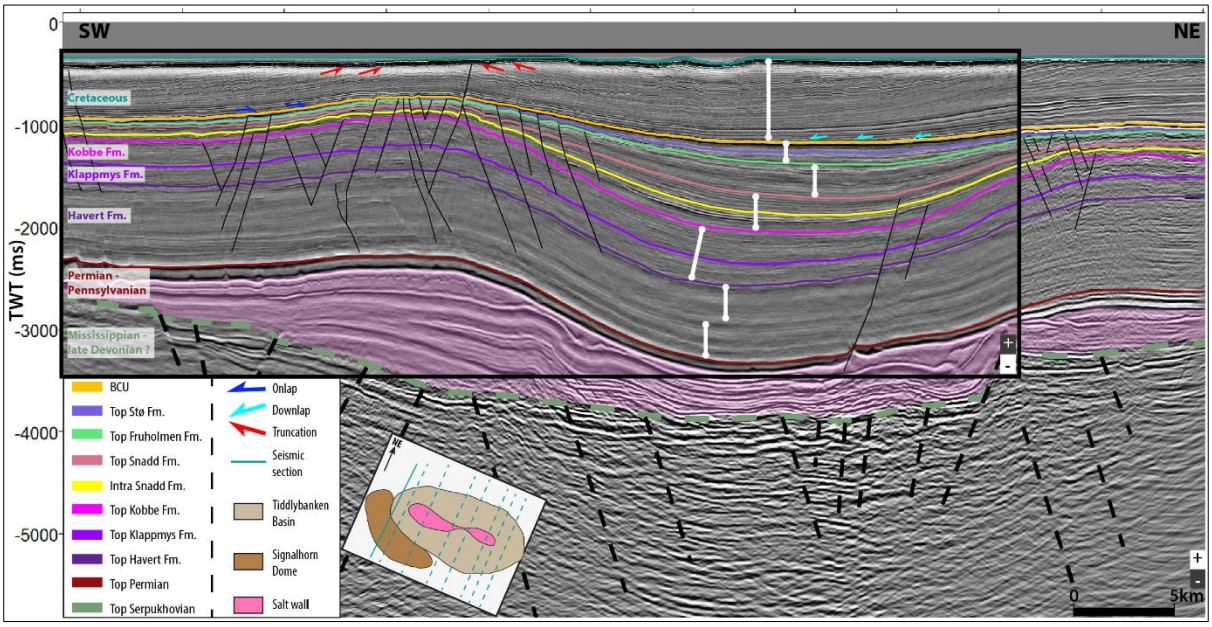

Figure 5.3: *Interpreted seismic profile illustrates along-strike salt wall variations, supra-salt sedimentation patterns, and stratal terminations in the northwestern part of the Tiddlybanken Basin. White circles connected by white lines display the thickness variations. Black box represents 3D seismic data that replaced 2D seismic data on the interpreted profile. Seismic data courtesy of NPD and Schlumberger Multiclient. Seismic polarity of the 3D and 2D is the opposite of each other.*

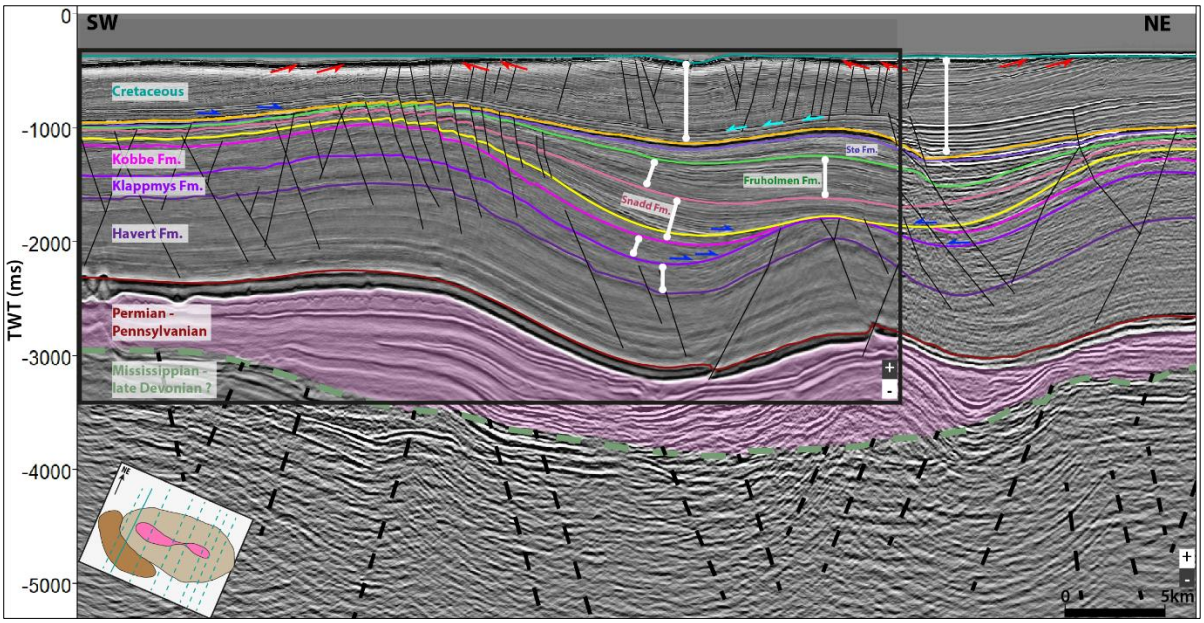

Figure 5.4: *Interpreted seismic profile illustrates along-strike salt wall variations, supra-salt sedimentation patterns, and stratal terminations in the northwestern part of the Tiddlybanken Basin. White circles connected by white lines display the thickness variations. Black box represents 3D seismic data that replaced 2D seismic data on the interpreted profile. Seismic data courtesy of NPD and Schlumberger Multiclient. Seismic polarity of the 3D and 2D is the opposite of each other.*

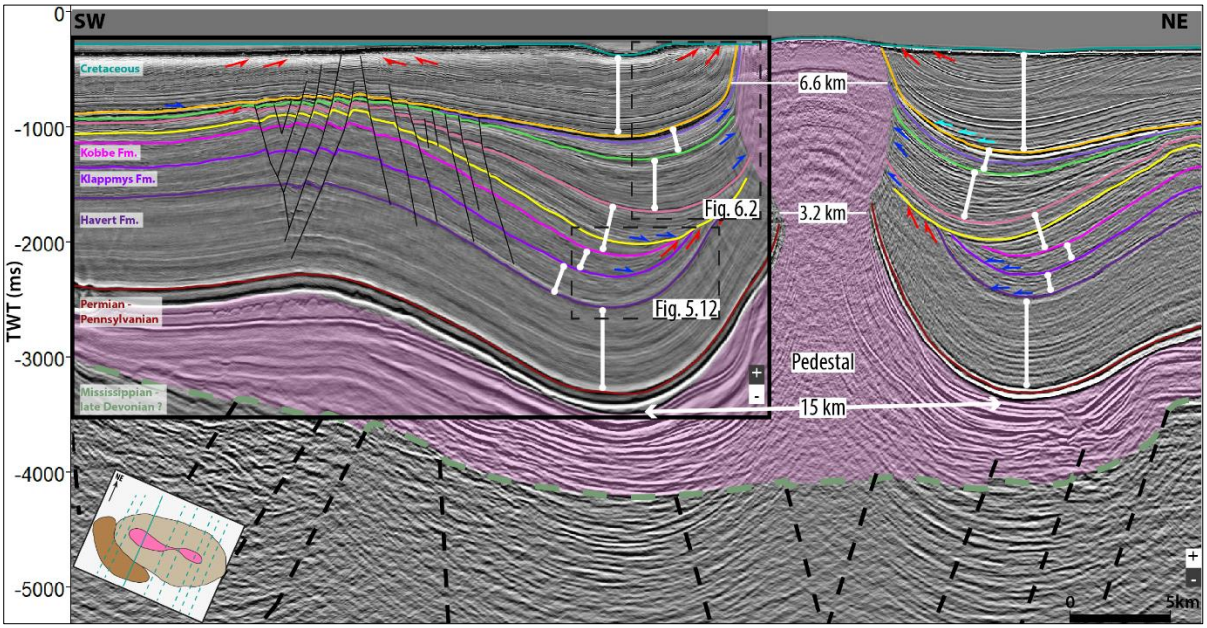

Figure 5.5: *Interpreted seismic profile illustrates along-strike salt wall variations, supra-salt sedimentation patterns, and stratal terminations in the northwestern part of the Tiddlybanken Basin. White circles connected by white lines display the thickness variations. Black box represents 3D seismic data that replaced 2D seismic data on the interpreted profile. Seismic data courtesy of NPD and Schlumberger Multiclient. Seismic polarity of the 3D and 2D is the opposite of each other.*

5.1.2 Central segment

The center of the salt wall correlates to the transfer zone shown in Figure 2.5. The salt wall has a pedestal geometry with a width of ca. 14.4 km at the bottom (Figure 5.6). Upper Triassic-Jurassic sequences onlap on the southwestern margin of the salt wall, while on the northeastern side, the sequences subcrops below the thin Quaternary cover (Figure 5.6). Further towards the center, a more symmetrical pedestal with a stem width of ca. 18.4 km is present (Figure 5.7). The sequence S1 (Havert Formation), Realgrunnen Subgroup, and Cretaceous units subcrop below the thin Quaternary cover, while the sequences S2, S3, and S4 are pinching out and truncated at the unconformity towards the salt pedestal.

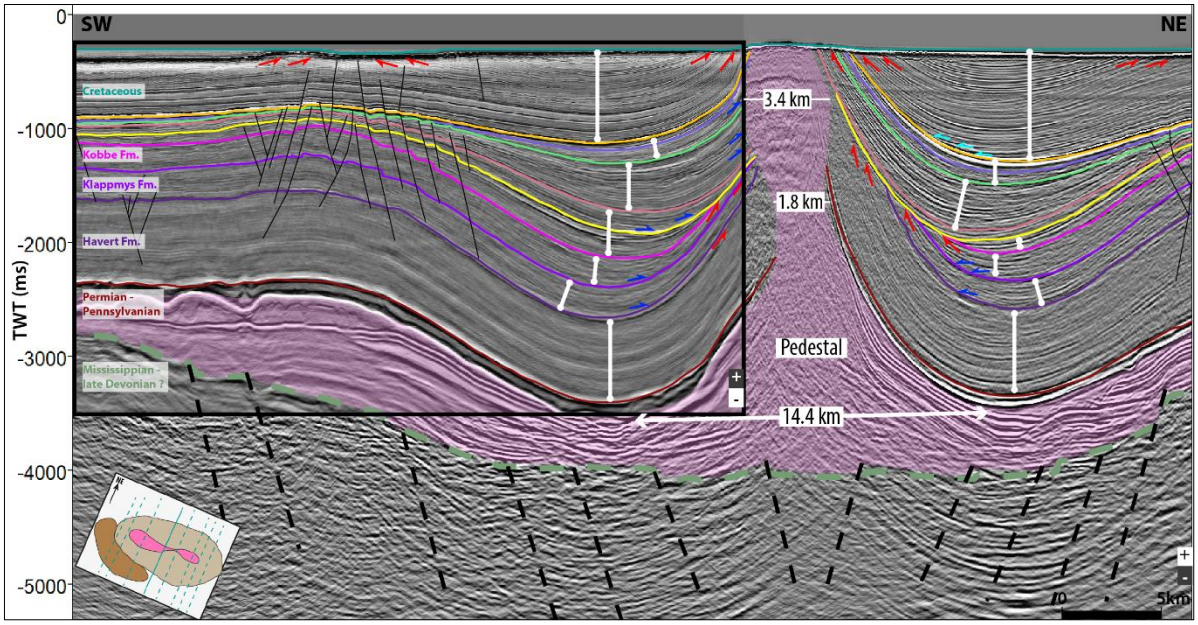

Figure 5.6: *Interpreted seismic profile illustrates along-strike salt wall variations, supra-salt sedimentation patterns, and stratal terminations in the northwestern part of the Tiddlybanken Basin. White circles connected by white lines display the thickness variations. Black box represents 3D seismic data that replaced 2D seismic data on the interpreted profile. Seismic data courtesy of NPD and Schlumberger Multiclient. Seismic polarity of the 3D and 2D is the opposite of each other.*

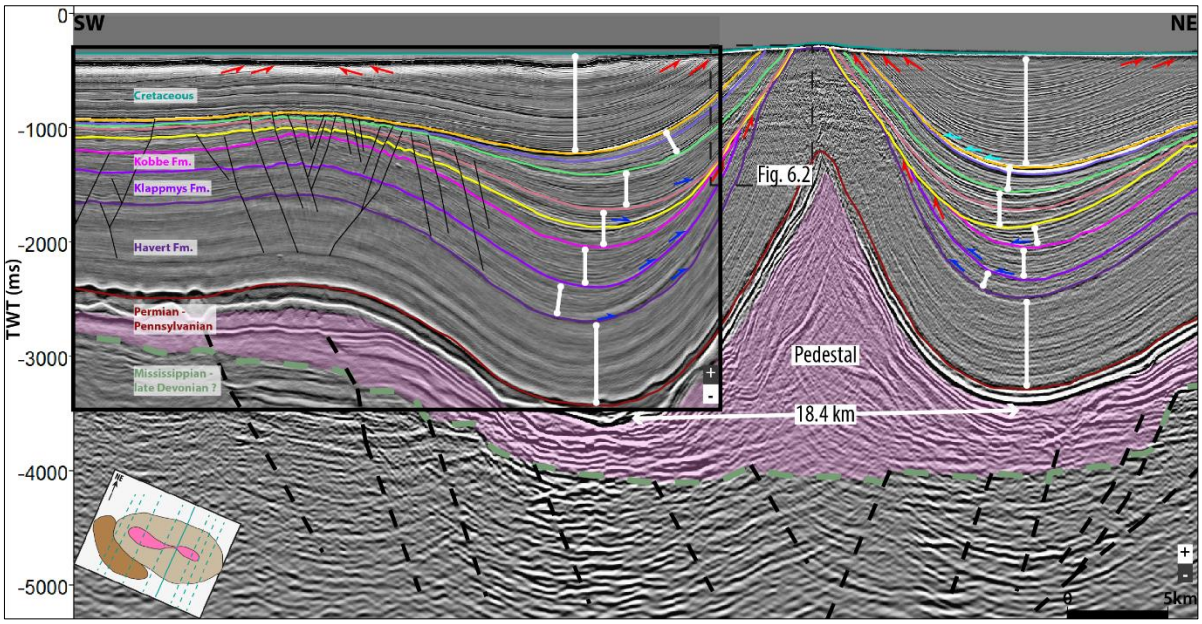

Figure 5.7: *Interpreted seismic profile illustrates along-strike salt wall variations, supra-salt sedimentation patterns, and stratal terminations in the northwestern part of the Tiddlybanken Basin. White circles connected by white lines display the thickness variations. Black box represents 3D seismic data that replaced 2D seismic data on the interpreted profile. Seismic data courtesy of NPD and Schlumberger Multiclient. Seismic polarity of the 3D and 2D is the opposite of each other.*

5.1.3 Southeastern segment

In the southeastern part of the salt wall, the sequences are not onlapping the salt wall; instead, the strata subcrop below the thin Quaternary cover (Figure 5.8). The southeastern part of the salt wall is observed to have the broadest base pedestal, stem, and bulb, ranging from ca. 17.6-18.8 km, ca. 3.5-5.3 km, and ca. 4.1-6.4 km correspondingly.

Further southeast, Upper Triassic-Cretaceous strata cover a pedestal-shaped salt structure (Figure 5.9). In the southeastern corner of the salt wall, a general uniform thickness is observed within the sequences. The thickness of Realgrunnen Subgroup strata (sequences S5 and S6) increases within the rim-syncline. However, the southeastern end comprises generally thinner sequences compared to the northwestern end of the salt wall (Figures. 5.3 and 5.10).

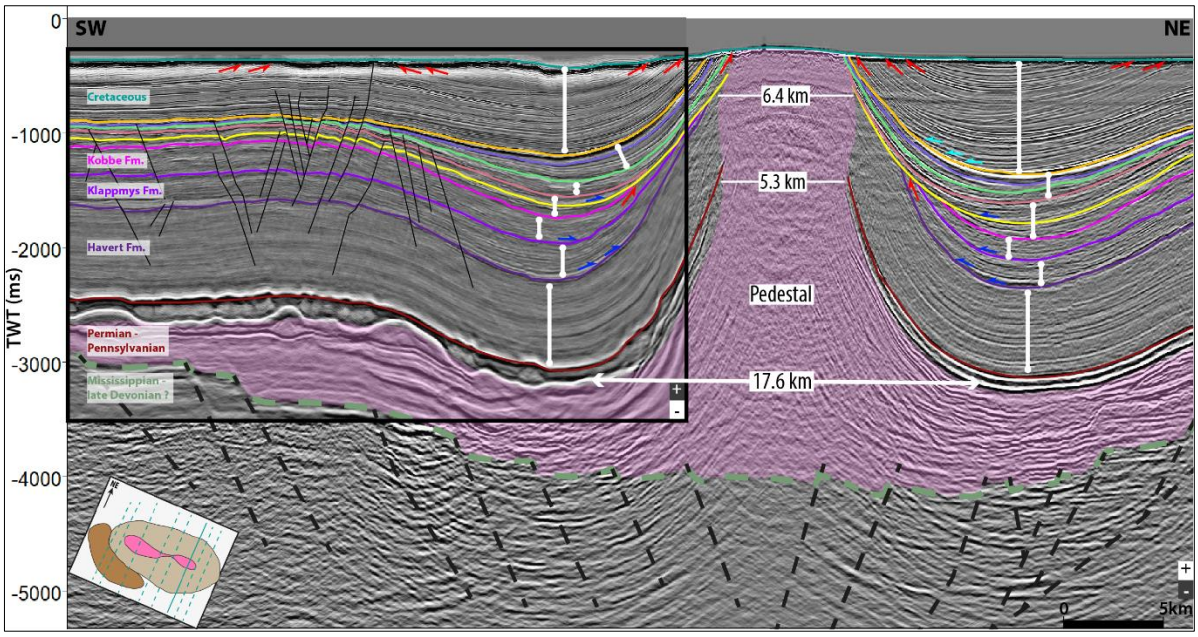

Figure 5.8: *Interpreted seismic profile illustrates along-strike salt wall variations, supra-salt sedimentation patterns, and stratal terminations in the northwestern part of the Tiddlybanken Basin. White circles connected by white lines display the thickness variations. Black box represents 3D seismic data that replaced 2D seismic data on the interpreted profile. Seismic data courtesy of NPD and Schlumberger Multiclient. Seismic polarity of the 3D and 2D is the opposite of each other.*

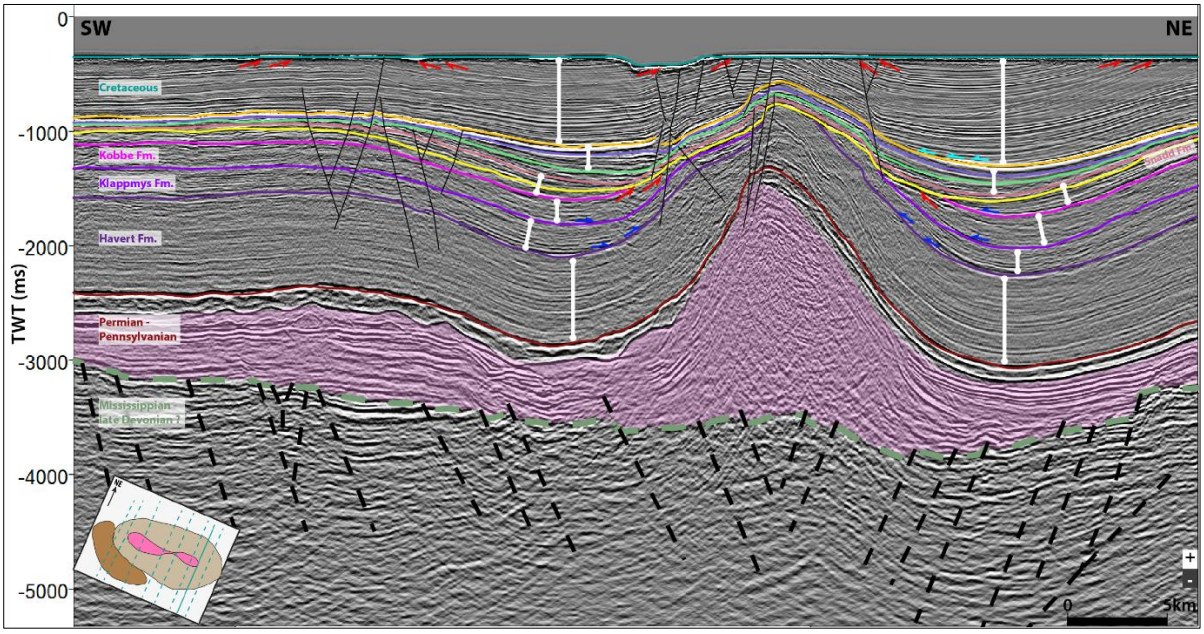

Figure 5.9: *Interpreted seismic profile illustrates along-strike salt wall variations, supra-salt sedimentation patterns, and stratal terminations in the northwestern part of the Tiddlybanken Basin. White circles connected by white lines display the thickness variations. Black box represents 3D seismic data that replaced 2D seismic data on the interpreted profile. Seismic data courtesy of NPD and Schlumberger Multiclient. Seismic polarity of the 3D and 2D is the opposite of each other.*

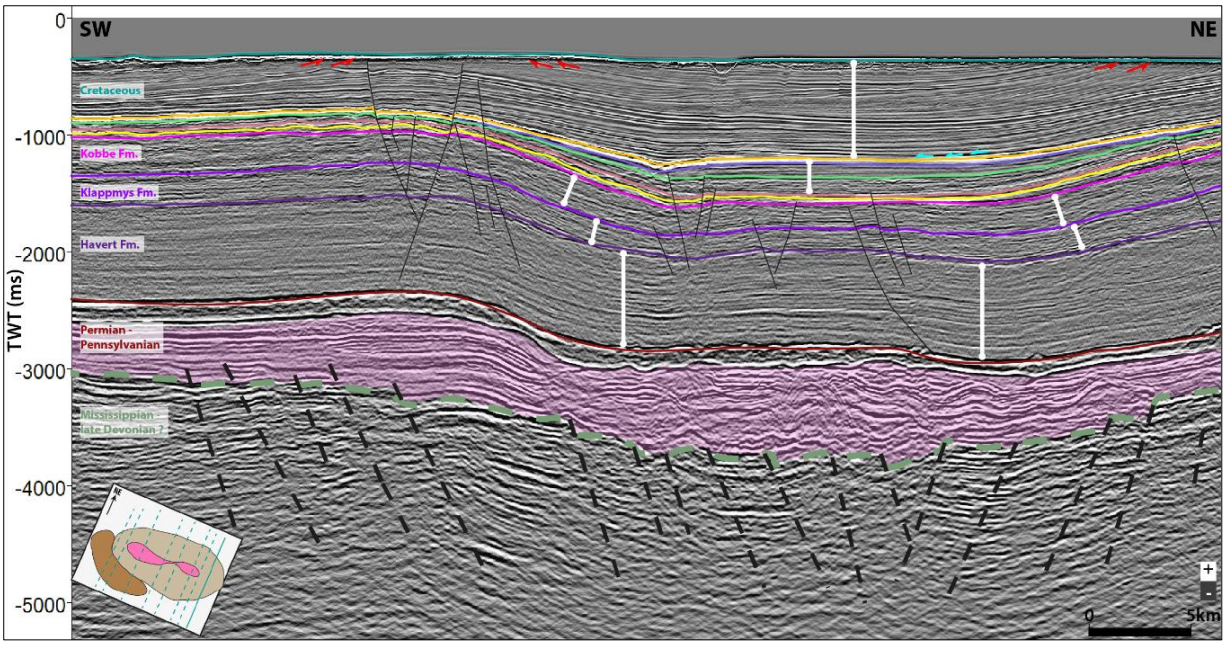

Figure 5.10: *Interpreted seismic profile illustrates along-strike salt wall variations, supra-salt sedimentation patterns, and stratal terminations in the northwestern part of the Tiddlybanken Basin. White circles connected by white lines display the thickness variations. Black box represents 3D seismic data that replaced 2D seismic data on the interpreted profile. Seismic data courtesy of NPD and Schlumberger Multiclient. Seismic polarity of the 3D and 2D is the opposite of each other.*

5.1.4 Signalhorn Dome

The Signalhorn Dome is located on the western and southwestern margin of the Tiddlybanken Basin and has an arc-shaped geometry with a salt pillow below it. The dome is NW-SE orientated, ca. 58 km long, and has an ellipsoid shape in map view (Figure 5.1). Antithetic and synthetic faults are observed over the dome (Figure 5.11). The normal faults are dipping and cutting through layers from Anisian (maybe deeper) and up to the thick Cretaceous units.

The seismic sections illustrate where the Signalhorn Dome is evident. Several normal faults are observed above the dome in the northwestern seismic sections (Figure 5.5), while towards the southeast, fewer faults are present (Figure 5.9). The faults in the northwestern part are also reaching a shallower level than in the southeastern part. A general trend of the upper Triassic-Jurassic formations is thinning towards the Signalhorn Dome and thickening in the basin (Figures 5.5, 5.6, and 5.17).

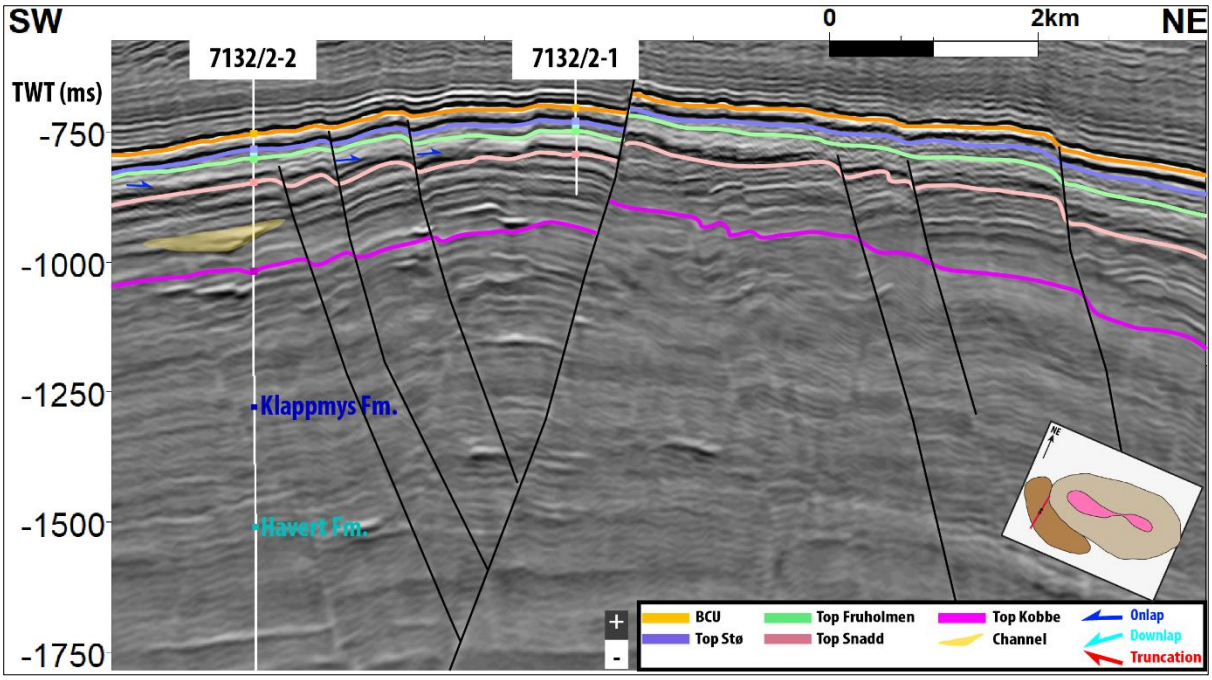

Figure 5.11: *The two wells, 7132/2-1 and 7132/2-2 penetrate the Signalhorn Dome. Seismic data courtesy of Schlumberger Multiclient.*

The sequence S5 (Fruholmen Formation) displays the most significant thinning towards the dome, where evidence of truncation is observed on both sides of the dome (Figurea 5.11 and 5.18). The sequence S6 is generally present as a thick sequence within the basin, while a thin blanket of the sequence covers the Signalhorn Dome (Figure 5.11).

5.2 Tectono-stratigraphic development

5.2.1 Induan-Olenekian (S1 and S2; Havert and Klappmys formations)

The sequence S1 (Havert Formation) is observed to have a uniform thickness, and there is no evidence of salt movement during this time (Figures 5.5 and 5.9). Sequence S2 (Klappmys Formation) is observed to have discordant contact with sequence S1 and a syn-kinematic infill structure. The sequence S2 onlaps its underlying strata and thins towards the flank of the salt wall creating a wedge-shaped geometry. It is truncated by a distinct unconformity (Figures 5.6 and 5.8). The unconformity is present in the basin and is most prominent near the salt wall. The sequence S1 is upturned along the flanks of the salt wall, whereas the sequence S2 is truncated

and pinches out towards the salt. The pinch-out is located further away from the salt wall towards the northwest.

5.2.2 Anisian (S3; Kobbe Formation)

The sequence S3 reaches a depth of more than -1600 ms TWT within the rim-syncline and up to -950 ms TWT on the Signalhorn Dome (Figure 5.13b). The salt wall is penetrating this horizon, where a rim-syncline surrounds it. Towards the southwest, an anticlinal is observed, which is the Signalhorn Dome. On top of the dome, wells 7132/2-1 and 7132/2-2 are drilled. The horizon generally deepens towards the north and gets shallower towards the south.

The sequence S3 is observed to have discordant contact with the underlying sequence S2 and displays a syn-kinematic infill (Figure 5.12). The sequence thins towards the flank of the salt wall and has a wedge-shaped geometry. Sequence S3 is upturned and pinches out towards the salt wall. The sequence is more upturned in the central and southeastern segments of the rim-syncline and reaches a relatively shallower level than in the northwestern segment (Figure 5.7).

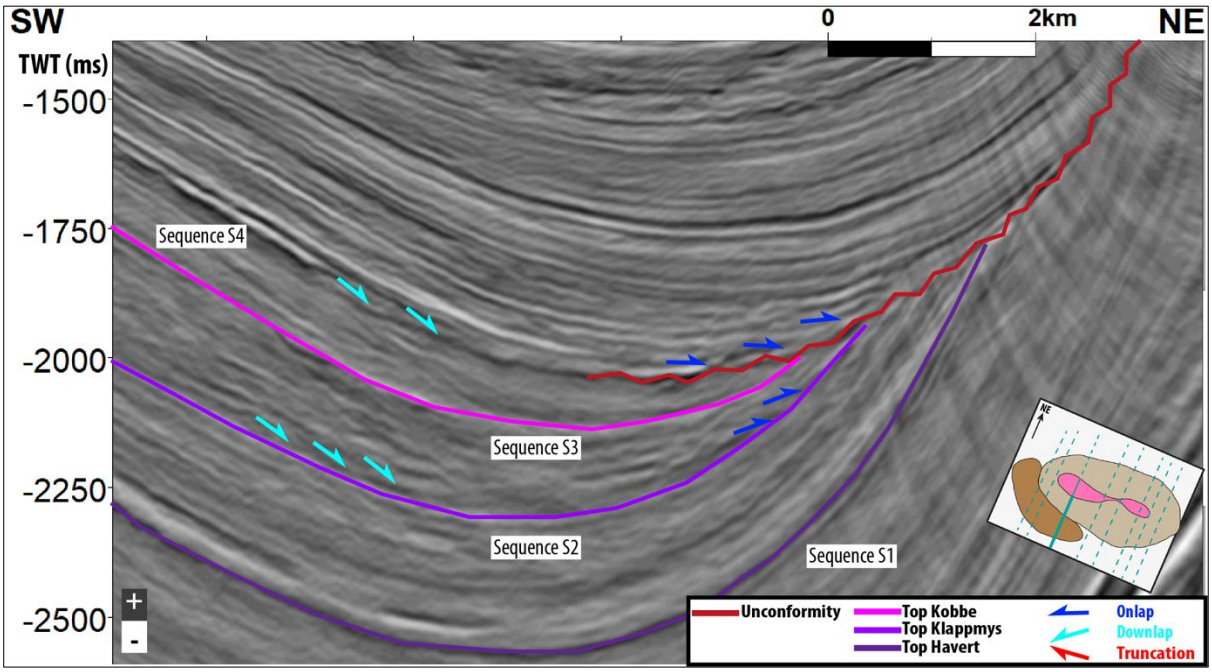

Figure 5.12: *Infill patterns from sequences S2 and S3, truncation and pinch-out of sequences S1, S2, S3, and lower S4 on the Base Carnian Unconformity. Seismic section zoom-in from figure 5.5B. Seismic data courtesy of Schlumberger Multiclient.*

5.2.3 Ladinian-Early Norian (S4; Snadd Formation)

The Top Snadd Formation surface is penetrated by the salt wall, and the time-structure map reaches down to ca. -1600 ms within the basin and up to ca. -800 ms above the Signalhorn Dome (Figure 5.13a). A general shallowing towards the south and a deepening towards the north can be seen on the time-structure map (Figure 5.13a). There is a shallower part north of the western salt wall, which can also be correlated with the same spot on the isochron map (Figure 5.13c).

The sequence S4 is characterized by onlapping reflections in the rim-syncline onto sequence S3 and the Base Carnian Unconformity towards the salt wall (Figures 5.5 and 5.6). The strata from the sequence S4b onlaps the northwestern overhang of the salt wall creating hook halokinetic sequences (Figures 3.6, 5.5, and 6.2) (*sensu* Giles and Rowan, 2012). The Signalhorn Dome shows no tectonic activity during deposition of sequence S4a (Figure 5.14a); instead, signs of minor doming of the Signalhorn Dome during the early Carnian time can be observed on the thickness map of sequence S4b (Figure 5.14b).

The sequence has a general thinning towards the Signalhorn Dome and the salt wall (Figures 5.4, 5.7, and 5.13c). The thickness is more or less uniform outside the basin area. Within the Tiddlybanken Basin, the thickness reaches up to 450 ms. The area surrounding the basin has thicknesses between 125 ms and 225 ms. The rim-syncline is more prominent on the western margin of the salt wall, having an elongated and isolated shape (Figures 5.7 and 5.13c). The northeastern rim-syncline is isolated from the southwestern rim-syncline. The northwestern part of the salt wall comprises a thicker sequence within the rim-syncline compared to the southeastern. The succession increases somewhat towards the north and decreases on the Signalhorn Dome and towards the southwest.

The sequence S4a (Lower Snadd Formation) has a constant thickness on the Signalhorn Dome and the Finnmark Platform, while in the basin, two main depocentres are located in the southwestern and northeastern rim-syncline (Figure 5.14). Sequence S4b is onlapping sequence S4a (Base Carnian Unconformity) and thins towards the salt wall (Figures 5.6 and 5.12). The sequence comprises two main depocentres that preserve the unit's thickest parts, where the most prominent one is located in the southeastern rim-syncline (Figure 5.14b).

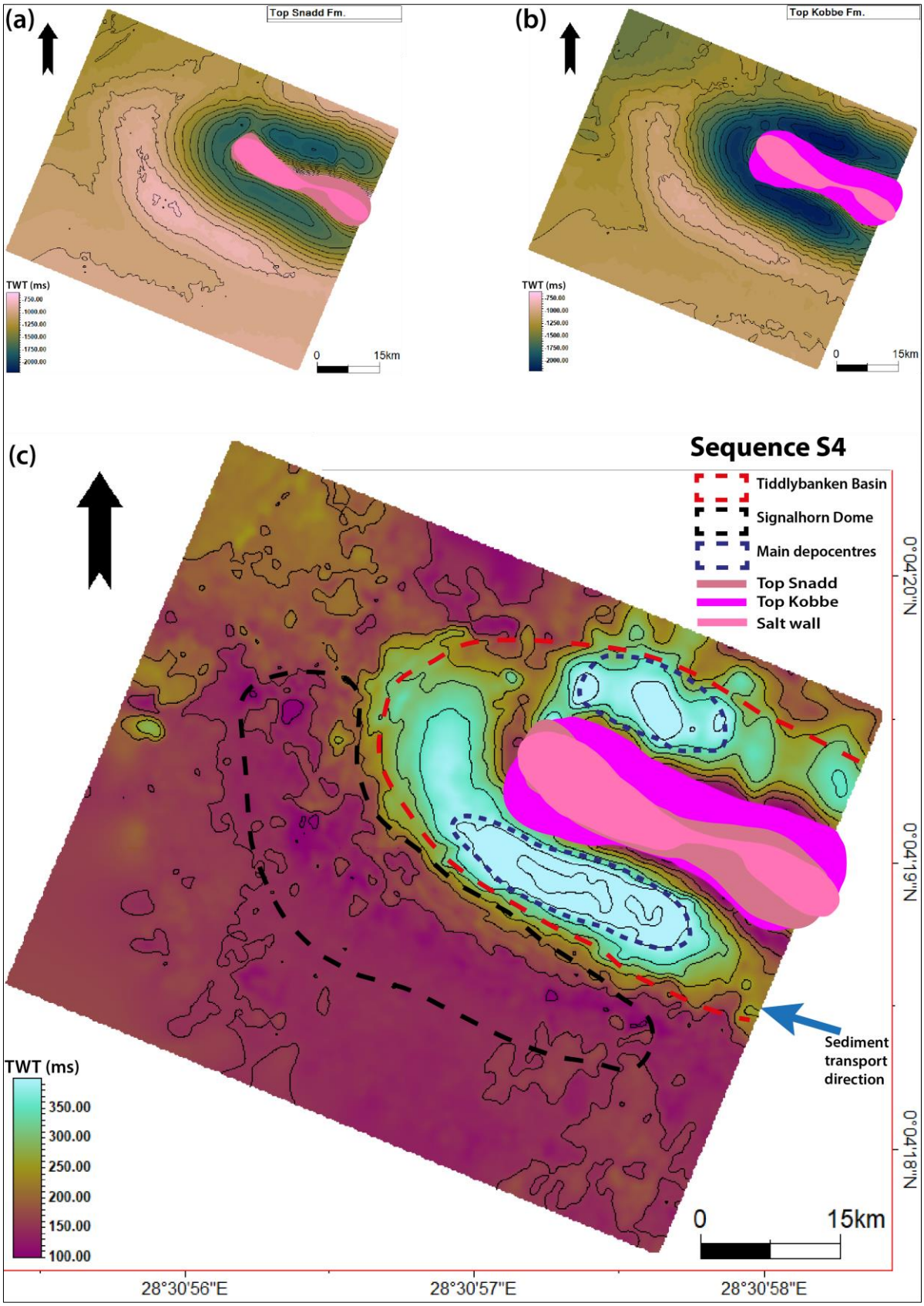

***Figure 5.13**: **(a)** Time-structure map of Top Snadd Fm. **(b)** Time structure map of Top Kobbe Fm. **(c)** Isochron map of the seismic sequence S4 (Snadd Formation) displaying major depocentres along the salt wall inside the Tiddlybanken Basin. Note the shift of the thickest depocentres during the evolution signifying the salt evacuation from different segments of the basin. Seismic data courtesy of Schlumberger Multiclient.*

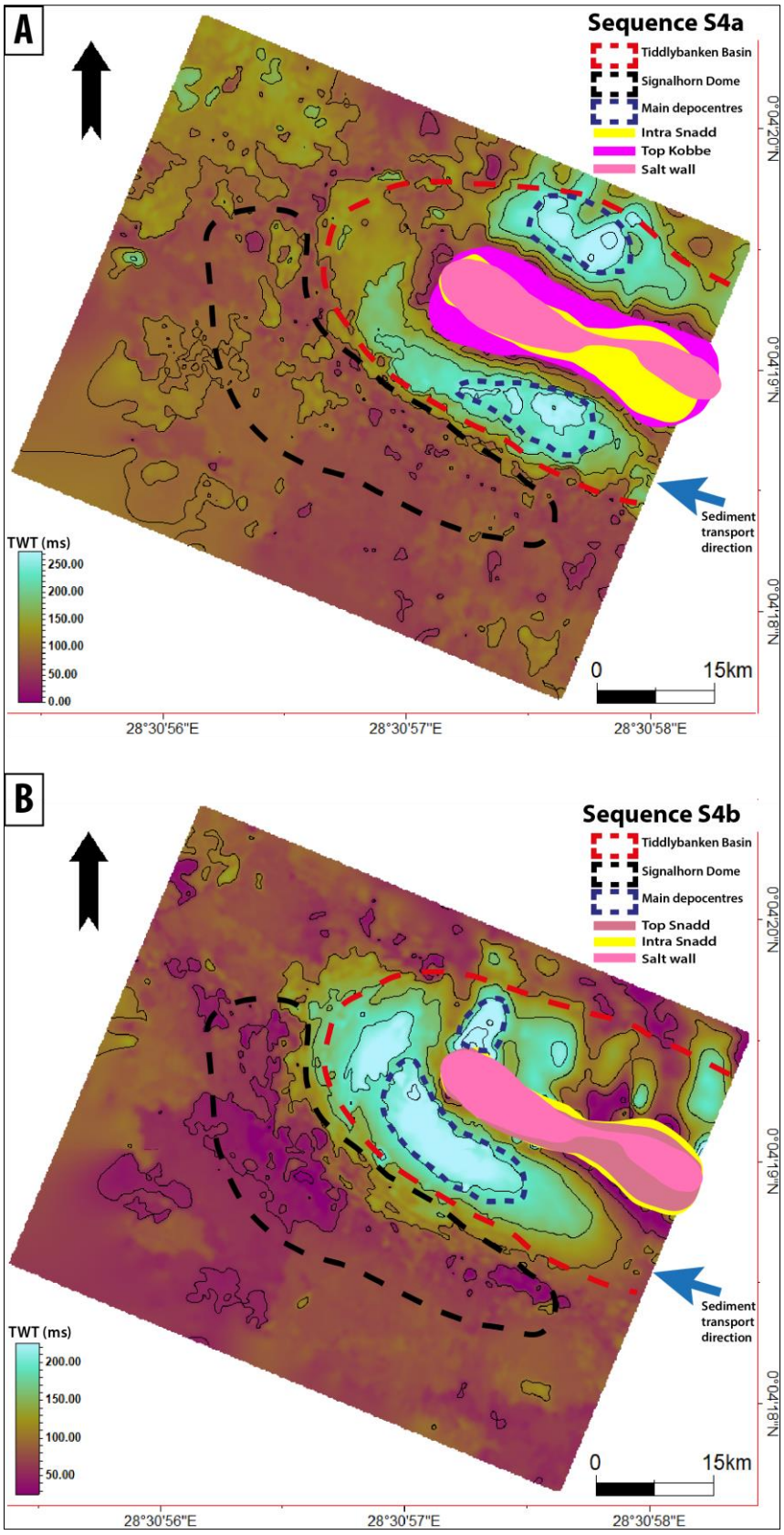

Figure 5.14: ***(a)*** *Isochron map of the seismic sequence S4a (Lower Snadd Formation) displaying major depocentres along the salt wall inside the Tiddlybanken Basin* ***(b)*** *Isochron map of the seismic sequence S4b (upper Snadd Formation) displaying major depocentres along the salt wall inside the Tiddlybanken Basin. Note the shift of the thickest depocentres during the evolution signifying the salt evacuation from different segments of the basin. Seismic data courtesy of Schlumberger Multiclient.*

An internal unconformity in sequence S4 (Snadd Formation) is observed and interpreted as a Base Carnian Unconformity (Figure 5.15). All the seismic sections are flattened on the Top Snadd Formation horizon to illustrate better the depositional relations within the Snadd Formation and the halokenesis.

Sequence S4 has distinctive thickness variation from NW-SE within the rim-syncline (Figure 5.15A). The sequence is divided into sub-sequences, where the northwestern part comprises three sub-sequences and the southeastern two (Figure 5.15B and C). The interpreted unconformity is observed between sub-sequence (1) and (2) based on stata terminations and seismic facies differences. The first sub-sequence (1) onlap Top Kobbe Formation and is apparently pinching out towards the salt wall (Figure 5.15B). However, sub-sequence (1) is truncated by an unconformity interpreted as the Base Carnian. The apparent pinch-out onto the unconformity is more than 2 km away from the salt wall (Figure 5.15B). The reflections within this unit are chaotic, discontinuous, and partly blurry. The second sub-sequence (2) generally has parallel and continuous reflections that onlap on the unconformity (Figure 5.15B). The reflections in the lower part of the sub-sequence are slightly different from the reflections above and onlap the unconformity. The pinch-out is somewhat more towards the salt wall than the sub-sequence (1). The third sub-sequence (3) has more parallel reflections and displays thinning towards the southwest (Figure 5.15B). The sub-sequence appears to consist of depositional downlaps and is gradually thinning towards the southeast within the southwestern rim-syncline (Figure 5.15A). The Top Snadd Formation horizon is, therefore, most likely also an unconformity. The reflections are parallel and continuous in the northeast and merge towards the southwest.

In contrast, the southeastern part of the salt wall looks very different (Figure 5.15C). Sub-sequence (1) and (2) are apparently pinching out ca. 2 km from the salt wall where the strata are somewhat thin and terminate on the unconformity. The reflections in these sub-sequences are discontinuous and chaotic, having no distinct impedance contrast. The interpreted Base Carnian Unconformity reflector has a clear and strong impedance contrast. The strata above the unconformity have an apparent thinning towards the northeast. The reflections are continuous and parallel in the southwestern part and become more discontinuous as they merge towards the northeast (Figure 5.15C).

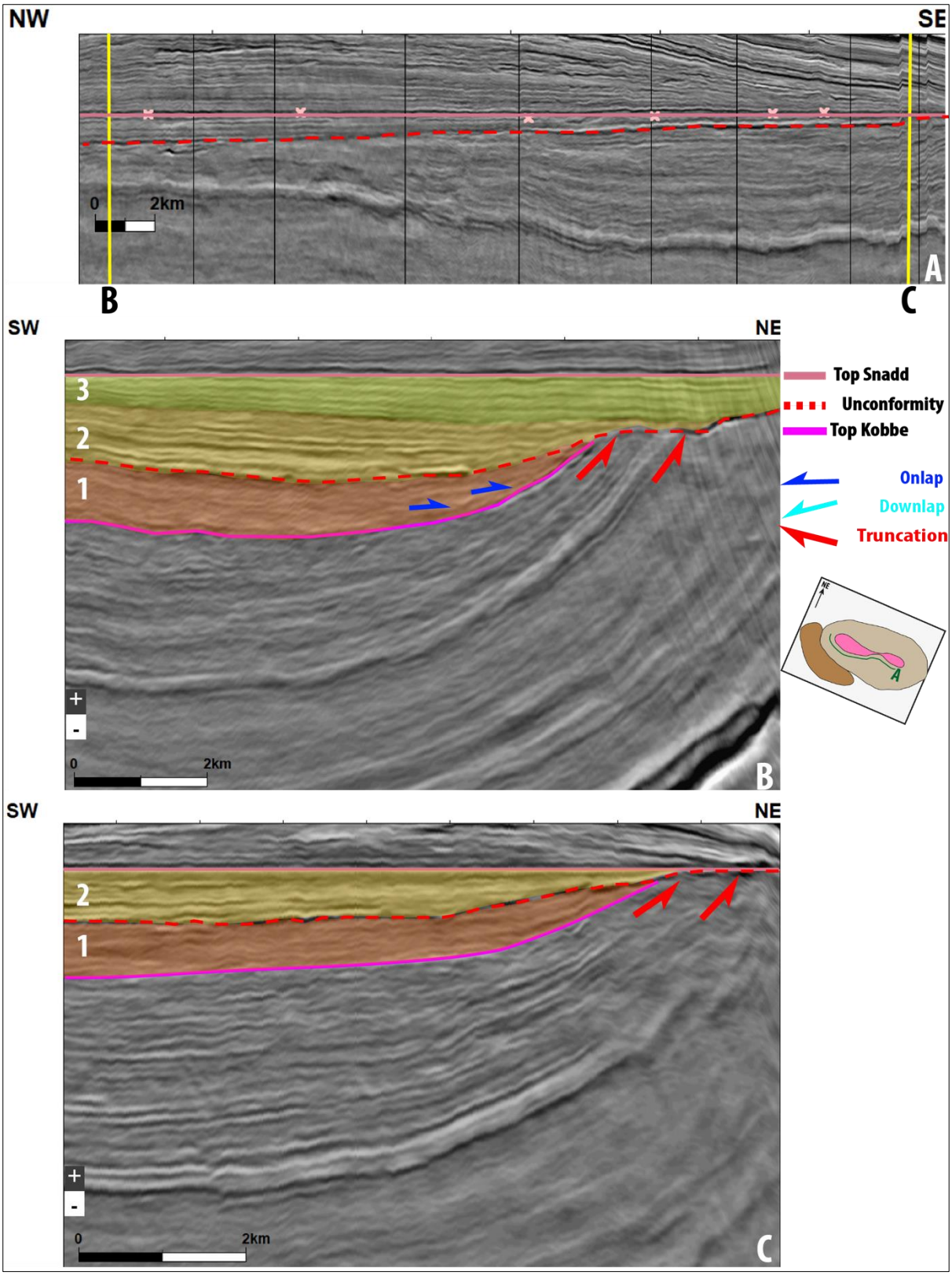

Figure 5.15: *These three flattened seismic sections illustrate the Base Carnian Unconformity.* ***A)*** *An arbitrary line crossing B and C illustrates the correlation between the two areas.* ***B)*** *Cross-section of the northwestern side of the salt wall, flattened on Top Snadd.* ***C)*** *Cross-section of the southeastern side of the salt wall, flattened on Top Snadd. Arbitrary line Fig. C in the study area. Seismic data courtesy of Schlumberger Multiclient.*

5.2.4 Norian-Rhaetian (S5; Fruholmen Formation)

The Top Fruholmen Formation surface reaches a depth of less than -800 ms on the Signalhorn Dome (Figure 5.16a). Two main depocenters are located within the northern rim-syncline reaching a depth of more than -1500 ms. There is a shallowing trend towards the south and deepening towards the north.

Sequence S5 has a general thickness of 20-100 ms outside the southwestern rim-syncline and is slightly thinner in the southwestern area (Figure 5.16c). Major depocentres surround the northwestern part of the salt wall that preserves the thickest part of sequence S5, while in the southeastern part, there is minor thickening (Figure 5.16c). The two wells located on the Signalhorn Dome record a 60 m thick sequence S5, indicating a >700 m thick S5 in the rim-syncline by measuring the ca. time interval (Figure 5.17). In the northwestern part of the salt wall, the sequence S5 terminates on the salt wall, while in the central and southeastern the sequence subcrops below the thin Quaternary cover. The sequence S5 thins towards the southwest, covering a wider region above the Signalhorn Dome (Figures 5.16 and 5.17). The upper part of sequence S5 displays discontinuous to continuous reflections above the Signalhorn Dome compared to clustered and stacked reflections within the southwestern rim-syncline of the basin. However, the reflections are parallel to sub-parallel in the lower package of the sequence S5 (Figures 5.17, 5.11, and 5.12).

The sequence S5 thins and is truncated on the Signalhorn Dome (Figure 5.17). The lower package of sequence S5 is still present on the Signalhorn Dome, but the upper package and sequence S6 are considerably thin or not present. Sequence S4 (Snadd Formation) has a constant thickness over the southeastern edge of the Signalhorn Dome; in comparison, sequences S5 and S6 are thinning towards the Signalhorn Dome in the north (Figure 5.17).

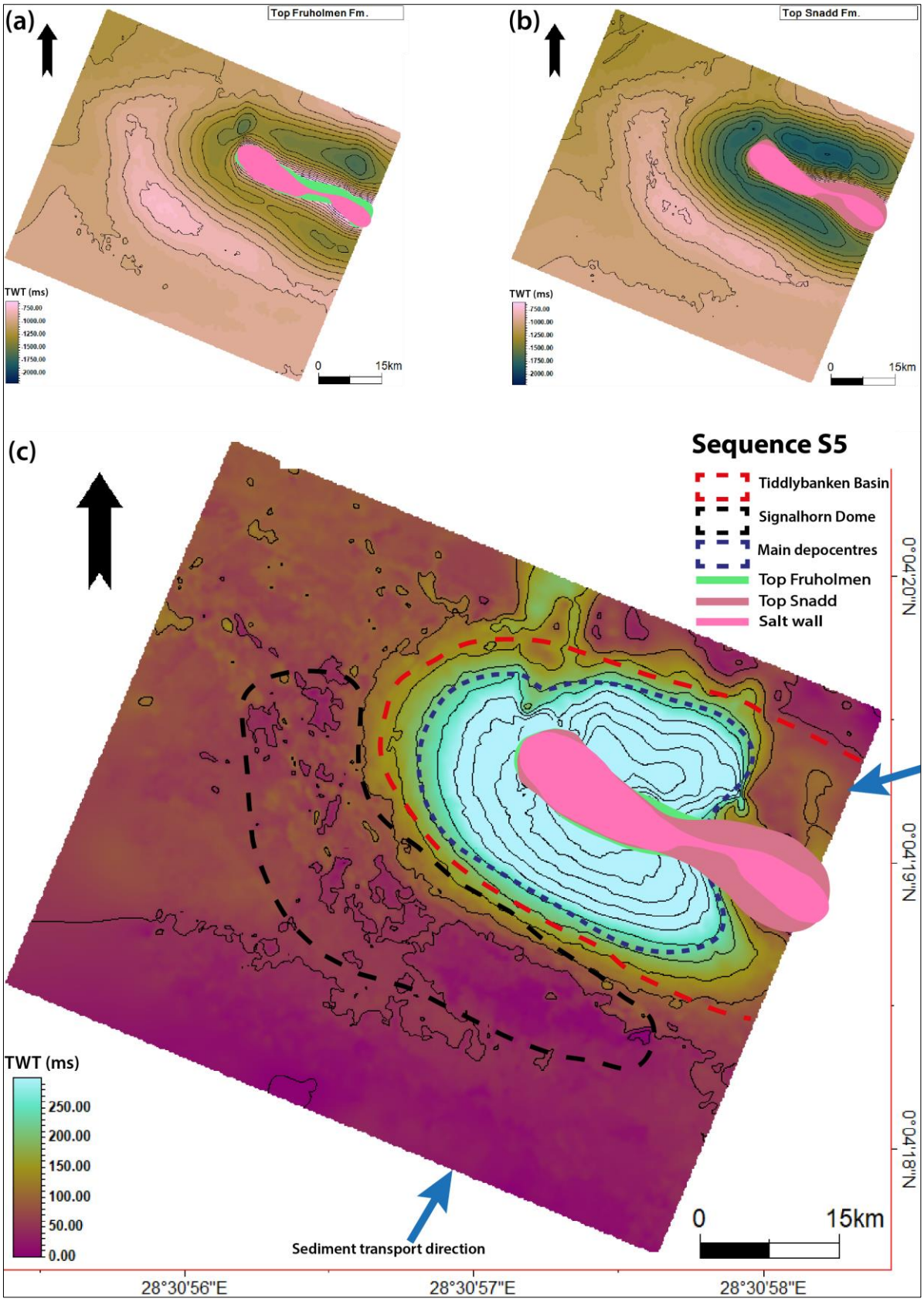

Figure 5.16: (a) *Time-structure map of Top Fruholmen Fm.* ***(b)*** *Time structure map of Top Snadd Fm.* ***(c)*** *Isochron map of the seismic sequence S5 (Fruholmen Formation) displaying major depocentres along the salt wall inside the Tiddlybanken Basin. Note the shift of the thickest depocentres during the evolution signifying the salt evacuation from different segments of the basin. Seismic data courtesy of Schlumberger Multiclient.*

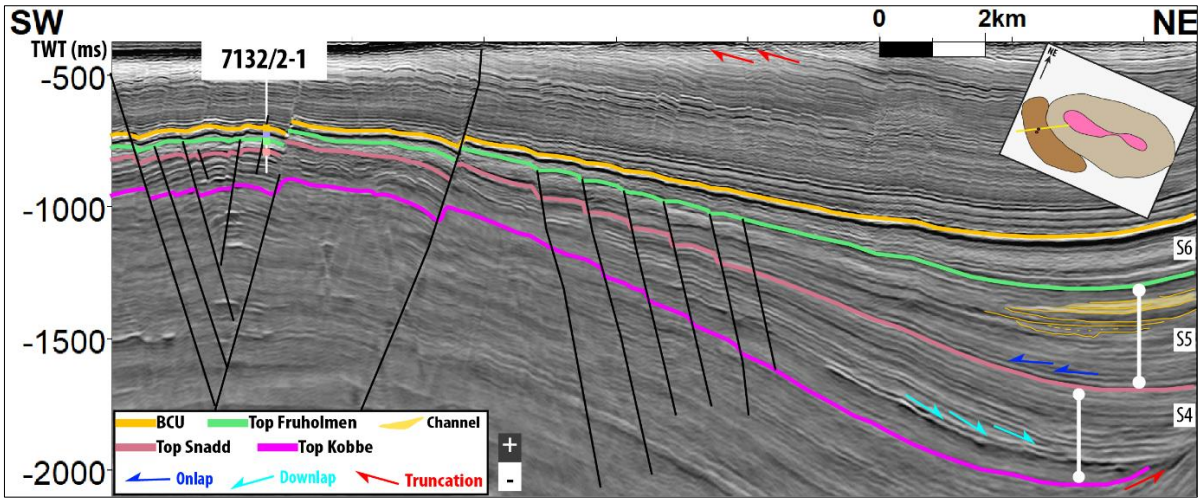

Figure 5.17: *Interpreted seismic section illustrates significant thickness variations from the rim-syncline to the Signalhorn Dome in sequences S4 (Snadd Formation) and S5 (Fruholmen Formation). The interpreted seismic horizons are tied from the well tops in well 7132/2-1. Seismic data courtesy of Schlumberger Multiclient.*

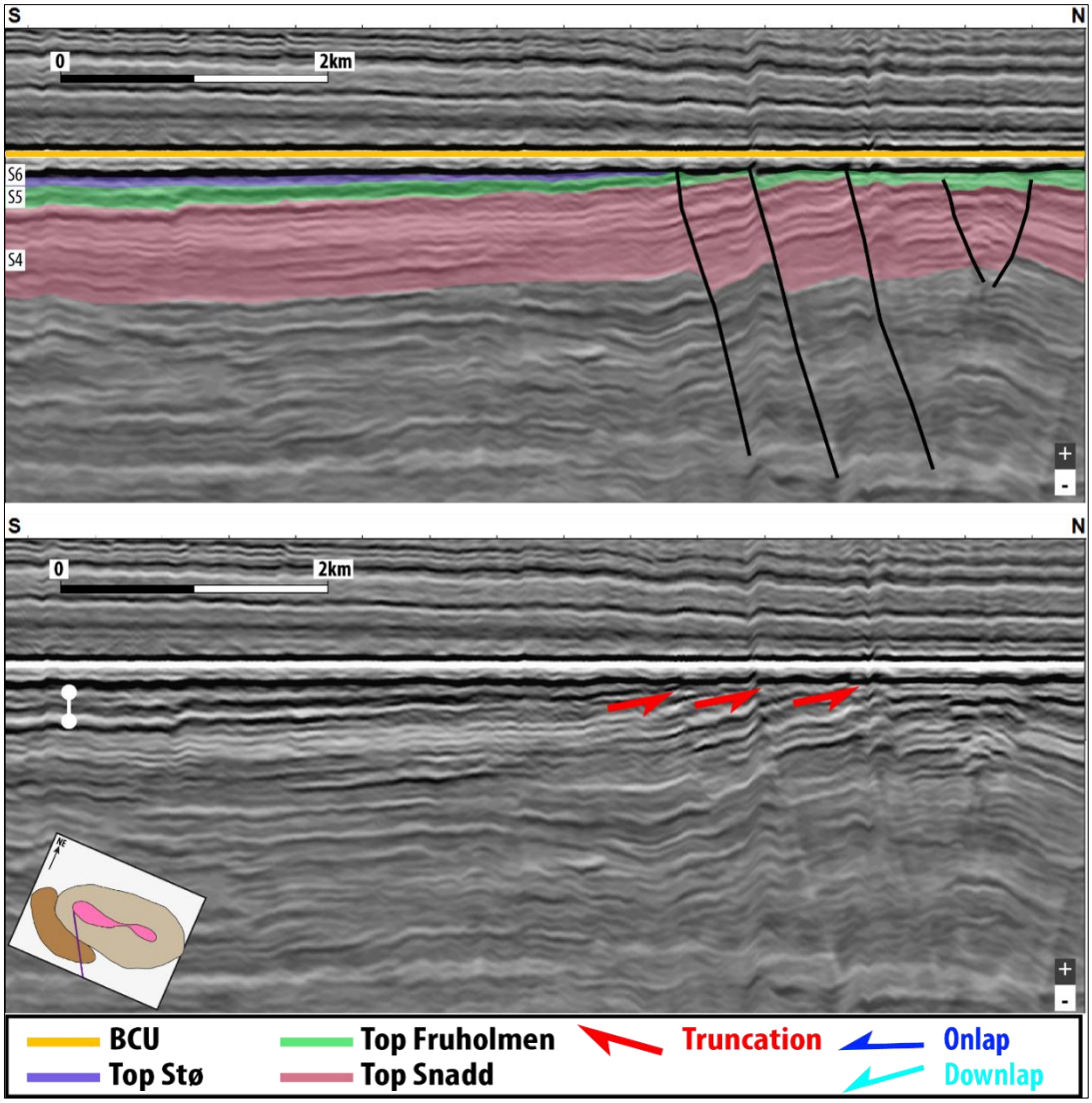

Figure 5.18: *Seismic section flattened on BCU with truncation of sequence S5 (Fruholmen Formation) from the south towards the Signalhorn Dome. The upper section illustrates where the different formations are present, while the bottom shows terminations and thickness variations. White circles connected by white lines display the thickness variations. Seismic data courtesy of Schlumberger Multiclient.*

5.2.5 Hettangian-Bajocian (S6; Tubåen, Nordmela and Stø formations)

The sequence S6 is bounded by Top Stø Formation, and Top Fruholmen Formation interpreted horizons and comprises the Tubåen, Nordmela, and Stø formations (Figure 4.4). The Top Stø Formation surface has a depth reaching from ca. -700 ms on Signalhorn Dome to ca. -1400 ms in the rim-syncline (Figure 5.19a). The surface is generally shallowing towards the south and deepening towards the northwest. The strata within sequence S6 terminate on the salt wall in the northwestern part, while in the central and southeastern, the sequence subcrops below the thin Quaternary cover.

The sequence S6 has a significant thickness increase from almost not present on the Signalhorn Dome to more than 75 ms within the basin (Figures 5.19c and 5.20A). The rim-syncline surrounds the entire salt wall, representing one significant depocenter. The sequence S6 thins above the southeastern part of the Signalhorn Dome, as apparent by thin thickness patches compared to the northwestern part. The thickness map shows minor thickening of the sequence towards the north.

The upper Jurassic seismic sequence displays minor thinning in the center of the Signalhorn Dome (Figure 5.21C). The rim-syncline shows signs of presence, evident by the sequence thickening. Two depocentres are located within the northeastern rim-syncline and minor thickening towards the north. The sequence is generally thinning towards the south, where it is recorded as a ca. 25 ms thick sequence (Figure 5.21C).

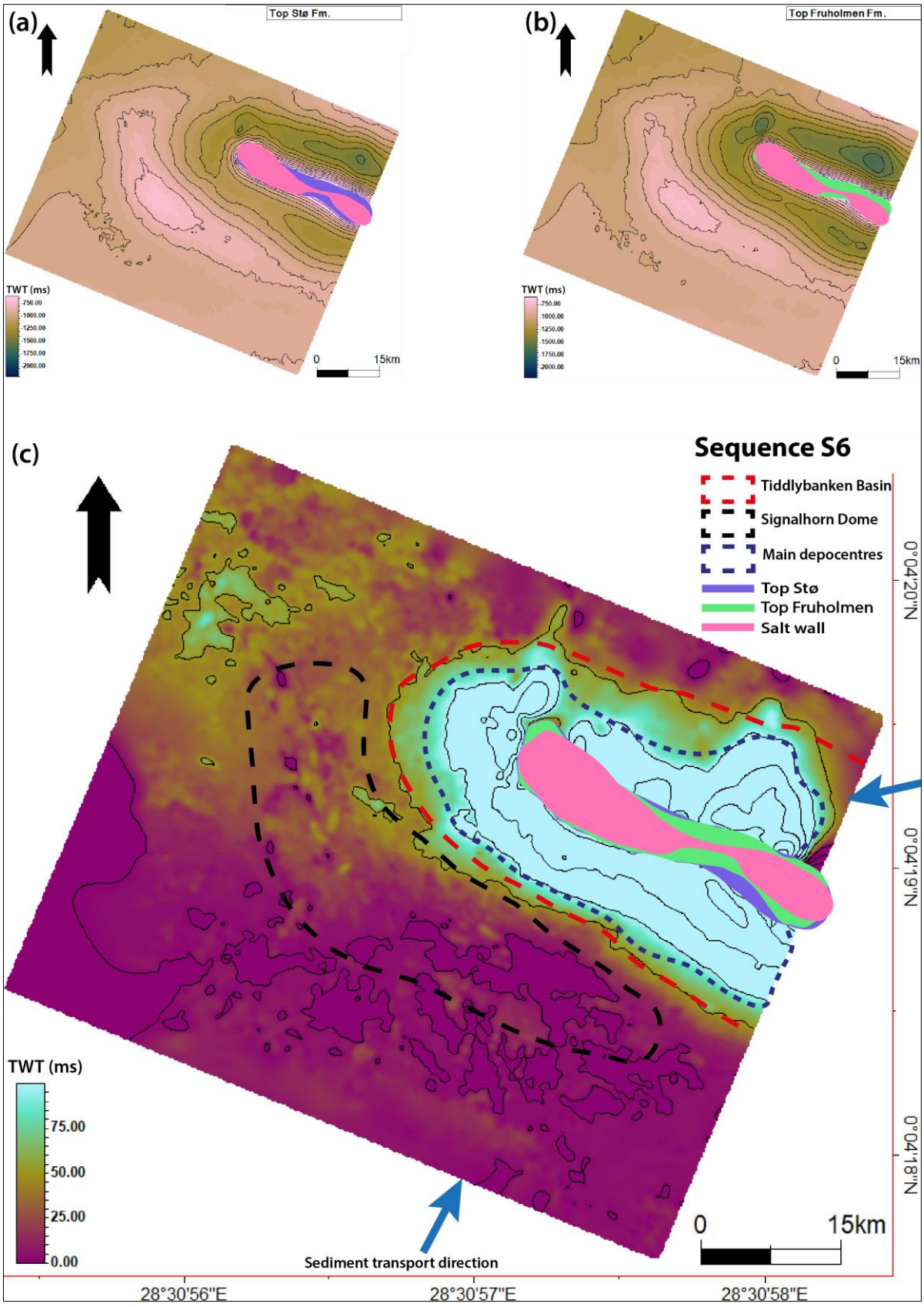

Figure 5.19: ***(a)*** *Time-structure map of Top Stø Fm.* ***(b)*** *Time structure map of Top Fruholmen Fm.* ***(c)*** *Isochron map of the seismic sequence S6 (Tubåen, Nordmela, and Stø formations) displaying major depocentres along the salt wall inside the Tiddlybanken Basin. Note the shift of the thickest depocentres during the evolution signifying the salt evacuation from different segments of the basin. Seismic data courtesy of Schlumberger Multiclient.*

Sequence S6 has continuous growth towards the basin and subcrops below the thin Quaternary cover in the southeastern part of the salt wall. The sequence is primarily present within the basin, whereas it thins and onlaps towards the Signalhorn Dome. The sequence S6 is further subdivided into four sub-sequences based on the seismic reflections pattern and apparent thickness. The sub-sequence (1) has an apparent onlapping on sequence S5, where the reflections are thick and wavy compared to the sub-sequence (2) (Figure 5.20B). Sub-sequence (2) is also onlapping Top Fruholmen Formation and thins towards the Signalhorn Dome, where the internal seismic reflections are parallel and continuous. Sub-sequence (3) is different from the other sub-sequences as the reflections display diffuse and dimmed characteristics with a wedge-shaped geometry. The internal reflections eventually merge into one distinct reflection towards the Signalhorn Dome that pinches out further northeast than the other sub-sequences (Figure 5.20B). The seismic sub-sequence (4) has continuous and parallel reflections that thin towards the Signalhorn Dome.

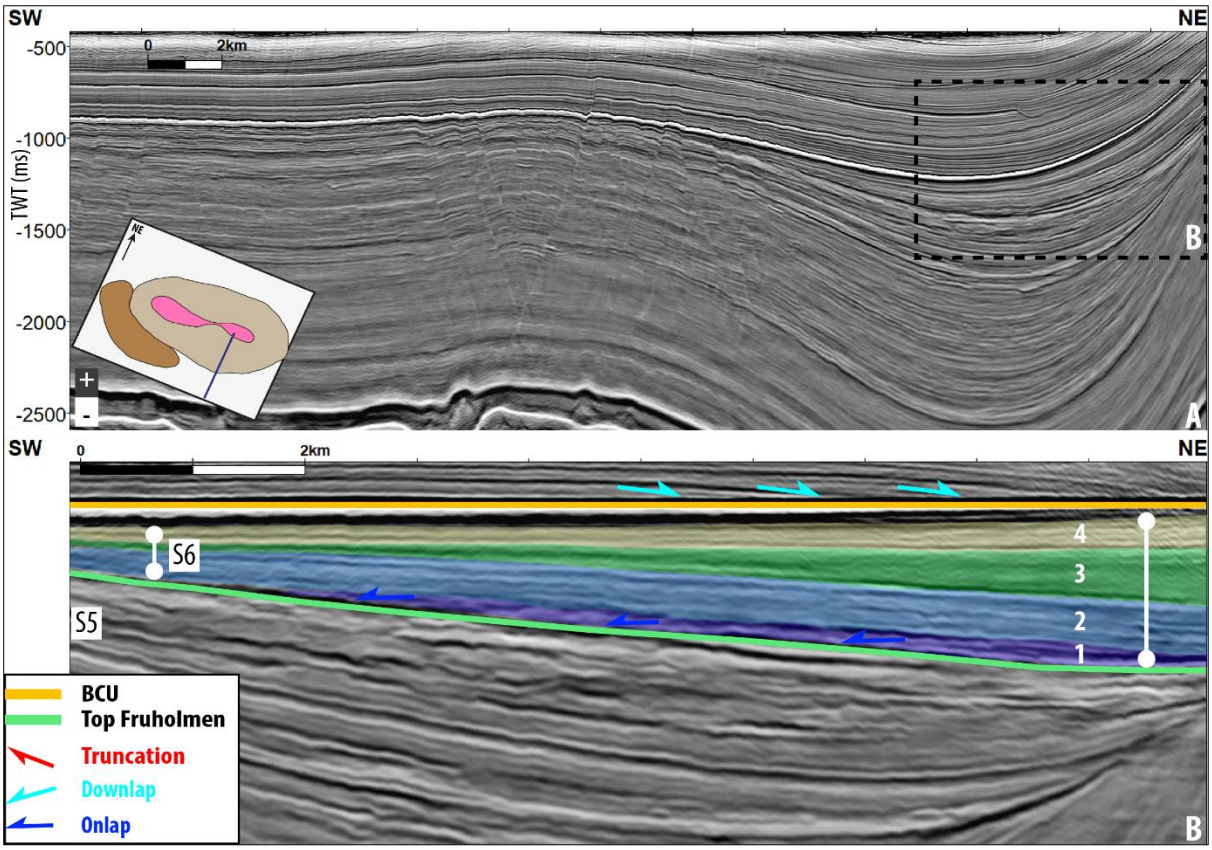

Figure 5.20: A) *Seismic section overview.* ***B)*** *Flattened seismic section on BSU showing drastic thickening of sequence S6 towards NE. Seismic data courtesy of Schlumberger Multiclient.*

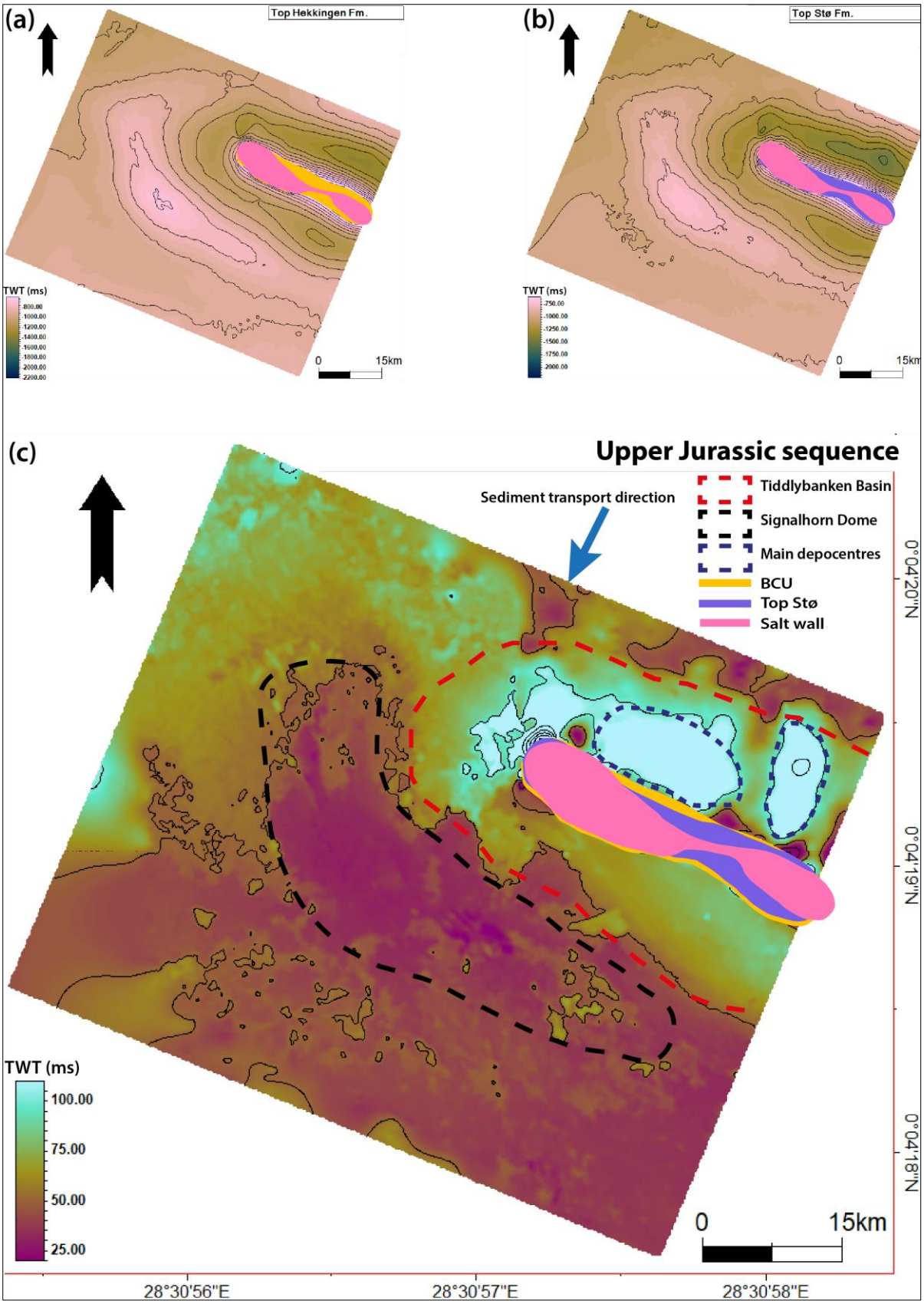

Figure 5.21: (a) *Time-structure map of Top Hekkingen Fm.* ***(b)*** *Time structure map of Top Stø Fm.* ***(c)*** *Isochron map of the upper Jurassic seismic sequence displaying major depocentres along the salt wall inside the Tiddlybanken Basin. Note the shift of the thickest depocentres during the evolution signifying the salt evacuation from different segments of the basin. Seismic data courtesy of Schlumberger Multiclient.*

5.2.6 Cretaceous

The lowermost Cretaceous strata onlap to the Base Cretaceous Unconformity (BCU), whereas the reflections upturned along the salt wall flanks and subcrop below the thin Quaternary cover (Figure 5.5, 5.7, and 5.9). The Cretaceous strata display significant erosion above the Signalhorn towards the western and southwestern margins.

5.3 Stratigraphy and facies analysis

The low resolution of conventional seismic data often obscures our understanding of the stratigraphic units incomplete development in the subsurface. Therefore, the presence of the two wells 7132/2-1 and 7132/2-2 are essential reference points for a detailed seismic interpretation and to understand the stratigraphic framework (Figures 4.4 and 5.22). This chapter focuses on descriptions of the stratigraphic units in the Tiddlybanken Basin.

5.3.1 Havert Formation (Sequence S1: Induan)

Description

The Havert Formation (sequence S1) is 1510 m thick in well 7132/2-2 and comprises high-value, serrated GR signals with internal funnel-shaped and bell-shaped higher GR-response (Figure 5.22). The base of the sequence has a strong seismic reflector that coincides with a pronounced shift in the well-log trend (Figure 5.22). Sequence S1 has a uniform thickness across the area that internally comprises parallel, medium-strong amplitude reflections.

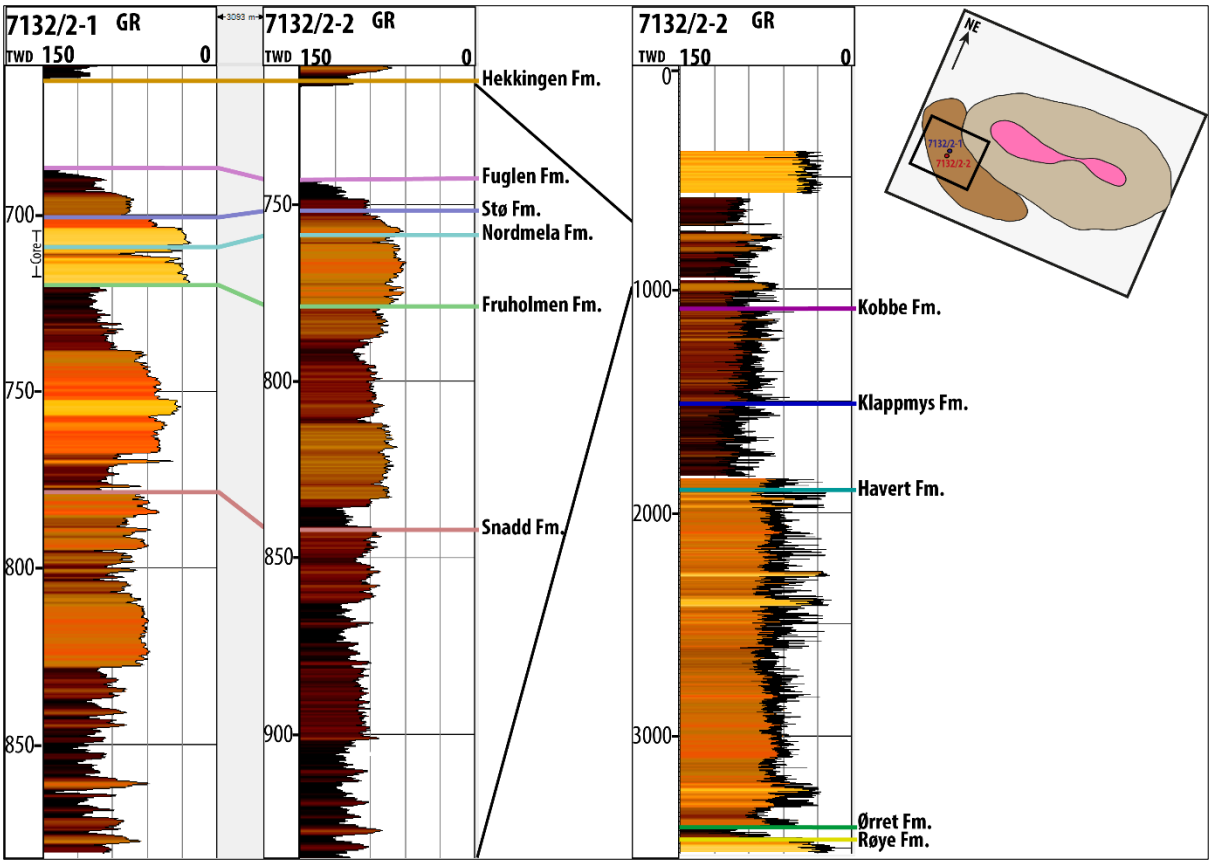

Figure 5.22: *Well correlations illustrating thickness variations in the Realgrunnen Subgroup, gamma-ray logs, and formation tops. The position of the interpreted core is shown to the left in brown color, and below it is an overview map with the location of the two wells. The low GR-values of Havert and the lowermost part of Klappmyss formations are due to a log shift and do not reflect an increase in sand content.*

Interpretation

Parallel reflections suggest steady depositional rates on a flat, uniformly subsiding surface, such as a basin plain. The serrated GR-motif reflects a heterogeneous lithology where high values represent an open marine environment (Strecker et al., 1999). The low GR values with bell-shaped characters represent sandstones deposited in channels, while the funnel shapes can be characterized as sheet floods or crevasse splays (Nystuen et al., 2014). The Havert Formation comprises an inter-bedded sequence between siltstone and shale, representing a deltaic depositional environment.

5.3.2 Klappmys Formation (Sequence S2: Olenekian)

Description

The Klappmyss Formation (sequence S2) is 426 m thick in well 7132/2-2. The base is marked as a transition to generally low GR-values and blocky units to a more serrated, cylinder-shaped higher-value GR-response (Figure 5.22). The strong base reflection coincides with a sharp increase in GR values. Sequence S2 has a uniform thickness across the area that slightly decreases towards the salt wall (Figures 5.4, 5.7, and 5.9). Reflections within the unit are sub-parallel and medium-strong. Base reflectors downlap locally within the basinal area.

Interpretation

The increasing GR-value suggests more fine-grained deposition, reflecting a deltaic to marginal marine environment. Lower GR-response in the upper part of the sequence indicates coarser material, which could reflect some channels. The sequence's uniform thickness and parallel seismic reflections indicate a stable depositional environment with constant subsidence, except for thinning towards the salt wall.

5.3.3 Kobbe Formation (Sequence S3: Anisian)

Description

The Kobbe Formation (sequence S3) is 386 m thick in well 7132/2-2. The transition from sequences S2 and S3 does not show a significant change in the well-log. Sequence S3 shows a similar trend as sequence S2, with high GR-response, a serrated cylinder shape, and a slight coarsening upward trend (Figure 5.22). Blocky low GR-values are present in the upper part of the formation, displayed as ca. 5-10 m thick units. Medium-strong seismic amplitude reflections with frequent swales characterize this package. Scattered high amplitude swaley/lensoid reflections and downlapping reflectors within the basin are observed.

Interpretation

The serrated GR-response indicates interbedded shale with sandstone, while lensoid reflections commonly indicate channelization (Schwab et al., 2007). The sequence S3 shows various

depositional environments, where a high gamma-ray value indicates shales and a low response sandstone. The low-value peaks and blocks in the GR-log indicate channels that characterize the upper part and can be interpreted as a deltaic to inner neritic environment. Based on the high-value GR-log curve peaks, the lower part of the sequence reflects a more marginal marine to deltaic paleoenvironment.

5.3.4 Snadd Formation (Sequence S4: Ladinian-Early Norian)

Description

The Snadd Formation (sequence S4) is 205 m thick in well 7132/2-2. The well-log displays a gradual transition from S3 into the sequence S4 (Figure 5.22). Serrated high-value GR-response dominates in well 7132/2-2, while intervals with serrated bell-shapes or blocky low-value GR-signals dominate well 7132/2-1. The thickness of the blocky low GR-value units is measured up to ca. 25 m and thinner peaks of ca. 5-10 m. The gamma log of 7132/2-1 displays an upward coarsening trend, while the 7132/2-2 displays an upward fining trend.

Parallel to sub-parallel seismic reflections with a medium to high amplitude reflection dominate the sequence. The lower package (sequence S4a) comprises stacked, discontinuous, and more complex reflections, while the upper package (sequence S4b) is characterized by more parallel reflections (Figure 5.12). Two distinct reflections within the basin are parallel and have a very strong amplitude reflection, were weaker, more chaotic reflections onlaps the strong reflections. Internal reflections are dominantly sub-parallel with frequent swales and lenses that occasionally concentrate and stack to form larger bowl-shaped, incising features (Figures 5.11 and 5.17).

Interpretation

The serrated GR-response indicates an interbedding between sandstone (low-value GR) and shale (high-value GR). The well log data suggests a prograding deltaic environment in the study area during the Carnian. The detailed paleoenvironment could be interpreted as deltaic to marginal marine, but lacustrine-fluvial deposits are also apparent (Figure 5.22). Lensoid reflections, bell-shaped curves, and low GR-values indicate channelization (Schwab et al.,

2007). The high-amplitude reflection on the seismic sections illustrates truncation patterns below and onlapping above, indicating a subaerial unconformity internally in sequence S4 (Base Carnian Unconformity). Sub-parallel, chaotic reflections dowlapping towards the basin might indicate derived alluvial fans (Figure 5.12).

Depositional elements

Generally, three channel systems are observed and described at different stratigraphic levels within sequence S4 (Figures 5.23 and 5.24). These channels are described in detail from deepest to shallowest stratigraphic level.

An enormous channel system is recognized in the sequence S4 (Figure 5.23). The system has an S-N orientation and dominates the southwestern margin of the Tiddlybanken Basin. Well 7132/2-2 is drilled through one of the big channels in this system (Figures 5.11 and 5.23). The main channel shows evidence of lateral accretion and sinuosity in the northwestern part of the study area, while towards the south, smaller distributary channels dominate (Figure 5.23). Lateral accretion of up to 10 km indicates low avulsion frequency during this time. Meandering channels with a medium degree of sinuosity have an isolated character and are generally observed in the southwestern and southeastern parts of the area.

In sequence S4b (above the Base Carnian Unconformity), a distinct channel (channel type 1) cross-cuts the northwestern salt wall in a NE-SW direction and continues in a southeastern direction (Figure 5.24).

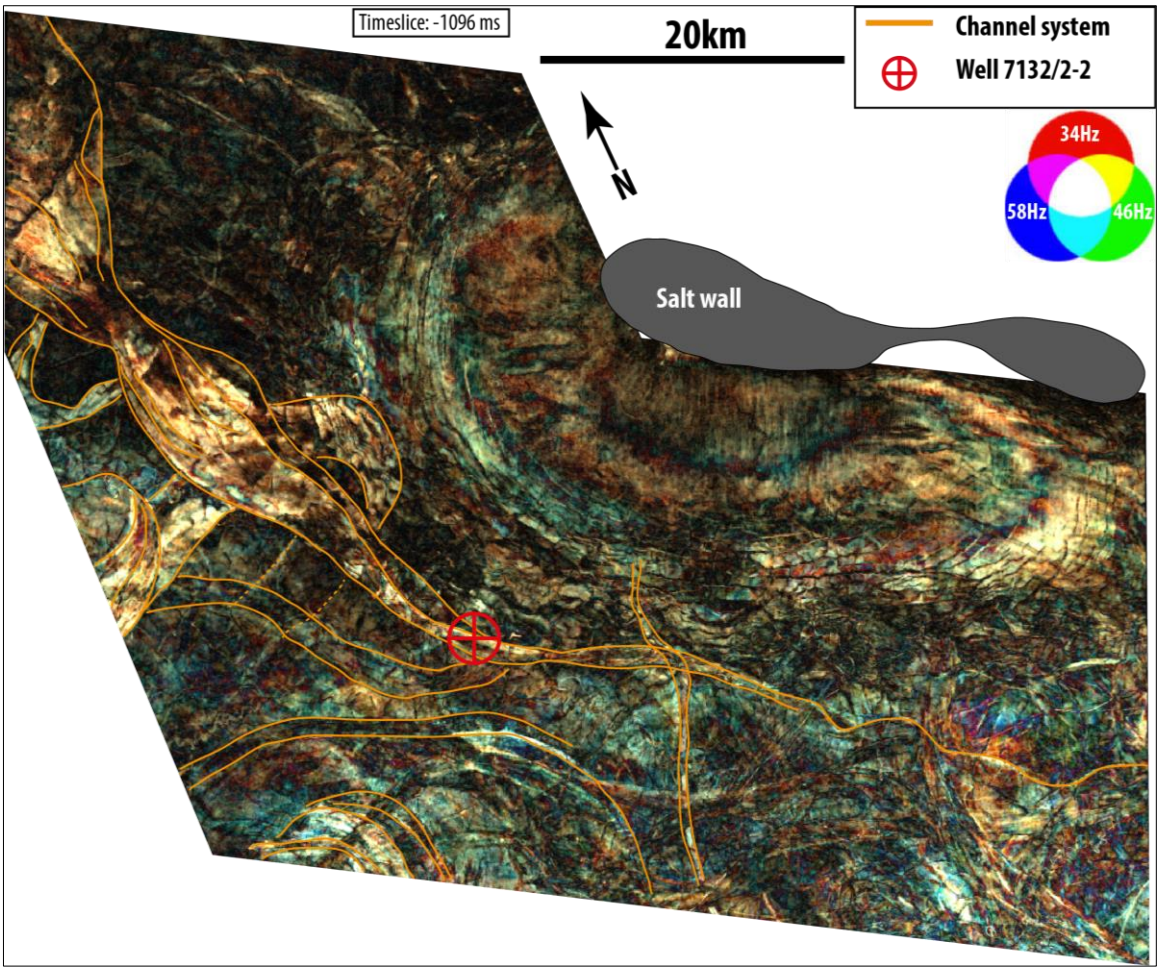

Figure 5.23: *Representative spectral decomposition attribute map of the lower part of sequence S4 (timeslice -1096). The RGB blend cube was flattened at -1000 ms. Channel systems located on the Finnmark Platform are colored in orange. Seismic data courtesy of Schlumberger Multiclient.*

Channel type 1 is most likely covering the entire salt wall. Observations of channels crossing the salt wall have significant importance on the salt mobilization evolution (discussed in 6.1.3). The available 3D-seismic cube (ST14004) does not cover the rest of the Tiddlybanken Basin, hindering mapping the complete channel pathways. Channel type 1 accreted laterally up to 2 km and is highly sinuous. A high sinuosity feature is interpreted as an expansion of a point-bar with a near channel cut-off that might become an ox-bow lake later (Figure 5.24C). Channel type 2 is a low sinuosity channel system located on the Finnmark Platform and most likely dominated the entire platform (Figure 5.24B). The interpreted channel type 2 has an S-N orientation that splits into two branches indicating avulsion and shows minor signs of lateral accretion and low sinuosity.

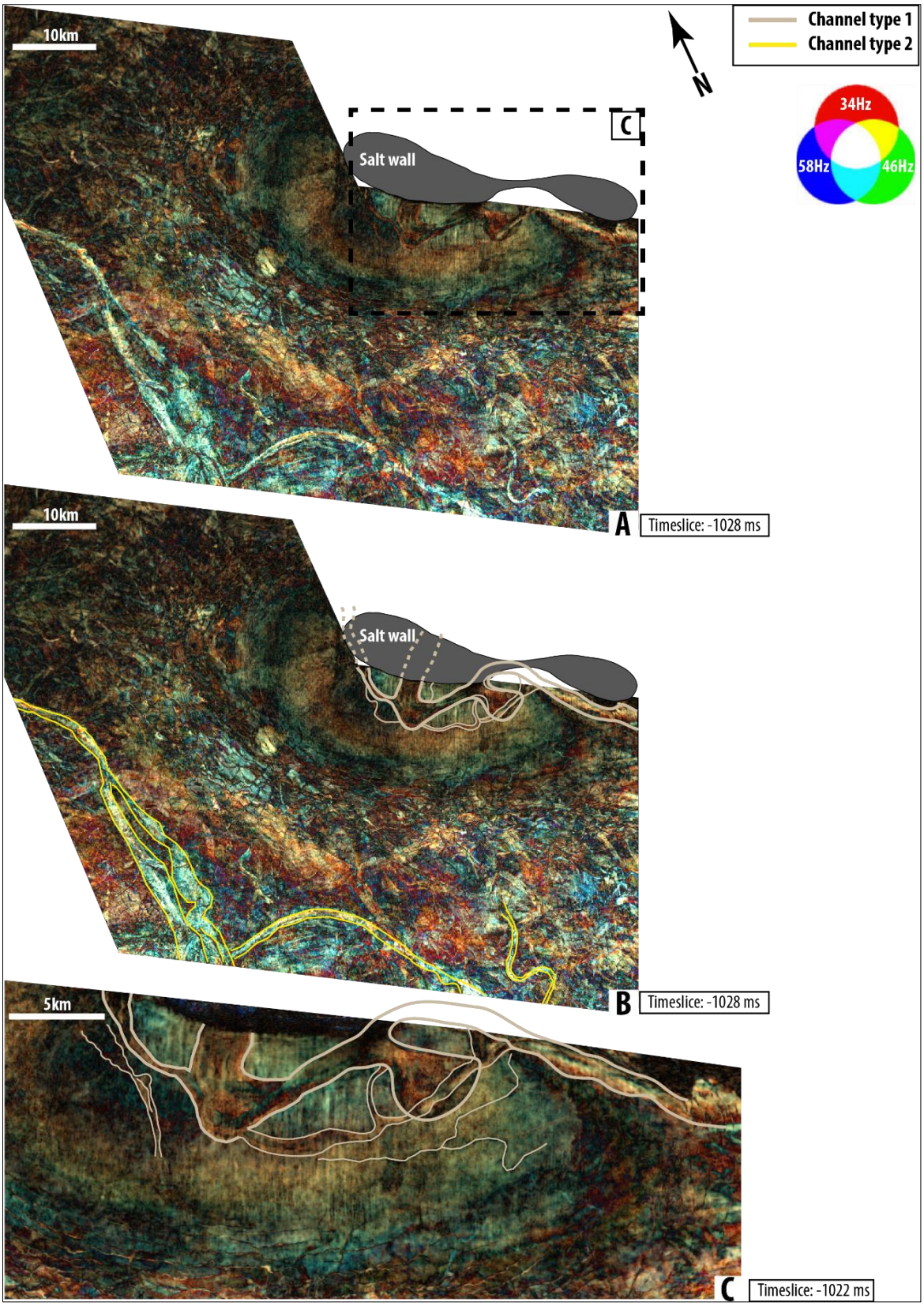

Figure 5.24: *Spectral decomposition attribute maps of timeslice -1028 to -1022 from sequence S4. The RGB blend cube was flattened at -1000 ms.* ***(A)*** *Uninterpreted overview map of the area. Inset locates figures B and C.* ***(B)*** *Channel interpretation of two different channel systems (-1028 ms). The youngest channel system is colored in yellow and the older in beige.* ***(C)*** *Zoom-in illustrates the channel system crosscutting the salt wall at timeslice -1022 ms, indicating an inactive salt wall during deposition of a particular package related to sequence S4 (Snadd Formation). Seismic data courtesy of Schlumberger Multiclient.*

5.3.5 Fruholmen Formation (Sequence S5: Norian-Rhaetian)

Description

The Fruholmen Formation (sequence S5) is 62 m thick in well 7132/2-2 and 60 m thick in well 7132/2-1. The biostratigraphy indicates the presence of an unconformity between Nordmela and Fruholmen formations, nearly 40 m.y. is missing in the two wells. The report from well 7132/2-1 states that middle Norian to ?Hettangian is missing, while in well 7132/2-2, middle Norian to ?Toarcian is missing. The well-log from well 7132/2-2 displays a high-value GR-response with a predominantly serrated cylinder, bell, and funnel-shaped curve (Figure 5.22). The well-log from 7132/2-1 shows high-value GR-response in the upper and lower part. A low-value serrated egg-shaped block dominates in the center and comprises a thickness of nearly 30 m. The low-value peak is ca. 5 m thick, corresponding to a thick sand layer.

A distinct high-frequency seismic reflection marks the base of the sequence that corresponds to the shift from low to high gamma response. The thickness variation is highly variable. The sequence S5 thickens considerably in the basin where medium-strong amplitude reflections with parallel to sub-parallel features are present in the lower part. In contrast, the upper part of sequence S5 is more chaotic and swaley. Internal high amplitude seismic reflections are present within the basin with typical strong troughs character. Where the sequence is thin, a strong reflector separates sequence S4 from sequence S5 (Figure 5.18). Internally, strong seismic reflections with frequent swales and lenses form large bowl-shaped incised features.

Interpretation

The high GR-value intervals represent mudstone-rich periods, indicating deltaic to marginal marine deposits, while the blocky, low-value intervals represent amalgamated sandstones. Fining-upward well-log responses and lateral accreting reflections likely reflect bar migration (Schwab et al., 2007). The egg-shaped low GR-response in well 7132/2-1 can be interpreted as bar migration (Figure 5.22). Spots of bowl-shaped, high amplitude seismic reflections might indicate channel deposits. The rim-syncline comprises large amounts of what seems to be migration of channel bars (Figure.5.17), where the channel follows the topography towards the north.

Depositional elements

In the lower part of sequence S5, a channel crosscutting the central part of the salt wall is observed with an NNW-SSE orientation (Figure 5.25B). Channel type 2 exhibits lower sinuosity than the other channels in the dataset and may have formed in a more distal position in the depositional system. Smaller meandering channels were sourced from the margin, indicating a relatively low gradient towards the rim-syncline. Shallower in the sequence S5, a meandering channel formed within the rim-syncline (Figure 5.25C). Channel type 1 developed into a meandering channel with high lateral accretion and sinuosity in the uppermost part of sequence S5. The channel belt has a SE-NW orientation and reaches a width of 6 km due to lateral accretion.

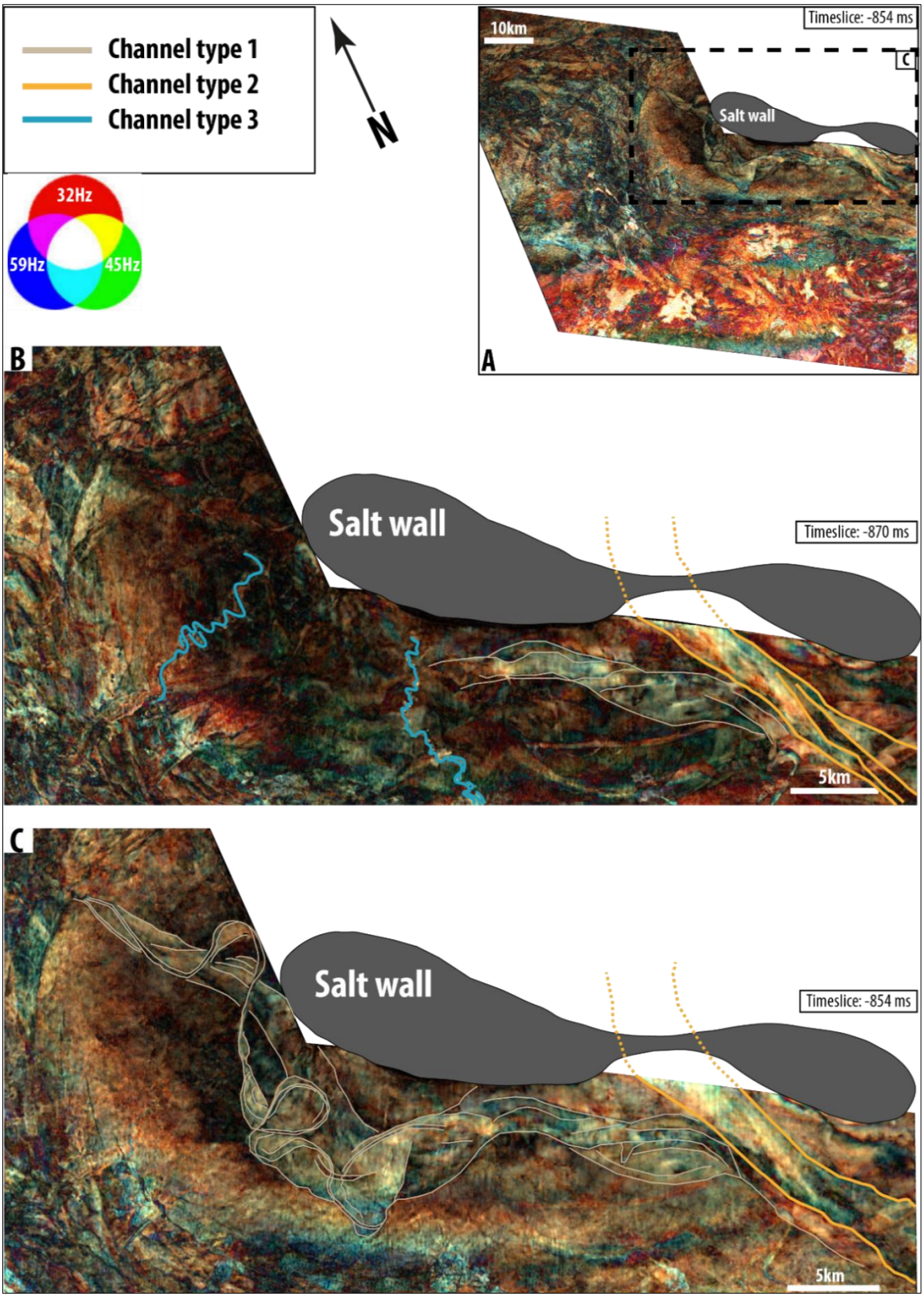

Figure 5.25: *Spectral decomposition attribute maps of timeslice -870 to -854 from the sequence S5. The RGB blend cube was flattened at -855 ms.* ***(A)*** *An overview map of the area. Inset locates figures B.* ***(B)*** *The lower part of sequence S5 (-870 ms) illustrates an older channel system (orange) crosscutting the central part of the salt wall. Signs of a younger channel system (beige) start to form in the rim-syncline. Smaller channel fills (blue) sourced from the Signalhorn Dome indicate erosion on the dome.* ***(C)*** *A significant meandering channel system developed within the rim-syncline in the uppermost part of sequence S5 (-854 ms). Seismic data courtesy of Schlumberger Multiclient.*

5.3.6 Tubåen, Nordmela, and Stø formations (Sequence S6: Hettangian-Bajocian)

Description

The Nordmela and Stø formations are 27 m thick in well 7132/2-2 and 20 m thick in well 7132/2-1. The two well logs from this sequence are displayed differently due to a shift in the GR-log (Figure 5.22). Well 7132/2-1 generally shows low GR-values, including a cylinder-shaped block at the bottom and a bell shape at the top. The transition from sequence S5 to S6 is significant, as it shifts from relatively high GR-response to low. Well 7132/2-2 is characterized by serrated higher GR-response and no distinct base separating sequence S5 to S6.

Sequence S6 is thicker in the basin and is characterized by bifurcated and lensoid seismic reflections. In some areas of the basin, the sequence S6 becomes quite chaotic. The transition from sequence S5 to S6 is a high-amplitude reflector that marks the shift from high-value GR-response to a smooth cylinder shape with low GR-values (Figure 5.22). Towards the salt wall, the high amplitude reflections become more distinct, parallel, and eventually onlap to the salt wall in the northwestern part of subcroppes below the thin Quaternary cover in the southeastern.

The core from well 7132/2-1 is 12 meters which includes Stø and Nordmela formations (Figure 5.26). The Nordmela Formation is composed of three upward fining units, separated by thin mudstone beds with coal, plant fragments, and root structures The sandstones at the base of these FU-units consist of poorly sorted quartz-rich sandstone units with rip-up clasts and quartz pebbles. The sandstones are cross-bedded near the base, while planar bedding dominates towards the top. An erosive unconformity separates the Nordmela Formation from the Stø Formation. The Stø Formation consists of very coarse-grained sand at the base, while it consists of more medium-grained sand in the upper part. Some subtle traces after parallel lamination are observed in this thin sandstone package. There is no direct evidence from the biostratigraphy of marine influence, but the presence of the microplankton Schizocystia rara in the Nordmela Formation might suggest nearshore or brackish environment.

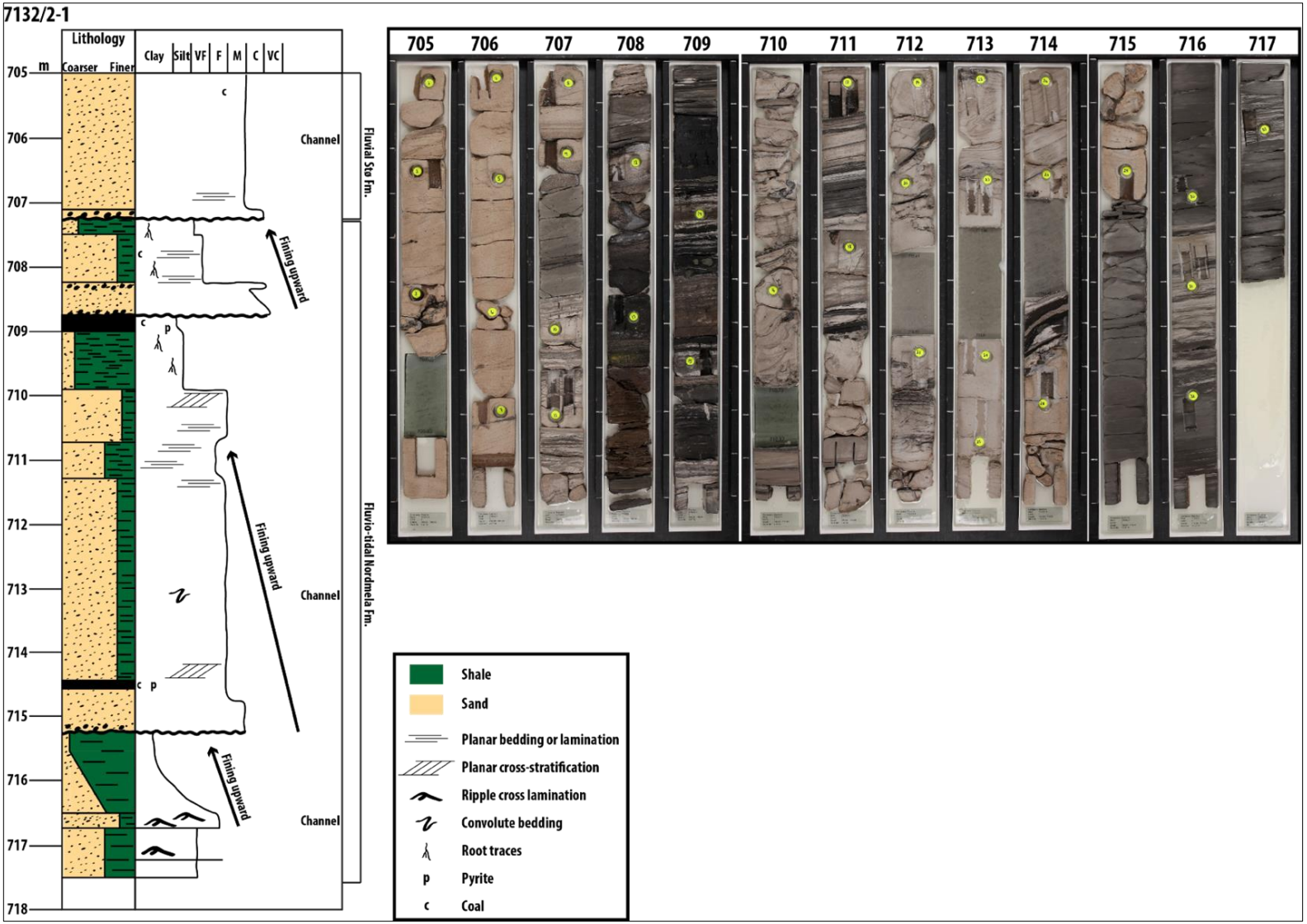

Figure 5.26: *Illustration of a brief core interpretation and core photos of the analyzed well 7132/2-1. The Nordmela Formation comprises fluvio-tidal deposits throughout the core, while the lower Stø Formation comprises fluvial channel deposit*

Interpretation

The sudden abrupt change in GR-signal value across the boundary between sequences S5 and S6 reflects an influx of large quantities of sand (Figure 5.22). The Nordmela Formation is composed of mainly sand-rich marginal marine to deltaic deposits. The Stø Formation show an overall upward fining trend, indicating a relative transgression. Different channel deposits of ca. 5 m are observed in the core and the GR log. The interpreted Stø Formation probably represents fluvio-tidal to a marginal marine environment

Depositional elements

Within the lower part of sequence S6, three different channels are mapped. The lowermost channel (channel type 1) has a similar trend as channel type 2 in sequence S5 and displays an NW-SE orientation that crosses the central and southeastern part of the salt wall (Figures 5.25B and 5.27B). Channel type 1 has low sinuosity and broad area coverage (ca. 4 km) and is the oldest one in this package (Figure 5.27B). In the upper part of the sequence S6 channel type 2 becomes a high-sinuosity channel with an NW-SE orientation. The meandering channel with migrated bars appears to be an extension of a possible tidal inlet (Figure 5.27C). The youngest channel system (channel type 3) is thinner with no signs of accretion (Figure 5.27D). Channel type 3 shows a more E-W orientation that most likely extends above the salt wall.

Three channelized features are observed in the upper part of sequence S6 (Figure 5.28). Two of the channels are more or less straight, with minor to no signs of sinuosity. These are interpreted as tidal inlets 1 and 2 due to their straight geometry, minor widening towards the basin, and sudden termination (Figure 5.28B). Tidal inlet 1 is relatively significant, cutting the southeastern salt wall with a NE-SW orientation. The NE-SW oriented tidal inlet 2 is smaller, displays bending character, and crosses the northeastern part of the salt wall. On the other hand, a thin meandering channel is observed entering the basin in the central part with a NE-SW orientation. Towards the uppermost part of the sequence S6, wavy features interpreted as possible coastlines have a SE-NW orientation and dominate where the present rim-syncline is (Figure 5.28C). The apparent tidal inlets displayed in the RGB-blends indicate a relative transgressional sequence and a more marine-influenced environment during deposition of the Stø Formation.

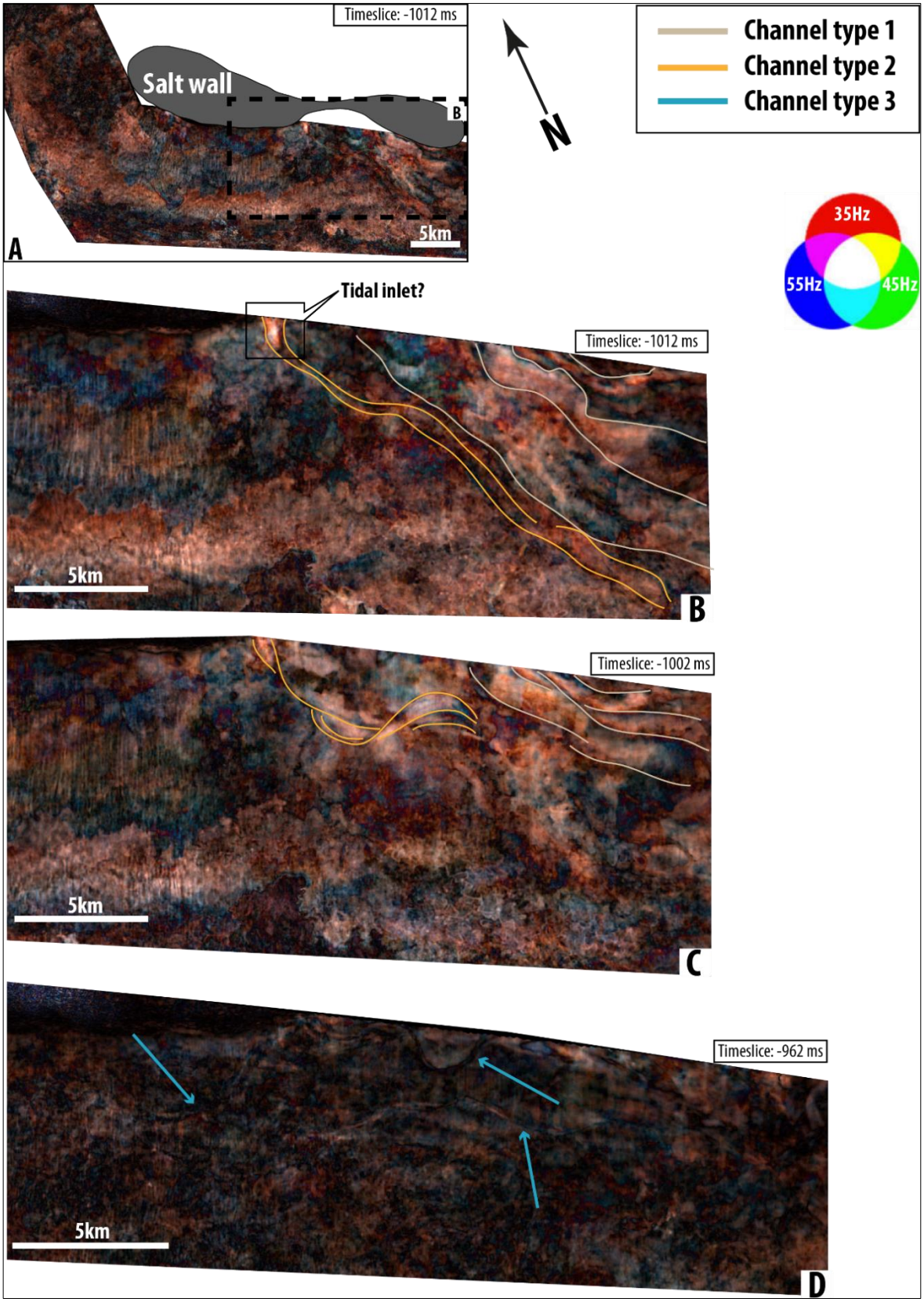

Figure 5.27: *Spectral decomposition attribute maps of timeslice -1012 to -962 from the sequence S6. The RGB blend cube was flattened at -993 ms.* ***(A)*** *An overview map of the area. Inset locates figures B, C, and D.* ***(B)*** *The lower part of sequence S6 illustrates an older channel system (Channel type 1) crosscutting the central part of the salt wall.* ***(C)*** *Shallower in the sequence, signs of a younger channel system (Channel type 2) start to form a more meandering system up from the possible tidal inlet.* ***(D)*** *A meandering channel system (Channel type 3) developed along and above the salt wall. Seismic data courtesy of Schlumberger Multiclient.*

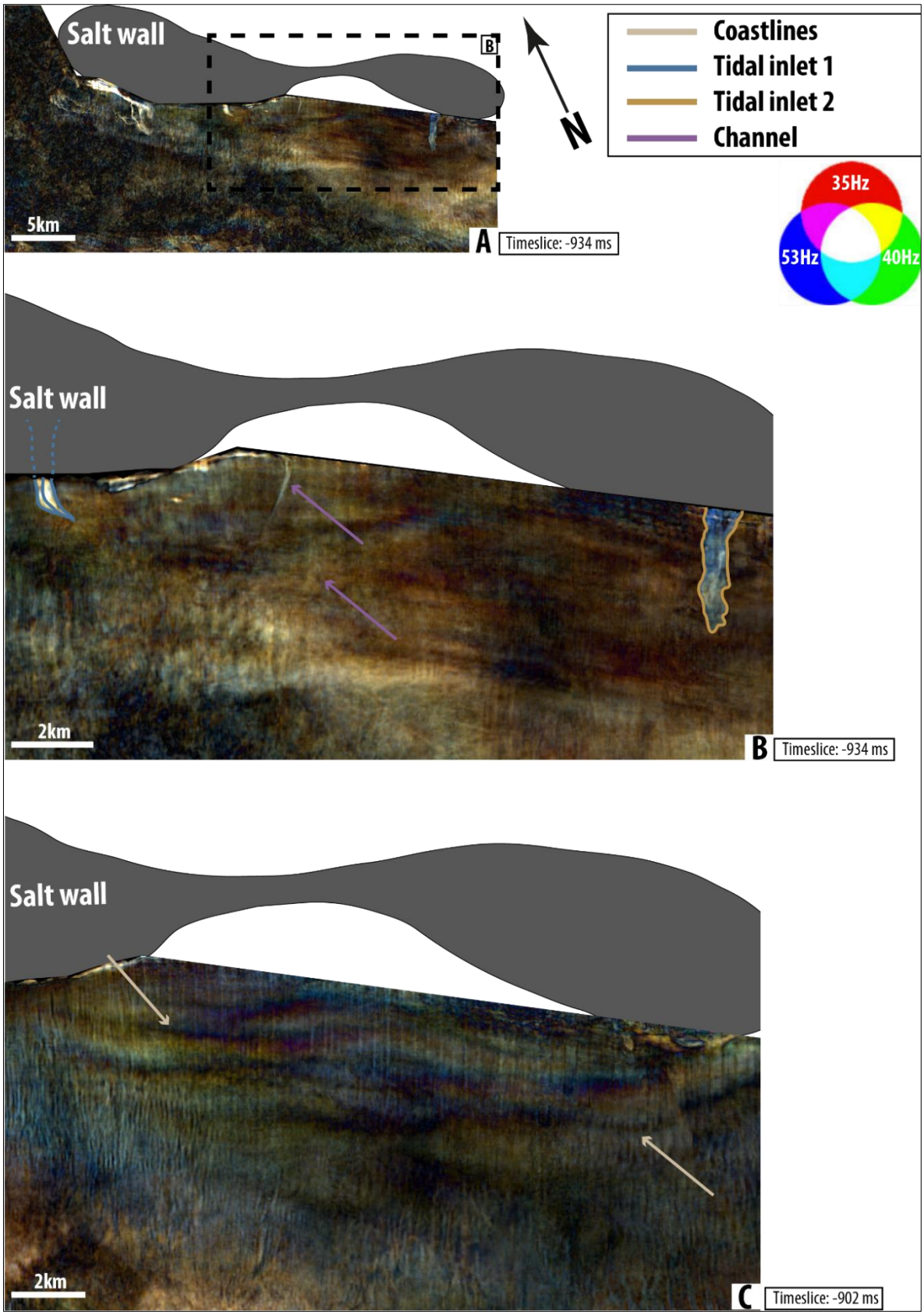

Figure 5.28: *Spectral decomposition attribute maps of timeslice -934 to -902 from the sequence S6. The RGB blend cube was flattened at -918 ms.* ***(A)*** *An overview map of the area at timeslice -934. Inset locates figure B.* ***(B)*** *Time slice -934 ms shows possible tidal inlets and channel systems at the top of sequence S6.* ***(C)*** *Time slice -902 ms shows possible coastlines prograding towards the salt wall. Seismic data courtesy of Schlumberger Multiclient.*

6 Discussion

In the previous chapter 5, the structural evolution and stratigraphic architecture/infill patterns were presented. In this chapter, results are used to discuss the timing and triggering mechanisms for salt mobilization (section 6.1) and the impact of structural development on sediment distribution (section 6.2) by integrating thickness maps, attribute maps, well and core data correlation. Moreover, suggestions for further work are presented in section 6.3.

6.1 Timing and triggering mechanisms for salt mobilization

6.1.1 Minor salt mobilization (earliest Triassic)

During Induan-Olenekian, prograding sedimentary systems entered from the southeast and were deposited during regional subsidence and tectonically stable conditions (Figure 2.8c)(Gilmullina et al., 2020; Glørstad-Clark et al., 2010; Klausen et al., 2015). The sedimentary wedge of sequence S1 (Havert Formation) that entered the study area triggered salt mobilization due to differential loading (Figure 3.7). The continuous deposition of sequence S2 (Klappmys Formation) resulted in the formation of a salt pillow structure (Figures 3.2 and 3.7). Growth of the salt structure during deposition resulted in a discordant contact with the sequence S1 and a syn-kinematic infill in the rim-syncline (Figures 5.6 and 5.8). The salt pillow development occurred at different rates along the strike due to the variability in Pennsylvanian to early Permian layered evaporites. The northwestern part of the salt pillow moved more rapidly during deposition of sequence S2 (Klappmys Formation) than in the southeastern part.

The pillow structure was earlier believed to have developed due to contractional stresses related to the Permo-Triassic Uralian Orogeny to the southeast (Figure 3.3b)(Rowan & Lindsø, 2017). The generally uniform thickness of sequences S1 and S2 infers that no tectonic events were active during this time, except for abrupt thickness change commonly seen near the salt wall (Figures 5.5, 5.8, and 6.1). This confirms the study by Hassaan et al. (2020b) that salt mobilization was initiated by differential loading.

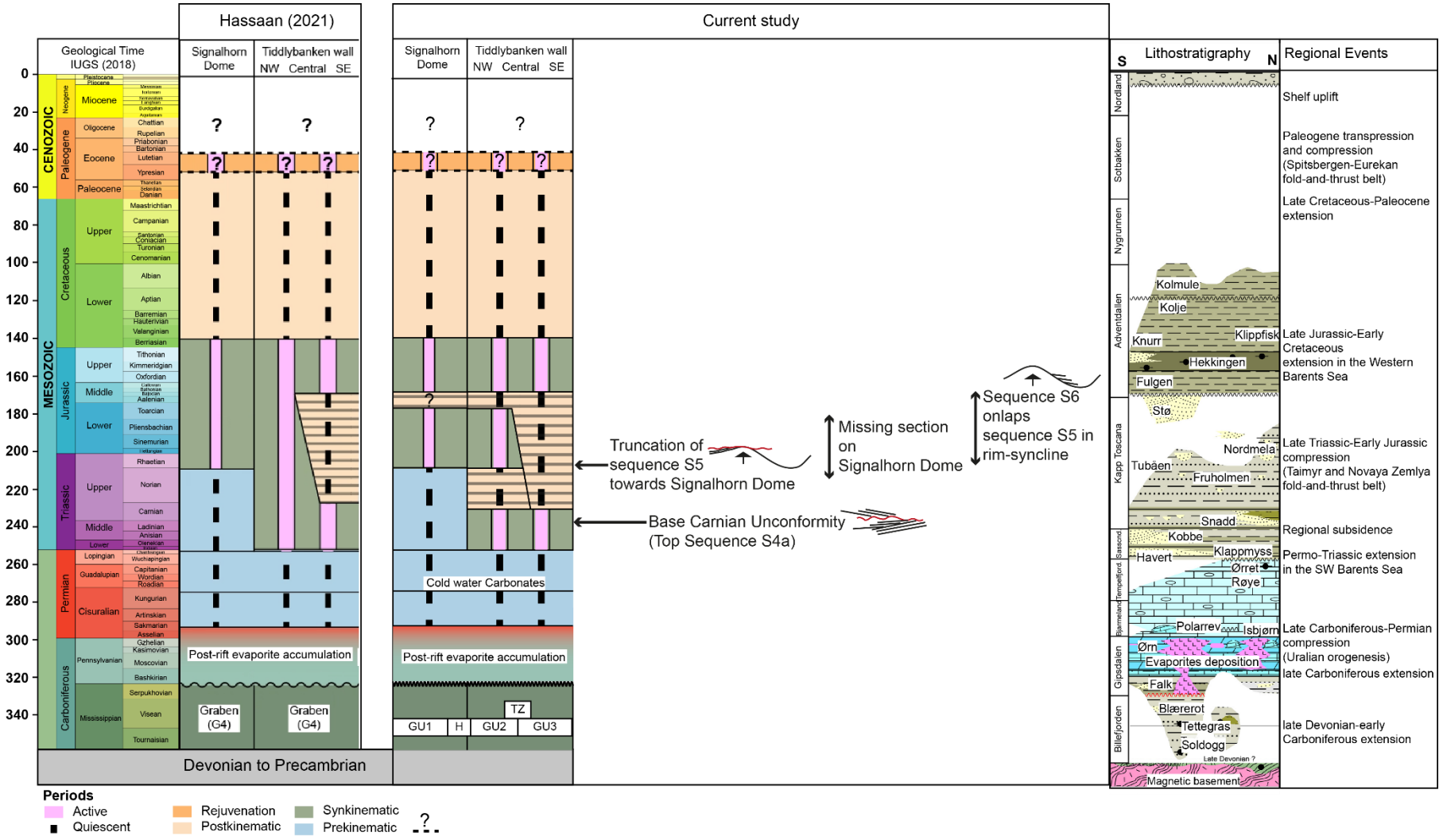

Figure 6.1: *Comparison between Hassaan (2021) and the current study of the growth timing of the evaporite-cored Signalhorn Dome and salt mobilization in the Tiddlybanken Basin. Different stages (i.e., prekinematic, synkinematic, postkinematic, and rejuvenation) show age relations between the time of overburden deposition and the time of salt flow (Jackson and Talbot, 1991; Jackson and Hudec, 2017). Pink bars represent the salt mobilization phases, while the dashed lines highlight the quiescent phases. Key observations from figure 5.2, lithostratigraphy, and regional event.*

6.1.2 Pedestal and Pillow development (Middle Triassic)

During Anisian, sequence S3 (Kobbe Formation) was deposited around the salt pillow, which enhanced the salt withdrawal and created a large salt pedestal in the northwestern part and a well-developed pillow structure in the southeastern part (Figures 3.2 and 3.7) (Hassaan et al., 2020b). The variable halite feeding caused differences in the salt structure from the post-rift evaporite layers and pre-salt half-graben architecture (Figures 2.5 and 2.7). Sequence S3 displays thinning towards the flanks of the salt wall, indicating that the sequence was deposited during movement of salt (Figures 5.6, 5.8, and 6.1), creating a syn-kinematic infill pattern in the rim-syncline and discordant contact with the underlying sequence S2 (Figure 5.12).

6.1.3 Salt piercement and passive diapirism (Middle-Late Triassic)

During Ladinian, the salt wall growth continued as the sequence S4a (lower Snadd Formation) was deposited (Figures 5.14 and 6.1). As the salt wall rose towards the surface, the overburden eroded, and the rim-syncline subsided, forcing the salt to move into the growing salt wall (Figure 3.8). The sequences S1, S2, S3, and S4a were uplifted and eroded in the earliest Carnian, creating an angular unconformity, named Base Carnian Unconformity, above and near the salt wall (Figures 5.5, 6.3, and 6.4). Distinct truncation patterns and upturned sequences are observed throughout Tiddlybanken Basin (Figures 5.5, 5.6, and 5.7). Previous studies, (Hassaan et al., 2020b; Rowan & Lindsø, 2017) interpreted Top Kobbe Formation to be the unconformity that is, in this study, interpreted to be a Base Carnian Unconformity (Figure 5.15). Therefore, it is considered that the erosion of the underlying sequences happened later than earlier believed. The extra load from sequence S4a, along with Havert (S1), Klappmys (S2), and Kobbe (S3) formations, in the rim-syncline caused differential compaction, forcing the salt to move into the growing salt wall (Figures 3.2, 3.7, and 3.8). Enough movable salt was available in the study area, causing doming and erosion of the sequences surrounding the salt wall (Figures 3.3b and 3.7).

In the northwestern part, erosion of the roof allowed the salt to pierce through the thin deposits above and commence passive diapirism (Figure 3.4). As salt-withdrawal continued, the rate of

subsidence increased in the rim-syncline as the thick sequence S4 deposited and created syn-kinematic infill patterns. The sequence S4b (upper Snadd Formation) terminates on the salt wall creating hook halokinetic sequences (Figure 5.5, 5.16, and 6.2B) (*sensu* Giles and Rowan, 2012) as also observed by Hassaan et al. (2020b). The stacked hook halokinetic sequences create tabular composite halokinetic sequences (CHS), which means that the sediment accumulation rate is relatively slow compared to the salt wall growth. Typically, a thin layer of sediments is deposited above the salt wall, and due to the significant availability of halite, the roof repeatedly fails. Major depocentres were created in the northwestern part of the rim-syncline after deposition of sequence S4b (upper Snadd Formation). The sequence S4 has a greater thickness in the northwestern part of the rim-syncline than the southeastern, indicating that the subsidence increased towards the northwestern part after the uplift and erosion from the Base Carnian Unconformity (Figures 5.14 and 5.15).

The salt structure did not reach further than a pedestal stage in the less halite-rich central and southeastern parts, but due to the development of a structural high, the sequence S4b (upper Snadd Formation) thins towards the salt wall (Figures 5.6 and 5.8). However, sequence S4b also covered the salt wall, resulting in upturning of the sequence due to the main rejuvenation phase in Eocene (Figure 6.2A). Subcropping of a sequence below the thin Quaternary cover indicates that the sequence earlier covered the salt wall, but later the salt penetrated through.

The evolution of the salt wall during this stage shows apparent differences between the northwestern, central, and southeastern parts (Figures 5.5, 5.7, and 5.8). The southeastern and central parts lacked mobile halite in the layered evaporitic sequence (Figures 2.7, 5.7, and 5.8)(Hassaan et al., 2020b). The thickest mobile halite-rich lithology was accumulated in the northwestern part of the basin, causing penetration of the overburden (Figure 2.7)(Hassaan, 2021). The transfer zone acted as a physical barrier between the mobile halite-rich lithology and the non-mobile/mixed lithologies (Figure 2.5), which later impacted the amount of erosion of older sediments in the northwestern part of the salt wall versus the central and southeastern. This highlights the significant role of halite in the evolution of individual salt structures and the infill processes in rim-synclines (Figures 2.7 and 6.2).

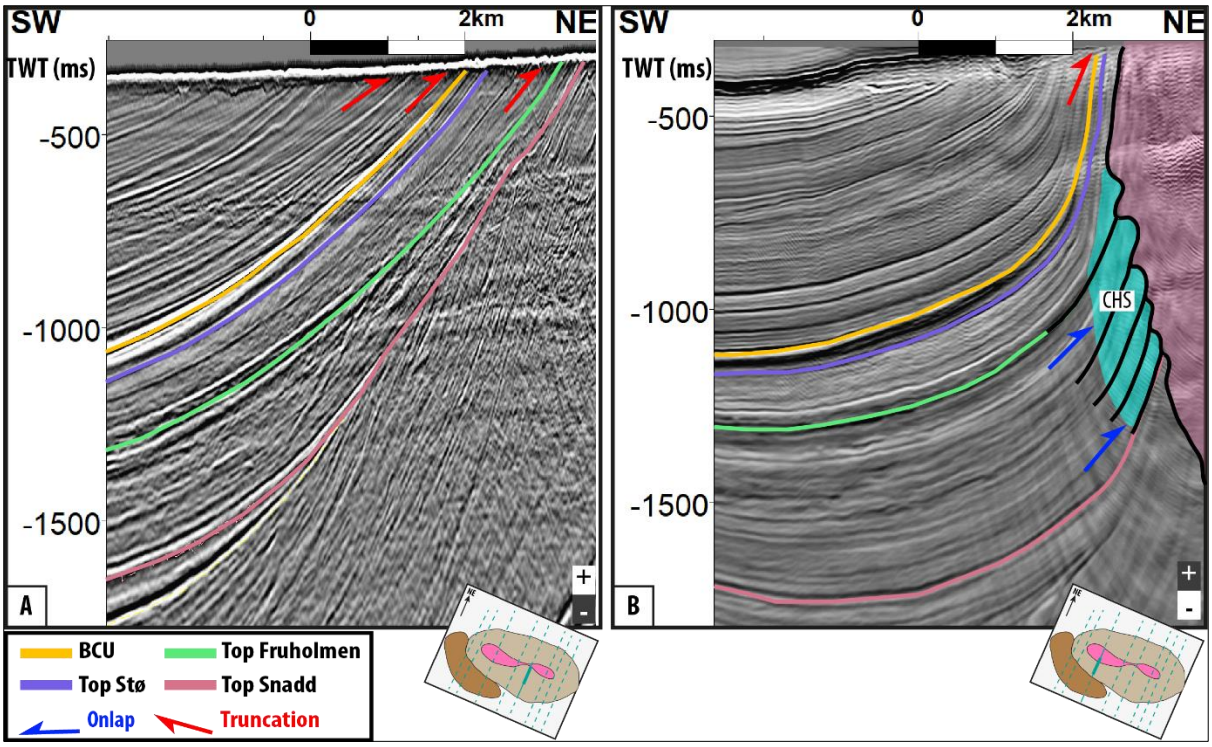

Figure 6.2: ***(A)*** *Sequences subcrops below the thin* Quaternary cover*, indicating inactivity of salt during the deposition.* ***(B)*** *Sequences terminate on the salt wall, indicating salt wall growth during deposition of the sequences. Seismic data courtesy of Schlumberger Multiclient.*

Salt mobilization locally controlled sediment accommodation throughout the western Barents Sea, including the Maud and Nordkapp basins (Glørstad-Clark et al., 2010; Hassaan, 2021; Rojo & Escalona, 2018). In the current study, evidence of repeated salt wall growth has been somewhat diachronous at different stratigraphic levels. During the active phase of the salt wall in the early-middle Triassic, depocenters formed at different locations within the rim-syncline, which would also impact the channel routing (Figures 5.14 and 6.5). During late Carnian, the salt wall became inactive due to lack of mobile halite or thick overburden (Figures 2.5, 2.7, and 6.1). Channel systems formed above the salt wall, which is major evidence of inactivity (see sections 5.3.4 and 6.2.1 for more details). This falsify the hypothesis in earlier studies by Rowan & Lindsø (2017) and Hassaan et al. (2020b), which believed passive diapirism continued from middle Triassic to upper Jurassic in the northwestern part of the salt wall (Figure 3.4).

6.1.4 Minor rejuvenation phase (Late Triassic)

Major depocenters have preserved a significantly thick sequence S5 (Fruholmen Formation) within the rim-syncline (Figure 5.16C); however, the sequence S5 shows extensive thinning towards the Signalhorn Dome (Figure 5.17). The sequence S5 displays a thickness of ca. 60 m in the two wells and presumably preserves a thickness greater than 700 m within the rim-syncline, as documented in sections 5.3.4 and 5.4.5.

The northwestern part of the salt wall comprises a very thick sequence S5 (Fruholmen Formation) that passively filled the rim-syncline as the basin subsided (described in section 5.3.4). The sediment loading and compaction drove the subsidence of the rim-syncline, and less dense salt moved out from the subsiding area into the rising salt wall (Figures 3.1 and 3.8). However, the sedimentation rate versus growth of salt wall controls the basin-infill geometries (Figures 3.6 and 3.10). The sequence S5 terminates on the salt wall, creating hook halokinetic sequences (elaborated in the previous section; Figures 3.6 and 6.2).

In the central and southeastern parts of the salt wall is sequence S5 thinner within the rim-syncline and reached only to pedestal stage during this minor rejuvenation phase (Figure 6.1). The sequence S5 subcrops below the thin Quaternary cover and shows no signs of tinning towards the salt wall, meaning that the sequence was deposited above the salt wall in a continuously subsiding local basin (Figure 6.4). Differential deposition of sequence S5 within the Tiddlybanken Basin was controlled by the availability of mobile halite within the study area (elaborated in chapter 2 and the previous section).

Thinning and onlapping towards the Signalhorn Dome indicate that a structural high was present, resulting in periods of condensation and non-deposition (Figures 5.16C, 5.17, and 6.3). Thickness variations observed in the study area within the sequence S5 (Fruholmen Formation) have also been observed in nearby areas. The Fruholmen Formation (S5) deposits are relatively thin on the Bjarmeland Platform, ca. 50 m, while on the Atlantic margin and in the Eastern Barents Sea, it has a thickness of 579 m (Gilmullina et al., 2020).

Seismic sections of the Signalhorn Dome display truncation patterns indicating an angular unconformity on the dome (Figures 5.18 and 6.3). The biostratigraphic reports from the two

wells on the Signalhorn Dome record a missing section from middle Norian to ?Toarcian in 7132/2-2 and from middle Norian to ?Hettangian in 7132/2-1, representing a time gap up to 40 m.y. Similar truncation patterns are also documented elsewhere in the Barents Sea, for example, on the Svalis Dome (Müller et al., 2019; Müller et al., 2022, in press), suggesting that there has been a significant erosional event during the Triassic-Jurassic transition. The current study shows that when the Signalhorn Dome was developed, it resulted in tilting and erosion of a thick Fruholmen Formation (sequence S5) during the Triassic-Jurassic transition, which has not been observed in previous studies of the Tiddlybanken Basin (Figure 5.18). Hassaan et al. (2020b), Rowan & Lindsø (2017), and Reppen (2016) did not discover distinct truncation patterns on the dome, in addition to a missing section displayed in the previously (2019, released in 2021) drilled wells.

The angular unconformity in sequence S5 can be related to far-field compressional stresses from Novaya Zemlya (Figures 2.2 and 2.8a). These stresses reactivated the pre-salt Carboniferous rift structures, resulting in salt structure growth, uplift, and erosion of the sequence S5 on the Signalhorn Dome (Figures 5.5, 5.6, and 6.3), as also inferred by Hassaan et al. (2020b). However, the Novaya Zemlya fold-and-thrust belt was moving during the late Triassic-early Jurassic (220-190 Ma) (Buiter et al., 2007), which means that the stresses could have started to affect the study area already during the early-middle Norian.

The lower part of sequence S5 shows a more parallel reflection configuration, interpreted as an uniform deposition in a subsiding basin with no salt activity (Figure 6.3). The upper part is different and displays more chaotic reflections and a greater thickness increase in the rim-syncline (Figures 5.4, 5.5, and 5.6). The salt wall seemes to have been rejuvenated during the deposition of upper part of sequence S5, based on the RGB-blends and signs of internal thickness variations. This may be due to the inversion of the Carboniferous rift system which occurred during upper Triassic-lower Jurassic. Salt withdrawal accelerated and caused increased subsidence and therefore increased thickness of the upper sequence S5 (Figures 5.5 and 5.16). This may infer that the propagating stresses reached the study area during late Norian. The propagated stresses are interpreted as the cause of other structures throughout the Barents Sea through inversion of older structures. The Haapet and Veslekari domes and the composite West Fedynsky (two domes informally named Alpha and Beta) were also most likely generated from the propagating stresses (Figure 1.1) (Hassaan, 2021). A regional uplift

has been interpreted based on the truncation trends in the Northern Barents Sea Basin. The reactivation of older structures aligns with the ongoing Novaya Zemlya fold-and-thrust belt in the east (Müller et al., 2019). Correlation across the Barents Sea shows that lower to upper Triassic strata is tilted and overlain unconformably by onlapping lower to middle Jurassic strata (Figure 6.3). Pronounced truncation of middle to upper Triassic deposits on the southern Finnmark Platform suggests that the Norwegian mainland also experienced uplift and erosion in the latest Triassic (Müller et al., 2019).

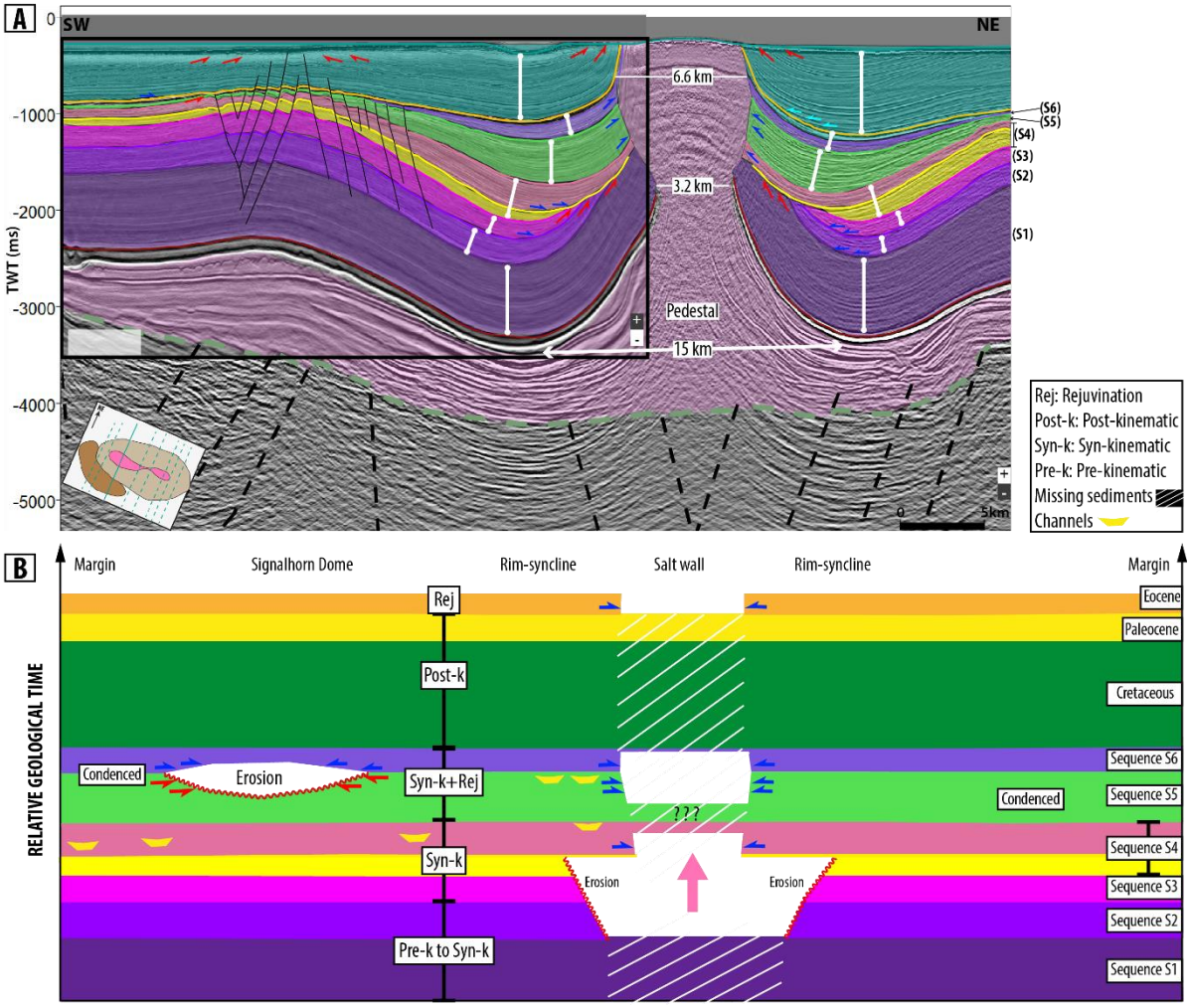

Figure 6.3: (A) *Interpreted seismic section in the northwestern part of the salt wall.* ***(B)*** *The wheeler diagram demonstrate the temporal change of local salt growth processes that have created genetic stratal depositional patterns adjacent to the salt wall. The wheeler diagram is a 2D representation of the interpreted seismic sections with relative geological time as the vertical axis and space in meters as the horizontal axis. Seismic data courtesy of Schlumberger Multiclient.*

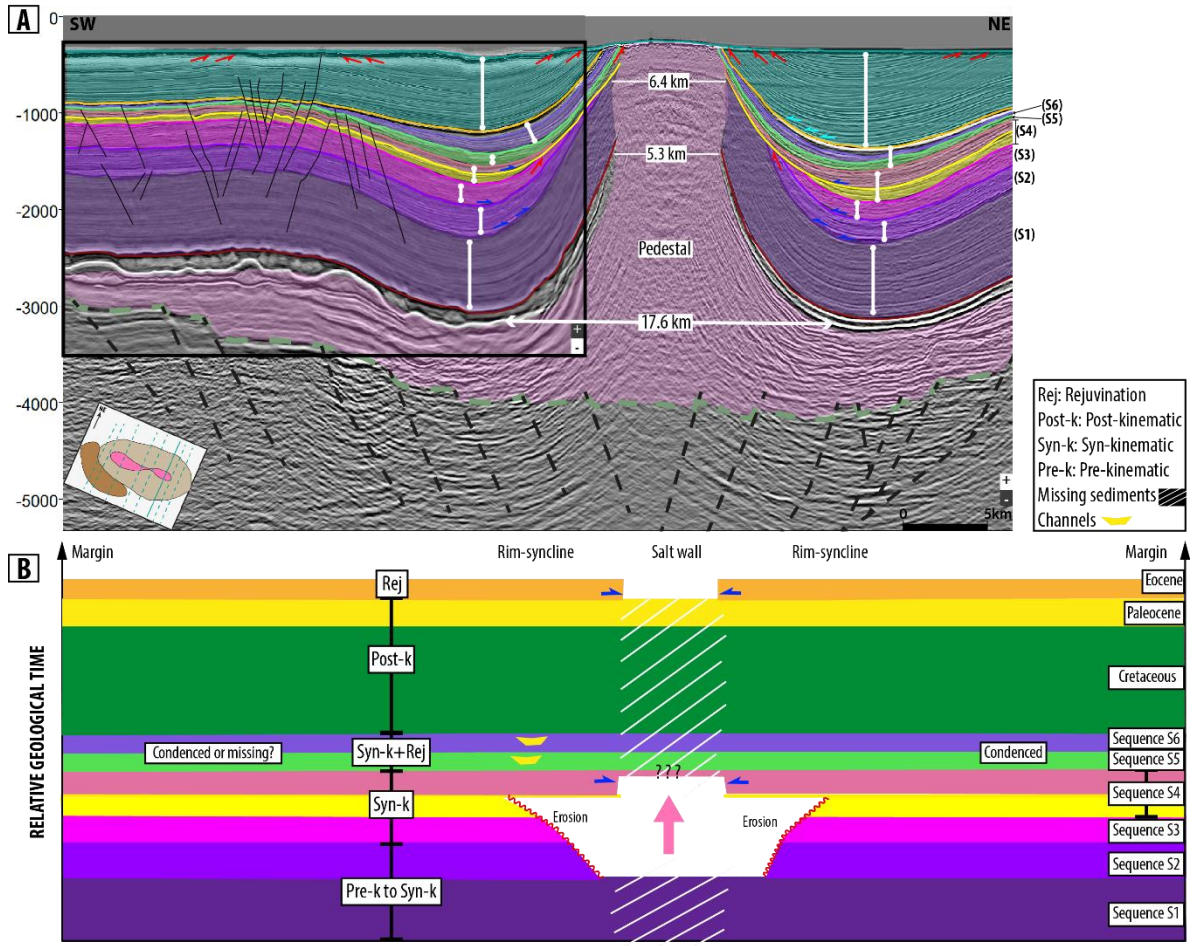

Figure 6.4: ***(A)*** *Interpreted seismic section in the southeastern part of the salt wall.* ***(B)*** *The wheeler diagram demonstrate the temporal change of local salt growth processes that have created genetic stratal depositional patterns adjacent to the salt wall. The wheeler diagram is a 2D representation of the interpreted seismic sections with relative geological time as the vertical axis and space in meters as the horizontal axis. Seismic data courtesy of Schlumberger Multiclient.*

Far-field compressional stresses from a fold-and-thrust belt like Novaya Zemlya may significantly affect smaller-scale structures. Compressional stresses cause reactivation and inversion of older structures (Hassaan et al., 2020a), resulting in the development of new structures (e.g., domes) and salt mobilization on a local scale, even from great distances. Erosion of the uplifted structures will later be eroded, for instance, the erosion of the sequence S5 (Fruholmen Formation) on the Signalhorn Dome (Figure 6.3).

Thickness increases and terminations towards the salt wall commonly indicate that the salt wall was active; however, this study suggests that it is more complex. The salt wall was likely active in pulses, discussed in more detail in section 6.2, causing different infill architecture at different levels within the rim-syncline, as observed in the upper and lower package of sequence S5 (Figures 5.4 and 5.5). However, the Signalhorn Dome is interpreted to be active during the

entire late Triassic-early Jurassic (Figure 6.1). Because the sequence S5 (Fruholmen Formation) is eroded after the doming, determining if the Signalhorn Dome was also active in pulses could be challenging. This clearly highlights that the far-field stresses affecting the study area are more complex than earlier believed.

The upper part of sequence S4 (Snadd Formation) and the lower part of sequence S5 (Fruholmen Formation) were allowed to deposit above the entire salt wall during the inactive period in Carnian-Norian (Figures 5.24 and 5.25). As shown in RGB blends in section 5.4.4, a channel system crossed the northwestern part of the salt wall during late Carnian (Figure 5.24C). Besides, an extensive low-sinuosity channel system crossed the southeastern and central parts of the salt wall during deposition of lower part of S5 (Figure 5.25B). Therefore, the salt wall is interpreted to be inactive during late Carnian-early Norian, as also discussed in more detail in sections 6.2.1 and 6.2.2. Additionally, the upper package of sequence S4 and lower package of sequence S5 are displayed as more evenly thick packages (Figures 5.4 and 5.5).

During Norian-Rhaetian, the northwestern salt wall was rejuvenated and penetrated through its overburden (Figure 5.5, 6.3, and 6.5). Passive diapirism in the northwestern part of the salt wall accelerated, causing a thickness increase in the upper part of sequence S5 within the rim-syncline towards the salt due to accommodation creation (Figures 3.4 and 5.16C). The channel system that earlier crossed the salt wall re-routed along the salt wall into the subsiding rim-syncline (Figure 5.25C).

Hassaan et al. (2020b) concluded that the northwestern part of the salt wall was active during the entire deposition of sequence S5 based on thickness maps, which can also be seen on the thickness maps from this study (Figure 5.16C). This highlights the importance of analyzing and integrating several variants of data. It is important to integrate both well data, if its available, detailed seismic interpretation, including stratigraphic- and seismic facies analysis. The additional spectral decomposition attribute maps from the detailed seismic interpretation is used to image channel systems within the area, revealed the salt wall's inactivity during a period that was first believed to be active. This shows that an integrated interpretation approach of the detailed depositional sequences is needed to fully understand the salt basins evolution.

A detailed integrated analysis, like the one performed in this study, is essential to get a better understanding of the evolution on salt basins.

6.1.5 Pulsation phase (Early-Middle Jurassic)

The sequence S6 (Tubåen, Nordmela, and Stø formations) thins towards the Signalhorn Dome and is uniformly thick in the rim-syncline (described in section 5.3.5). In the northwestern part, the sequence S6 passively filled the subsiding rim-syncline and terminated on the rising salt wall (Figures 5.4 and 5.5). However, the uppermost part of sequence S6 subcrops below the thin Quaternary cover (Figure 5.5), indicating that this package was once deposited above the salt wall during an inactive phase (Figures 6.1 and 6.3).

The Nordmela and Stø formations are recorded in the wells and thinly blanket the Signalhorn Dome (Figures 5.11 and 5.22). The two formations are present as a thick unit within the Tiddlybanken Basin; however, it uncertain if the Tubåen Formation is present as it has not been recorded in the wells (Figures 5.5, 5.8, and 5.22). An important hiatus between the sequence S5 (Fruholmen Formation) and the Nordmela Formation on the Signalhorn Dome is strengthened by the truncation patterns within sequence S5 (Fruholmen Formation) (Figure 5.18). In contrast, truncation of sequence S6 is not observed, suggesting condensation or non-deposition on the Signalhorn Dome. A condensed Stø Formation has also been recorded throughout the southwestern Barents Sea Basin by Klausen et al. (2018b), resulting from a persistent low-accommodation setting since the early Jurassic.

Onlapping terminations towards the Signalhorn Dome show a structural high was present during the deposition of sequence S6 and was instead deposited where accommodation was available, in the rim-syncline (Figures 5.5 and 5.6). Thickness variations of the sequence S6 (Tubåen, Nordmela, and Stø formations) are recorded throughout the entire Barents Sea Basin. The Nordmela Formation is represented as a thick sedimentary unit in the Hammerfest Basin and the Bjørnøyrenna Fault Complex (Olaussen et al., 1984), while in the Hoop area, the formation is significantly thinner (Klausen et al., 2015). The Bjarmeland and Finnmark platforms were likely uplifted during the deposition of lower to middle Jurassic strata (Müller et al., 2019; Müller et al., 2022, in press).

In the central and southeastern parts of the salt wall, sequence S6 subcrop below the thin Quaternary cover (Figures 5.7 and 5.8). This suggests a subsiding basin developed above the salt wall's central and southeastern parts during the deposition of S6 (Figures 5.20 and 6.4). The previous study by Hassaan et al. (2020b) suggested a possible restoration of the Tiddlybanken Basin, illustrating a sag basin in the southeastern part of the salt wall during the middle Jurassic. The current study strengthens this suggestion with more detailed evidence through RGB blends and biostratigraphic evidence (Figures 5.26 and 5.28).

The core analysis from well 7132/2-1 indicates a fluvial dominated environment during Nordmela Formation deposition, evidenced by coal beds, plant fragments, roots, and upward fining sequences (Figures 5.22 and 5.26). During the deposition of the lower part of sequence S6 (most likely Nordmela Formation), channel systems and a possible tidal inlet crossed the inactive central and southeastern parts of the salt wall, while the northwestern part still rose towards the surface (Figure 5.27B; discussed in section 6.2.3). The combination of these observations strengthens the interpreted fluvial to tidal depositional environment (Figures 5.26 and 5.27B, C).

The upper part of sequence S6 (most likely Stø Formation) displays tidal inlets and meandering channels routed towards southwest that developed above the entire salt wall, indicating that it was inactive (see section 5.3.6 for details; Figure 6.5). The Stø Formation show signs of a transgressional environment illustrated by the GR-log and the tidal inlets on the RGB-blends (Figures 5.22 and 5.28B). When the subsidence rate is higher than the sediment input, channels are poorly interconnected, and lacustrine or marine sediments will deposit in the basin (Banham & Mountney, 2013; Ryseth, 2000). The area's transgressional character also corresponds to Klausen et al. (2018b), who documented this on a regional scale. Deposits from the Stø Formation in the Barents Sea were interpreted to reflect variations in the relative sea-level during an overall transgression of the basin (Klausen et al., 2018b).

Various seismic sections display sub-sequences with different characters within the sequence S6, described in section 5.3.5 (Figure 5.20). A sudden change in accommodation creation versus sedimentation rate is shown in the lower sub-sequence (3) in the upper unit of sequence S6 (Figure 5.20B). An internal wedge shape shows an abrupt thinning towards the Signalhorn

Dome, compared to the sub-sequences below and above. They comprise a different sedimentation/accommodation rate. Based on these speculations, the transgressive Stø Formation could represent the wedge-shaped sub-sequence.

6.1.6 Main rejuvenation phase (Early-Middle Eocene)

During the early Cretaceous, a tectonically stable period dominated the area while a Lower Cretaceous shelf platform deposited and buried the Signalhorn Dome and Tiddlybanken Basin (Figures 5.3, 5.6, and 5.10)(Hassaan et al., 2020a; Midtkandal et al., 2020). Far-field stresses from the Eurekan/Spitsbergen Orogeny likely rejuvenated the Signalhorn Dome and the salt wall in the early-middle Eocene, which also uplifted and eroded post-middle Cretaceous strata (Figures 5.4, 5.8, and 6.1)(Gac et al., 2020; Hassaan et al., 2020b). The northwestern and southeastern parts of the salt wall subcrop below the thin Quaternary cover, causing upturned Upper Jurassic to Lower Cretaceous and Upper Triassic to Lower Cretaceous strata, respectively (Figures 5.5 and 5.8). The salt did not reach the seafloor in the central part during the rejuvenation; on the other hand, the strata were upturned along the salt wall (Figure 5.7).

6.2 Impact of structural development on sediment distribution

The interaction between fluvio-deltaic systems and salt diapirism characterizes the basin infill of the Triassic-Jurassic succession in the study area (Figure 6.5). The Tiddlybanken Basin is a salt-influenced basin that experienced increased subsidence and accommodation creation due to local salt tectonics (Figures 3.3 and 3.4). The salt wall had a repeating growth in different geological times and stratigraphic levels, creating depocenters within the rim-syncline at various locations and times (Figures 6.1, 6.3, and 6.4).

Sediment loading combined with tectonic stresses were most likely the triggering mechanisms within the study area, resulting in the diversion of the fluvial systems (Figures 5.25 and 6.5). External factors such as sediment source area and climatic variations affect the rate and amount of sediment supply. Moreover, it controls the composition and availability of sediments, which

respond to the area's subsidence rate and drainage pathway (Figures 3.9 and 3.10). Increased subsidence affected the channel system within the rim-syncline due to salt wall growth (Figure 6.5). The channel systems are routed with the topography; therefore, evidence of crosscutting channels above the salt wall indicates inactivity of salt mobility (Figures 5.24C and 5.25B)(Howlett et al., 2020). The channel systems interpreted are characterized by meandering and anabranching rivers, delivering sediments to the salt-walled rim-syncline (Figures 5.24, 5.25, and 5.27).

6.2.1 Snadd Formation (S4: Ladinian-Early Norian)

Salt-related basins in the eastern Norwegian Barents Sea area are significantly affected and controlled by sediment load from the regional fluvial system generally sourced from the southeast (Glørstad-Clark et al., 2010; Hassaan et al., 2020b; Klausen et al., 2015; Line et al., 2020). This study documents that a local source area most likely affected the prograding system (Figure 6.5). The first phase of salt wall growth initiated by differential loading resulted in uplifted strata. The local high was eroded in the earliest Carnian (Figures 5.15 and 6.1). The doming above the salt wall in the Tiddlybanken Basin is such a local sediment source area, which impacted the general sediment system and has not been documented earlier. Sediments from Permian-late Triassic were eroded and redeposited during this event (Figures 5.5, 5.6, and 5.8). This acted as an additional minor source of sediment in the large-scale Snadd depositional system (Figure 6.5).

The Norwegian Barents Sea depositional environments of the Snadd Formation (S4) have been studied on a regional scale by Glørstad-Clark et al. (2010) and Klausen et al. (2015). An interpretation of one massive transportation system resulted in the construction of facies maps, which gives a general overview. The previous chapters showed that local changes (e.g., salt growth and subsidence) in the study area affected the depositional processes (Figures 3.9, 5.20, and 6.5).

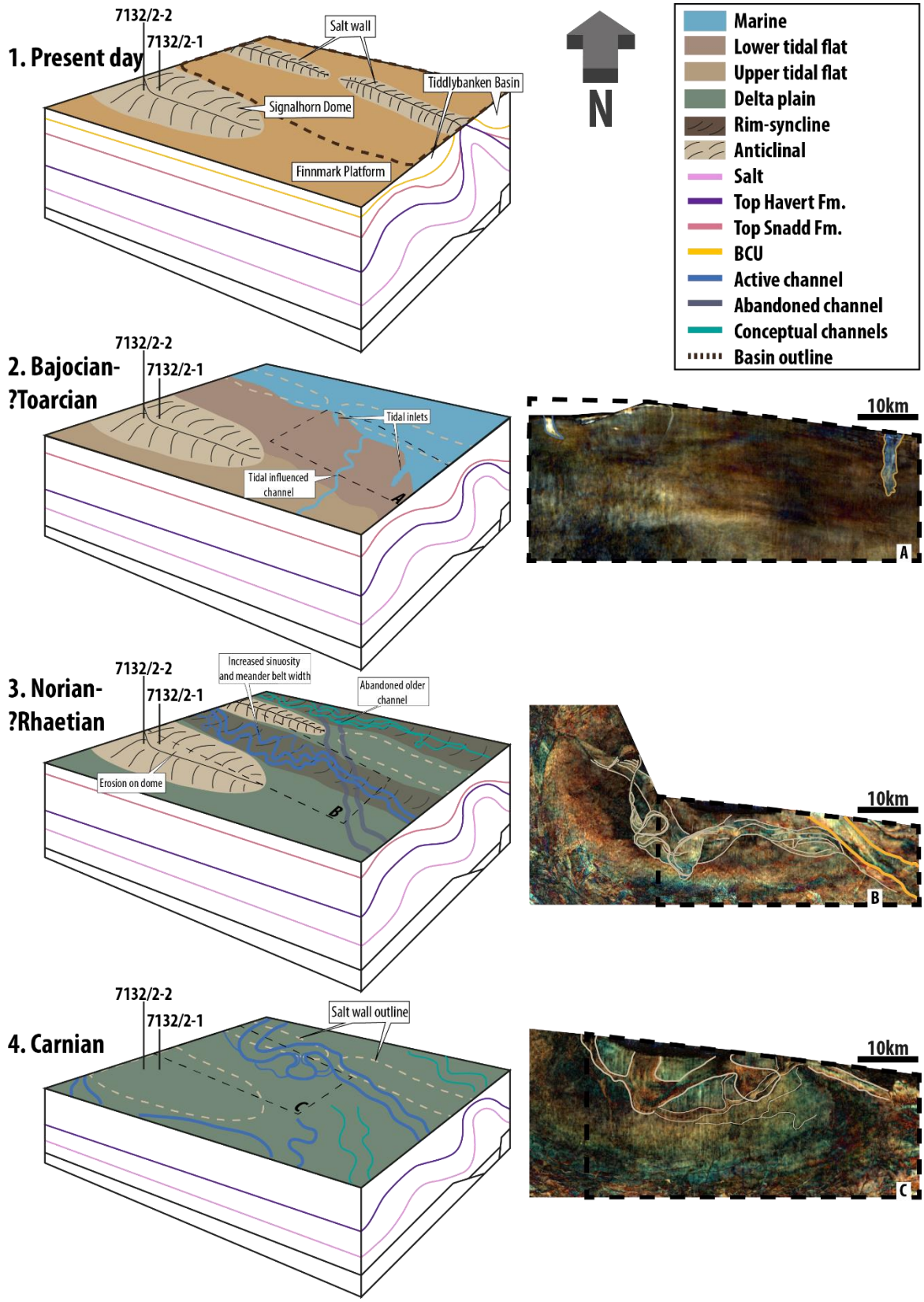

Figure 6.5: *Dynamic evolution of channel systems within the study area.* ***1.*** *Present-day illustration with the Signalhorn Dome, Tiddlybanken Basin, and the Finnmark Platform.* ***2.*** *Schematic model of the Bajocian-?Toarcian depositional environment, with a local basin and tidal inlets above the southeastern salt wall.* ***3.*** *Schematic model of the Norian-?Rhaetian comprised of a high-relief salt wall and a well-defined rim-syncline.* ***4.*** *Schematic model of the Carnian time comprised of channel complexes that easily crossed over low-relief, inactive salt wall. Seismic data courtesy of Schlumberger Multiclient.*

The channel system entering the Tiddlybanken Basin during deposition of sequence S4 is expected to be routed downwards into the rim-syncline. Identified channels are expected to extend beyond the study area, across the Finnmark Platform, and some might be routed into the Nordkapp Basin (Figures 5.23 and 5.24). The oldest channel system within the sequence S4 (Snadd Formation) is located on the Finnmark Platform and on the Signalhorn Dome, which was an exploration target and interpreted in the well log (Figures 5.11 and 5.23). The channel system shows no signs of re-routing due to doming of the surface, indicating a tectonically stable environment (Figure 6.1). Reppen (2016) reconstructed the paleogeography during the deposition of the Snadd Formation. The author documented the same N-S oriented channel system (Figure 5.23), interpreted to continue into the Nordkapp Basin in the northwest. During the deposition of sequence S4a, the salt wall created positive topographic relief and a rim-syncline surrounding it (Figures 5.14a and 5.15). It is expected that smaller channels sourced from the high-relief fold, developed by the salt wall growth, distributed sediments into the subsiding rim-syncline. Additionally, the regional system was routed towards negative topography, down into the rim-syncline.

The topographic highs and lows created by salt wall growth control the sediment routing of the transportation system (Figure 6.5). Therefore, the mapped channel systems indicate the salt wall's activity (Figures 6.1 and 6.5). During late Carnian, a channel system crossed the northwestern part of the salt wall, which acted as a negligible topographic relief (Figure 6.5). The channel system included one wide main channel crossing the northwestern salt wall in a NE-SW orientation, as described in section 5.4.4 (Figure 5.24C). Smaller channels are interpreted as distributary channels. It is essential to mention that channels crossing the salt wall may be difficult to determine if they are sourced from the topographic high formed by the salt wall growth or if the channels are a part of the regional channel system. Reppen (2016) and Hassaan et al. (2020b) stated that the salt wall was active during the entire deposition of the Snadd Formation (sequence S4) (Figure 6.1). In contrast, this study shows that the salt wall was inactive during the deposition of the upper Snadd Formation (S4b) confirmed by the crossing channel (Figures 6.3, 6.4, and 6.5).

Previous studies analyzed thickness maps of the study area (Hassaan et al., 2020b; Rowan & Lindsø, 2017). Thickness variations indicate when salt was active during a period, but it is essential to consider the imaging challenges on steeply dipping flanks (Figures 5.5, 5.6, and

5.8). For example, the thickness map of sequence S4 (Snadd Formation) illustrates a stratal thickening towards the salt wall (Figure 5.13c), indicating that the salt wall was active. The time-thickness is measured vertically along the seismic trace (true vertical thickness) and will therefore display a greater thickness on the dipping strata than the true stratigraphic thickness. The spectral decomposition attribute maps disprove an active salt wall (Figure 5.24C). The salt wall was inactive in the upper Snadd Formation until the salt moved again during early Rhaetian (Figure 5.25C). This is an important observation from the current study that might apply to other salt basins in the Norwegian Barents Sea and worldwide.

6.2.2 Fruholmen Formation (S5: Norian-Rhaetian)

The routing and geomorphology of depositional systems can be analyzed in terms of a ratio between the rate of salt structure growth or uplift and the sediment accumulation rate (Howlett et al., 2020). During deposition of sequence S5 (Fruholmen Formation), the first stage is characterized by a low-relief, segmented salt wall that creates minor diversions of channel systems that are mainly influenced by the regional margin gradient (Figure 5.25B and 6.5). The central and southeastern parts of the salt wall did not affect the topography during the deposition of the lower part of sequence S5, allowing the N-S oriented channel belt to cross the low-relief salt-cored fold (Figure 5.25B and 6.5).

The northwestern part might have been a low-relief salt-cored structure, creating minor diversions of the channel systems. In the previous section, a channel crossing the northwestern part during deposition of upper sequence S4 (Snadd Formation) was discussed (Figure 5.24C). However, the initiation of salt wall growth during sequence S5 (Fruholmen Formation) is diffuse. Still, as discussed in section 6.1.4, far-field stresses from the Novaya Zemlya fold-and-thrust belt most likely initiated the salt mobilization during middle Norian (Figures 6.1 and 6.5).

During deposition of the upper part of sequence S5 (Fruholmen Formation), the rate of salt wall growth was dominantly high relative to sediment accumulation in the northwestern part of the salt wall. A high-relief structure was developed, resulting in blocking, ponding, and diversion of the channel system (Figure 5.25C). Ponding is encouraged by local changes in a

gradient from high-relief down-dip salt walls, which block the transportation system from exiting the basin (Howlett et al., 2020).

Sequence S5 moved gradually in response to structural growth of the salt wall through lateral migration (Figure 6.5). The channel belt entered and exited the rim-syncline through confinement as a relatively narrow erosional channel (Figure 5.25C). Sinuosity and meander belt width increased due to accommodation for lateral migration (Figure 5.17). In offshore Angola, gradually diverting and ponding channel systems during times of high structural growth of salt structures were observed by Howlett et al. (2020). The study interpreted several channel-lobe systems within a specific area comprising different salt-cored structures. In contrast, the current study analyzed mainly one system that re-routed along one specific salt wall as it grew (Figures 5.17 and 5.25).

6.2.3 Tubåen, Nordmela, and Stø formations (S6: Hettangian-Bajocian)

The first stage during the deposition of sequence S6 is defined by a high-relief salt-cored structure in the northwestern part of the salt wall. The developed topographic high caused diversions and blockage of the channel systems most likely sourced from Fennoscandia and the Caledonides provenance area to the south. In the central and southeastern parts, the channel systems were largely able to transverse low-relief fold structures (Figures 5.27B and 6.1; section 5.3.6). Since the sediment routing of the transportation system is controlled by the topographic highs and lows created by the movement of salt, it can be possible to determine if the salt wall was inactive or active during deposition of the sequences. This indicates that the extensive crossing channel system is clear evidence of an inactive salt wall (Figure 5.27B, C). Younger and smaller channels with an NW-SE orientation were routed towards the northwestern part of the salt wall and are interpreted to cross over the low-relief fold that earlier was a high-relief fold (Figure 5.27D).

Towards the top of sequence S6, the entire salt wall was most likely inactive at this time and acted as a negligible topographic relief (Figures 6.1 and 6.5). The interpreted tidal inlets indicate that the sedimentation rate was not able to keep up with the subsidence, resulting in a

rise in relative sea-level (Figures 6.5). This is also discussed in section 6.1.5, where a tidal environment is interpreted for the Stø and Nordmela formations based on the core analysis and the RGB-blends displaying tidal inlets (Figures 5.26 and 5.28B).

6.3 Future research work

This study provides an improved understanding of the structural evolution and basin infill architecture in the Tiddlybanken Basin. Many questions remain unanswered, and in addition, several new questions have been raised during the investigation. The 3D seismic dataset in this study was far better than the ones used in previous studies. However, having 3D seismic data covering the entire basin would increase the understanding of the channel system dominating above the salt wall during a time when several studies interpreted the salt to be active. A detailed analysis of the composite halokinetic sequences of the central salt wall could help to reveal the relative 4D competing behavior of the salt structure and rim-syncline. The Tiddlybanken Basin has a multi-layered feeding system along the strike of the uni-directional and isolated salt wall. It would be useful to perform forward numerical modeling and analog modeling, including heterogeneities of layered evaporites and salt as a parameter. This would increase the knowledge of triggering mechanisms for salt mobilization and the growth of salt structures from multi-layered evaporite systems.

The current and previous studies suggest two rejuvenation phases for the salt wall and dome, i.e., the Triassic-Jurassic transition and the early-mid Eocene. In addition to the deep-seated Carboniferous structures, far-field stresses propagating from east to west were most likely the cause of rejuvenation. Therefore, it would be helpful to use numerical modeling to understand better the basement inheritance, intensity, and propagation of far-field stresses, properties of salt structures on the post-salt sedimentation, reservoir distribution, and hydrocarbon re-migration. A more detailed analysis of the structural evolution has been done in this study. However, a 3D structural restoration with 3D thermal and geomechanical modeling could increase the structural evolution even more. Lastly, a complete analysis of the Realgrunnen Subgroup stratigraphic evolution of channel-lobe systems on the salt-influenced slopes would improve the understanding of sediment routings under the influence of salt structure growth in the evaporite-influenced Barents Sea region.

7 Conclusions

Improved quality seismic (3D and 2D), well, core data, and spectral decomposition are used to analyze and study the evaporite-influenced Tiddlybanken Basin and evaporite-cored Signalhorn Dome in the southeastern Norwegian Barents Sea. The Tiddlybanken Basin is an excellent example of a salt-influenced basin, base salt rift structures, and evaporite accumulation that influenced post-salt structural and sedimentary development. The basin has several factors controlling the infill architecture: rate of subsidence (also controlled by salt growth), rate and style of sediment supply, basement geometry, salt thickness and composition, climate, and drainage direction. The revealed study results and processes could have similar implications for nearby salt-influenced basins like the Nordkapp Basin and other similar evaporite-dominated basins in the southwestern Barents Sea and worldwide.

In the late Devonian-early Carboniferous (Mississippian), NE-SW-oriented regional stress regime formed three half-grabens beneath the Tiddlybanken Basin and Signalhorn Dome defining the basement geometry. The structural variations between the grabens separated by structural horst and transfer zone caused differential deposition of Pennsylvanian-early Permian post-rift layered evaporite sequences. The layered evaporites with variable thickness and mobile character were deposited in the graben system that was later covered by early Permian carbonates.

Thick deltaic wedges prograded through the southeastern Norwegian Barents Sea, causing differential loading and salt mobilization during the early-middle Triassic in the Tiddlybanken Basin. A massive erosion of the domed lower-middle Triassic strata was determined to be a lower Carnian unconformity instead of an upper Anisian unconformity, as suggested by previous studies. Passive diapirism continued in pulses in the northwestern part of the salt wall, while the central and southeastern parts were inactive and did not reach further than the pedestal stage. Salt tectonics and the corresponding sea-floor topography within the Tiddlybanken Basin impacted the routing and geomorphology of channel systems. During Carnian, the salt wall was inactive, allowing channel systems to cross the salt wall that also eroded and transported older sediments domed by the salt wall.

In the late Triassic-?early Jurassic, the development of the Signalhorn Dome, and the rejuvenation of the northwestern part of the salt wall were caused by far-field compressional stresses from Novaya Zemlya fold-and-thrust belt. Reactivation and inversion of deep-seated structures caused by compressional stresses from the Novaya Zemlya fold-and-thrust belt east of the basin is a probable cause of the distinct truncation patterns and unconformities seen on the Signalhorn Dome and other domes nearby in southeastern Norwegian Barents Sea. The wells on the Singnalhorn Dome support a considerable hiatus caused by the structural development. High-relief salt-cored structures confined the channel systems, forcing re-routing towards the lower-relief structure and depocenters. The growth of the northwestern part of the salt wall during ?Rhaetian caused diversion and ponding of a massive Fruholmen channel system. As the salt wall was in an inactive phase, the channel systems were allowed to essentially follow the regional basin floor gradient with minimal diversions or ponding.

The early Cretaceous prograding strata covered the entire Signalhorn Dome and the salt wall during a tectonically stable period. Later, the main rejuvenation phase occurred during the early-middle Eocene, most likely caused by the compressional stresses from the transpressional Eurekan/Spitsbergen orogeny. The Signalhorn Dome and the salt wall were rejuvenated, but the reactivation caused minimal reactivation in the central part of the salt wall compared to the northwestern and southeastern parts. The Middle Triassic to Eocene succession over the crest of the salt wall and Signalhorn Dome are missing due to regional Cenozoic uplift and erosion of the Norwegian Barents Sea.

8 References

Baig, I., Faleide, J. I., Jahren, J., & Mondol, N. H. (2016). Cenozoic exhumation on the southwestern Barents Shelf: Estimates and uncertainties constrained from compaction and thermal maturity analyses. *Marine and Petroleum Geology, 73*, 105-130.

Banham, S. G., & Mountney, N. P. (2013). Evolution of fluvial systems in salt-walled mini-basins: A review and new insights. *Sedimentary Geology, 296*, 142-166. doi:10.1016/j.sedgeo.2013.08.010

Beauchamp, B. (1994). Permian climatic cooling in the Canadian Arctic. *Geological Society of America Special Paper, 288*, 229-246.

Bjorlykke, K. (2010). *Petroleum geoscience: From sedimentary environments to rock physics*: Springer Science & Business Media.

Brown, A. R. (2011). *Interpretation of three-dimensional seismic data*: Society of Exploration Geophysicists and American Association of Petroleum ….

Bugge, T., Mangerud, G., Elvebakk, G., Mørk, A., Nilsson, I., Fanavoll, S., & Vigran, J. O. (1995). The Upper Palaeozoic succession on the Finnmark Platform, Barents Sea. *Norsk Geologisk Tidsskrift, 75*(1), 3-30.

Buiter, S. J., & Torsvik, T. H. (2007). Horizontal movements in the eastern Barents Sea constrained by numerical models and plate reconstructions. *Geophysical Journal International, 171*(3), 1376-1389.

Crameri, F., Shephard, G. E. and Heron, P. J. (2020) The misuse of colour in science communication. Nature communications, 11 (1), pp 1-10.

Dengo, C., & Røssland, K. (1992). Extensional tectonic history of the western Barents Sea. In *Structural and tectonic modelling and its application to petroleum geology* (pp. 91-107): Elsevier.

Doré, A. (1995). Barents Sea geology, petroleum resources and commercial potential. *Arctic*, 207-221.

Eldholm, O., Tsikalas, F., & Faleide, J. (2002). Continental margin off Norway 62–75 N: Palaeogene tectono-magmatic segmentation and sedimentation. *Geological Society, London, Special Publications, 197*(1), 39-68.

Faleide, J. I., Bjørlykke, K., & Gabrielsen, R. H. (2010). Geology of the Norwegian continental shelf. In *Petroleum Geoscience* (pp. 467-499): Springer.

Faleide, J. I., Pease, V., Curtis, M., Klitzke, P., Minakov, A., Scheck-Wenderoth, M., . . . Zayonchek, A. (2018). Tectonic implications of the lithospheric structure across the Barents and Kara shelves. *Geological Society, London, Special Publications, 460*(1), 285-314.

Faleide, J. I., Tsikalas, F., Breivik, A. J., Mjelde, R., Ritzmann, O., Engen, O., . . . Eldholm, O. (2008). Structure and evolution of the continental margin off Norway and the Barents Sea. *Episodes, 31*(1), 82-91.

Faleide, J. I., Vågnes, E., & Gudlaugsson, S. T. (1993). Late Mesozoic-Cenozoic evolution of the south-western Barents Sea in a regional rift-shear tectonic setting. *Marine and Petroleum Geology, 10*(3), 186-214.

Fossen, H. (2016). *Structural geology*: Cambridge University press.

Gabrielsen, R. H., Faerseth, R. B., & Jensen, L. N. (1990). *Structural elements of the Norwegian continental shelf. Pt. 1. The Barents Sea region*: Norwegian Petroleum Directorate.

Gac, S., Minakov, A., Shephard, G. E., Faleide, J. I., & Planke, S. (2020). Deformation Analysis in the Barents Sea in Relation to Paleogene Transpression Along the Greenland-Eurasia Plate Boundary. *Tectonics, 39*(10), e2020TC006172.

Gernigon, L., Brönner, M., Dumais, M.-A., Gradmann, S., Grønlie, A., Nasuti, A., & Roberts, D. (2018). Basement inheritance and salt structures in the SE Barents Sea: Insights from new potential field data. *Journal of Geodynamics*.

Giles, K. A., & Lawton, T. F. (2002). Halokinetic sequence stratigraphy adjacent to the El Papalote diapir, northeastern Mexico. *AAPG Bulletin, 86*(5), 823-840.

Giles, K. A., & Rowan, M. G. (2012). Concepts in halokinetic-sequence deformation and stratigraphy. *Geological Society, London, Special Publications, 363*(1), 7-31.

Gilmullina, A., Klausen, T. G., Paterson, N. W., Suslova, A., & Eide, C. H. (2020). Regional correlation and seismic stratigraphy of Triassic Strata in the Greater Barents Sea: Implications for sediment transport in Arctic basins. *Basin Research, 33*(2), 1546-1579. doi:10.1111/bre.12526

Glørstad-Clark, E., Faleide, J. I., Lundschien, B. A., & Nystuen, J. P. (2010). Triassic seismic sequence stratigraphy and paleogeography of the western Barents Sea area. *Marine and Petroleum Geology, 27*(7), 1448-1475.

Gudlaugsson, S., Faleide, J., Johansen, S., & Breivik, A. (1998). Late Palaeozoic structural development of the south-western Barents Sea. *Marine and Petroleum Geology, 15*(1), 73-102.

Hassaan, M. (2021). *Evaporite-influenced rift basins and salt tectonics in the southeastern Norwegian Barents Sea.* (Degree of Philosophiae Doctor (PhD)). University of Oslo Norway, Oslo.

Hassaan, M., Faleide, J. I., Gabrielsen, R. H., & Tsikalas, F. (2020a). Carboniferous graben structures, evaporite accumulations and tectonic inversion in the southeastern Norwegian Barents Sea. *Marine and Petroleum Geology, 112*, 104038.

Hassaan, M., Faleide, J. I., Gabrielsen, R. H., & Tsikalas, F. (2020b). Architecture of the evaporite accumulation and salt structures dynamics in Tiddlybanken Basin, southeastern Norwegian Barents Sea. *Basin Research*.

Henriksen, E., Bjørnseth, H., Hals, T., Heide, T., Kiryukhina, T., Kløvjan, O., . . . Sollid, K. (2011b). Uplift and erosion of the greater Barents Sea: impact on prospectivity and petroleum systems. *Geological Society, London, Memoirs, 35*(1), 271-281.

Henriksen, E., Ryseth, A., Larssen, G., Heide, T., Rønning, K., Sollid, K., & Stoupakova, A. (2011a). Tectonostratigraphy of the greater Barents Sea: implications for petroleum systems. *Geological Society, London, Memoirs, 35*(1), 163-195.

Hochuli, P. A., & Vigran, J. O. (2010). Climate variations in the Boreal Triassic — Inferred from palynological records from the Barents Sea. *Palaeogeography, Palaeoclimatology, Palaeoecology, 290*(1-4), 20-42. doi:10.1016/j.palaeo.2009.08.013

Howlett, D. M., Gawthorpe, R. L., Ge, Z., Rotevatn, A., & Jackson, C. A. L. (2020). Turbidites, topography and tectonics: Evolution of submarine channel-lobe systems in the salt-influenced Kwanza Basin, offshore Angola. *Basin Research, 33*(2), 1076-1110. doi:10.1111/bre.12506

Hudec, M. R., & Jackson, M. P. (2007). Terra infirma: Understanding salt tectonics. *Earth-Science Reviews, 82*(1-2), 1-28.

International Union of Geological Sciences (IUGS) [2018], (http://www.iugs.org/).

Jackson, M. P., & Hudec, M. R. (2017). *Salt tectonics: Principles and practice*: Cambridge University Press.

Jackson, M. P., Roberts, D. G., & Snelson, S. (1995). Salt tectonics: a global perspective.

Jackson, M. P. and Talbot, C. J. (1991). A glossary of salt tectonics, Bureau of Economic Geology, University of Texas at Austin, pp. 44 Geologic Circular 91-4.

Jackson, M., and Vendeville, B. (1994). Regional extension as a geologic trigger for diapirism. Geological society of America bulletin, 106(1), 57-73.

Jacquin, T. (2015). Chrono- and Lithostratigraphic Framework of the Finnmark Platform. Retrieved from: https://www.geolink-s2.com

Jakobsson, M., Mayer, L., Coakley, B., Dowdeswell, J. A., Forbes, S., Fridman, B., . . . Rebesco, M. (2012). The international bathymetric chart of the Arctic Ocean (IBCAO) version 3.0. *Geophysical Research Letters, 39*(12).

Klausen, T. G., Müller, R., Poyatos-Moré, M., Olaussen, S., & Stueland, E. (2019). Tectonic, provenance and sedimentological controls on reservoir characteristics in the Upper Triassic–Middle Jurassic Realgrunnen Subgroup, SW Barents Sea. *Geological Society, London, Special Publications, 495*.

Klausen, T. G., Müller, R., Slama, J., & Helland-Hansen, W. (2016). Evidence for Late Triassic provenance areas and Early Jurassic sediment supply turnover in the Barents Sea Basin of northern Pangea. *Lithosphere, 9*(1), 14-28. doi:10.1130/l556.1

Klausen, T. G., Müller, R., Sláma, J., Olaussen, S., Rismyhr, B., & Helland-Hansen, W. (2018b). Depositional history of a condensed shallow marine reservoir succession: stratigraphy and detrital zircon geochronology of the Jurassic Stø Formation, Barents Sea. *Journal of the Geological Society, 175*(1), 130-145. doi:10.1144/jgs2017-024

Klausen, T. G., Ryseth, A. E., Helland-Hansen, W., Gawthorpe, R., & Laursen, I. (2015). Regional development and sequence stratigraphy of the Middle to Late Triassic Snadd formation, Norwegian Barents Sea. *Marine and Petroleum Geology, 62*, 102-122.

Klausen, T. G., Torland, J. A., Eide, C. H., Alaei, B., Olaussen, S., & Chiarella, D. (2018a). Clinoform development and topset evolution in a mud-rich delta–the Middle Triassic Kobbe Formation, Norwegian Barents Sea. *Sedimentology, 65*(4), 1132-1169.

Knutsen, S.-M., & Larsen, K. (1997). The late Mesozoic and Cenozoic evolution of the Sørvestsnaget Basin: a tectonostratigraphic mirror for regional events along the Southwestern Barents Sea margin? *Marine and Petroleum Geology, 14*(1), 27-54.

Koyi, H., Talbot, C. J., & Tørudbakken, B. O. (1993b). Salt diapirs of the southwest Nordkapp Basin: analogue modelling. *Tectonophysics, 228*(3-4), 167-187.

Kristensen, T. B., Rotevatn, A., Marvik, M., Henstra, G. A., Gawthorpe, R. L., & Ravnås, R. (2018). Structural evolution of sheared margin basins: the role of strain partitioning. Sørvestsnaget Basin, Norwegian Barents Sea. *Basin Research, 30*(2), 279-301.

Larssen, G., Elvebakk, G., Henriksen, L., Kristensen, S., Nilsson, I., Samuelsberg, T., . . . Worsley, D. (2005). Upper Palaeozoic lithostratigraphy of the southern part of the Norwegian Barents sea; GB Larssen, G. Elvebakk, LB Henriksen et al. *Bulletin/Norges geologiske undersokelse, 444*.

Larssen, G., Elvebakk, G., Henriksen, L. B., Kristensen, S., Nilsson, I., Samuelsberg, T., . . . Worsley, D. (2002). Upper Palaeozoic lithostratigraphy of the Southern Norwegian Barents Sea. *Norwegian Petroleum Directorate Bulletin, 9*, 76.

Lasabuda, A. P., Johansen, N. S., Laberg, J. S., Faleide, J. I., Senger, K., Rydningen, T. A., . . . Hanssen, A. (2021). Cenozoic uplift and erosion on the Norwegian Barents Shelf–A review. *Earth-Science Reviews*, 103609.

Line, L. H., Müller, R., Klausen, T. G., Jahren, J., & Hellevang, H. (2020). Distinct petrographic responses to basin reorganization across the Triassic-Jurassic boundary in the southwestern Barents Sea. *Basin Research*.

Lord, G. S., Mørk, M. B. E., Mørk, A., & Olaussen, S. (2019). Sedimentology and petrography of the Svenskøya Formation on Hopen, Svalbard: an analogue to sandstone reservoirs in the Realgrunnen Subgroup.

Mannie, A. S., Jackson, C. A. L., Hampson, G. J., & Fraser, A. J. (2016). Tectonic controls on the spatial distribution and stratigraphic architecture of a net-transgressive shallow-marine synrift succession in a salt-influenced rift basin: Middle to Upper Jurassic, Norwegian Central North Sea. *Journal of the Geological Society*, *173*(6), 901-915.

Mattingsdal, R., Høy, T., Simonstad, E., & Brekke, H. (2015). *An updated map of structural elements in the southern Barents Sea.* Paper presented at the 31st Geological Winter Meeting.

Midtkandal, I., Faleide, T. S., Faleide, J. I., Planke, S., Anell, I., & Nystuen, J. P. (2020). Nested intrashelf platform clinoforms—Evidence of shelf platform growth exemplified by Lower Cretaceous strata in the Barents Sea. *Basin Research, 32*(Clinoforms and Clinothems: Fundamental Elements of Basin Infill), 216-223.

Müller, R., Klausen, T., Faleide, J., Olaussen, S., Eide, C., & Suslova, A. (2019). Linking regional unconformities in the Barents Sea to compression-induced forebulge uplift at the Triassic-Jurassic transition. *Tectonophysics*.

Müller, R., Klausen, T., Line, L., Hafeez, A., Planke, S., Eide, F., . . . Olaussen, S. (2022, in press). Tectonostratigraphic development of the Upper Triassic to Middle Jurassic in the Hoop Area, Barents Sea: Implications for understanding ultra-condensed reservoir units. *Marine and Petroleum Geology*.

Mørk, M. (1999). Compositional variations and provenance of Triassic sandstones from the Barents Shelf. *JOURNAL OF SEDIMENTARY RESEARCH SECTION A AND B, 69*, 690-710.

Nystuen, J. P., Kjemperud, A. V., Müller, R., Adestål, V., & Schomacker, E. R. (2014). Late Triassic to Early Jurassic climatic change, northern North Sea region: impact on alluvial architecture, palaeosols and clay mineralogy. *From depositional systems to sedimentary successions on the Norwegian Continental Margin*, 59-99.

Olaussen, S., Dalland, A., Gloppen, T., & Johannessen, E. (1984). Depositional environment and diagenesis of Jurassic reservoir sandstones in the eastern part of Troms I area. In *Petroleum Geology of the North European Margin* (pp. 61-79): Springer.

Othman, A. A., Fathy, M., & Maher, A. (2016). Use of spectral decomposition technique for delineation of channels at Solar gas discovery, offshore West Nile Delta, Egypt. *Egyptian Journal of Petroleum, 25*(1), 45-51.

Peel, F. J. (2014). How do salt withdrawal minibasins form? Insights from forward modelling, and implications for hydrocarbon migration. *Tectonophysics, 630*, 222-235. doi:10.1016/j.tecto.2014.05.027

Reppen, I. (2016). *Structural evolution and fluvio-deltaic sedimentary architecture in salt-influenced rift-basins - examples from the Snadd Formation in the Nordkapp and Tiddlybanken basins.* (Master Master thesis). University of Stavanger,

Riis, F., Lundschien, B. A., Høy, T., Mørk, A., & Mørk, M. B. E. (2008). Evolution of the Triassic shelf in the northern Barents Sea region. *Polar Research, 27*(3), 318-338.

Rojo, L. A., Cardozo, N., Escalona, A., & Koyi, H. (2019). Structural style and evolution of the Nordkapp Basin, Norwegian Barents Sea. *AAPG Bulletin*(20,190,301).

Rojo, L. A., & Escalona, A. (2018). Controls on minibasin infill in the Nordkapp Basin: Evidence of complex Triassic synsedimentary deposition influenced by salt tectonics. *AAPG Bulletin, 102*(7), 1239-1272.

Rowan, M. G., & Giles, K. A. (2021). Passive versus active salt diapirism. *AAPG Bulletin, 105*(1), 53-63.

Rowan, M. G., & Lindsø, S. (2017). Salt Tectonics of the Norwegian Barents Sea and Northeast Greenland Shelf. In *Permo-Triassic Salt Provinces of Europe, North Africa and the Atlantic Margins* (pp. 265-286): Elsevier.

Rowan, M. G., and Weimer, P. (1998). Salt-sediment interaction, northern Green Canyon and Ewing bank (offshore Louisiana), northern Gulf of Mexico. AAPG Bulletin, 82(5), 1055-1082.

Ryseth, A. (2000). Differential subsidence in the Ness Formation (Bajocian), Oseberg area, northern North Sea: Facies variation, accommodation space development and sequence stratigraphy in a deltaic distributary system. *Norsk Geologisk Tidsskrift, 80*(1), 9-26. doi:10.1080/002919600750042645

Ryseth, A. (2014). Sedimentation at the Jurassic–Triassic boundary, south-west Barents Sea: indication of climate change. *From depositional systems to sedimentary successions on the Norwegian Continental Margin, 46*, 187-214.

Ryseth, A., Augustson, J. H., Charnock, M., Haugerud, O., Knutsen, S.-M., Midbøe, P. S., . . . Sundsbø, G. (2003). Cenozoic stratigraphy and evolution of the Sørvestsnaget Basin, southwestern Barents Sea. *Norwegian Journal of Geology/Norsk Geologisk Forening, 83*(2).

Schwab, A., Cronin, B., & Ferreira, H. (2007). Seismic expression of channel outcrops: Offset stacked versus amalgamated channel systems. *Marine and Petroleum Geology, 24*(6-9), 504-514.

Sheriff, R. E. (1977). Limitations on resolution of seismic reflections and geologic detail derivable from them: Section 1. Fundamentals of stratigraphic interpretation of seismic data.

Smelror, M., Petrov, O., Larssen, G. B., & Werner, S. (2009). Geological history of the Barents Sea. *Norges Geol. undersøkelse*, 1-135.

Stemmerik, L. (2000). Late Palaeozoic evolution of the North Atlantic margin of Pangea. *Palaeogeography, Palaeoclimatology, Palaeoecology, 161*(1-2), 95-126.

Strecker, U., Steidtmann, J., & Smithson, S. (1999). A conceptual tectonostratigraphic model for seismic facies migrations in a fluvio-lacustrine extensional basin. *AAPG Bulletin, 83*(1), 1320-1336.

Trusheim, F. (1960). Mechanism of salt migration in northern Germany. *AAPG Bulletin, 44*(9), 1519-1540.

Warren, J. K. (2016). *Evaporites: A geological compendium*: Springer.

Worsley, D. (2008). The post-Caledonian development of Svalbard and the western Barents Sea. *Polar Research, 27*(3), 298-317.